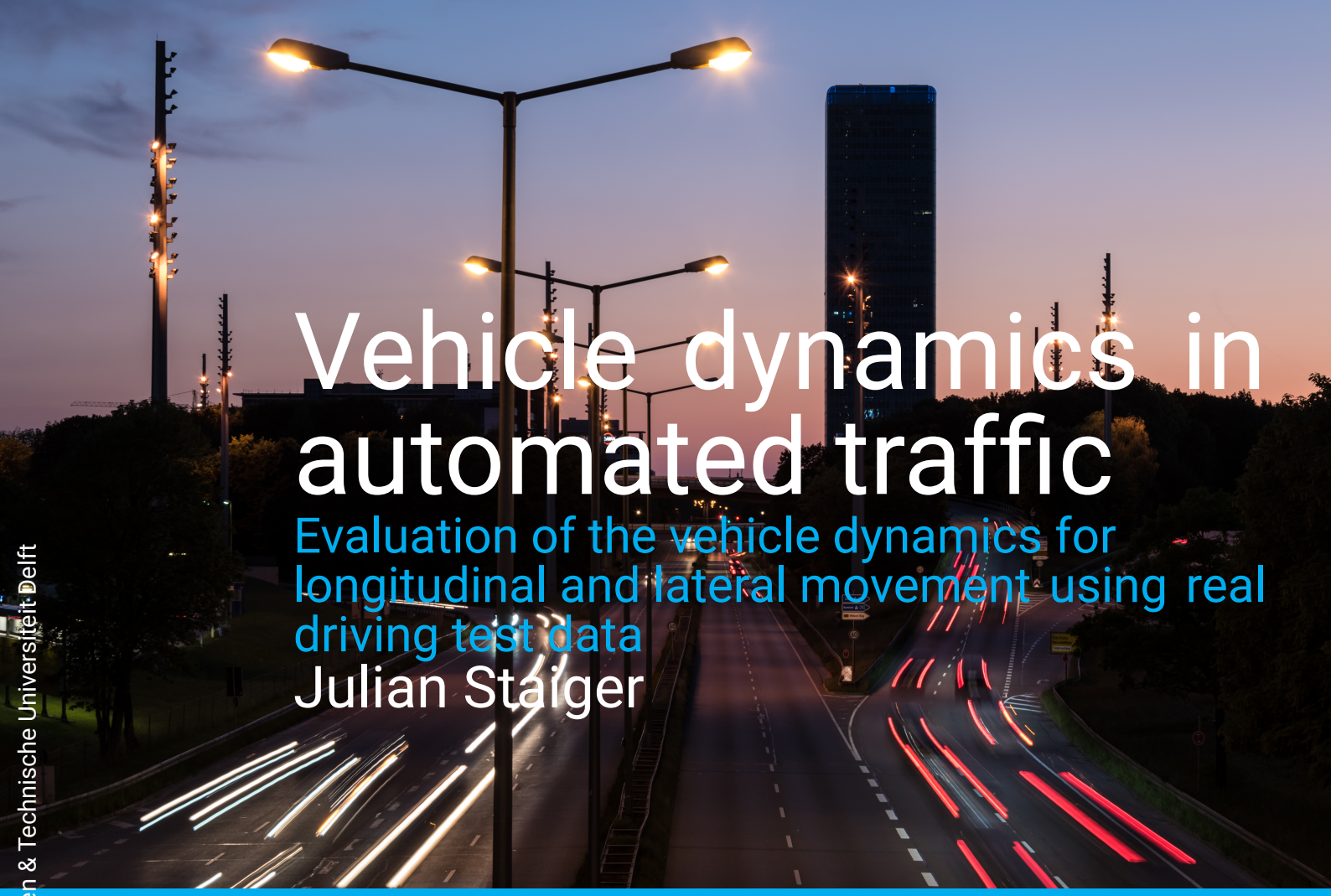

Vehicle dynamics in automated traffic

Evaluation of the vehicle dynamics for longitudinal and lateral movement using real driving test data

Julian Staiger

Hochschule München & Technische Universiteit Delft

TU Delft

HOCHSCHULE FÜR ANGEWANDTE WISSENSCHAFTEN MÜNCHEN

Vehicle dynamics in automated traffic

Evaluation of the vehicle dynamics for longitudinal and lateral movement using real driving test data

by

Julian Staiger

to obtain the degree of Master of Science
at the technische Hochschule München,
to be defended publicly on Wednesday May 27, 2020 at 15:00 PM.

Student number:	00170918	
Project duration:	November 1, 2019 – Mai 1, 2020	
Thesis committee:	Dr. Peter. E. Pfeffer,	Chairperson, Hochschule München
	Dr. ir. Simeon Calvert ,	Daily Supervisor, TU Delft
	Dr. ir. Meng Wang,	Committee member, TU Delft

An electronic version of this thesis is available at `http://repository.tudelft.nl/`.

TU Delft

HOCHSCHULE FÜR ANGEWANDTE WISSENSCHAFTEN MÜNCHEN

Preface

The motivation of this research has its origin in both my interest in the field of vehicle dynamics as well as in future mobility. In my opinion, there will always be a need for mobility of goods and people. The advent of automated or autonomous vehicles opens up new opportunities for mobility, but at the same time raises many questions about realisation, security and implementation. For me, the possibilities include an increase of driving comfort, the positive macroeconomic effects if, for example, travel time can be used as uninterrupted working time, or the ecological aspects through, for example, more intelligent use and fewer vehicle registrations. However, until we can make full use of all the advantages described above, several problems still need to be solved. The challenges include for example precise knowledge of how automated vehicles drive.

This thesis project would not have been possible without the help and support of a group of people. I want to thank my daily supervisor dr.ir. Simeon C. Calvert for his confidence in my abilities and giving me the chance to work on my master thesis in the course of an Erasmus exchange at the technical university in Delft. Beyond that, he was always a great help with daily questions, vital suggestions for important decisions during the project, and honest feedback. I was able to expand my knowledge immensely during the seven months I worked on the project. A general thanks go to all colleagues of the DiTTlab - Delft Integrated Traffic and Travel Laboratory. The academic atmosphere, as well as the scientific exchange among each other, impressed me emphatic. The working atmosphere in the laboratory and at the Faculty of Civil Engineering, in general, was something that kept my motivation high during the research project and strengthened my ambition to pursue an academic career after graduation. Furthermore, I would like to thank the whole thesis committee for devoting their time to review my report.

I would also like to thank Dr Panchamy Krishnakumari and MSc. Tin Nguyen for their support and fresh ideas that helped me to implement methods for the evaluation of the test data. Their original thinking and broad knowledge were always impressive and great support for me. The data processing would not have been possible without the excellent support of Dr Paul van Gent and Shubham Bhusari. I want to appreciate Paul and Shubham for their help understanding the unique data acquisition and post-processing in one of the field tests. Besides, I would like to thank Nagarjun Reddy and Shubham Bhusari for their support during the project. My thanks also to Johannes Keppler for the cover picture.

I am indebted to my family, especially my mother Susanne, for supporting me in every possible way throughout the thesis abroad and before through my studies in Germany. Finally, I would like to sincerely thank Anna Katherina Huber for her dedication to lecturing my thesis. My life and this work would be different without the aforementioned loved ones.

At this point, I will let my research unfold to you, dear reader.

Julian Staiger
Delft & München, May 2020

Vorwort

Die Motivation für diese Forschungsarbeit liegt grundsätzlich in meinem Interesse an Fahrdynamik sowie an neuen zukunftsorientierten Themen der Mobilität. Meiner Meinung nach wird es immer einen Bedarf an Mobilität geben, sei es die von Gütern oder Personen. Das Aufkommen von automatisieren beziehungsweise autonomen Fahrzeugen eröffnet neue Möglichkeiten dem faustischen Bestreben nach Fortschritt und Verbesserung naschzukommen. Dergestalt stehen Wissenschaftler vor neuen Herausforderungen wie diese neuen Technologien zielgerichtet eingesetzt werden können. Chancen der Automatisierung von Verkehr sind erhöhter Fahrkomfort, makroökonomische Effekte sowie ökologische Verbesserungen, um nur einige zu nennen. Herausforderungen, denen wir uns noch bis zur vollständigen Ausnutzung der positiven Effekte der Technologie stellen müssen, betreffen die Art und Weise wie automatisierte Fahrzeuge fahren.

Dieses Projekt wäre in dieser Form nicht ohne die folgenden Mitwirkenden möglich gewesen. Besonderer Dank gilt meinem Betreuer Dr. Simeon C. Calvert für sein Vertrauen in meine Fähigkeiten und die Chance, dass ich meine Thesis im Zuge einer Erasmus Kooperation an der Technischen Universität in Delft habe anfertigen können. Darüber hinaus stand er mir täglich mit bestem Rat zur Seite, machte wichtige Beiträge die direkt in die vorliegende Arbeit mit einflossen und gab mir stets ehrliches Feedback. Besonders deswegen konnte ich in den vergangenen sieben Monaten immens viel neues Lernen. Mein allgemeiner Dank gilt auch den Kollegen des DiTTlab - Delft Integrated Traffic and Travel Laboratory. Die besondere akademische Arbeitsatmosphäre und der gegenseitige Austausch beflügelten meine Motivation und waren die gesamte Zeit über Ansporn meiner Bemühungen. Insbesondere möchte ich hier auch meinen Dank an alle Mitglieder meines Thesis Komitees aussprechen. Ebenfalls danken möchte ich Dr. Panchamy Krishnakumari und MSc. Tin Nguyen für Ihre Hilfe und ihre Ideen die mir bei der Umsetzung dieses Projekts geholfen haben. Ihre immer frischen Denkansätze sowie ihr breites Spektrum an Wissen haben mich nachdrücklich beeindruckt. Die Datenanalyse in dieser Arbeit wäre auch ohne die Hilfe von Dr. Paul van Gent und Shubham Bhusari nicht möglich gewesen. Ich möchte Paul und Shubham für ihre Hilfe bei der Analyse der Datenstruktur einiger Experimente danken. Darüber hinaus danke ich auch Nagarjun und Shubham für ihre Hilfe und Empfehlungen, die Thesis betreffend, aus erster Hand. Vielen Dank auch an Johannes Keppler für das Titelbild.

Ich bin ebenfalls meiner Familie, besonders meiner Mutter Susanne, zu großem Dank verpflichtet. Ohne Ihre Unterstützung wäre eine Abschlussarbeit im Ausland sowie mein bisheriges Studium nicht möglich gewesen. Schlussendlich möchte ich mich ebenfalls bei Anna Katherina Huber für ihr Lektorat danken. Die vorliegende Arbeit wäre ohne die oben erwähnten eine andere geworden.

Julian Staiger
Delft & München, Mai 2020

Executive Summary

In the last years, significant developments in the field of Advanced Driver Assistance Systems (ADAS) have been achieved. Intelligent systems supported the improvement of traffic management and prediction, driver comfort, and vehicle safety. However, a detailed knowledge of the way vehicles move is crucial for these applications. The mobility behaviour has changed over the last decades significantly. Both the individual mobility and the mobility of goods is nowadays an essential part of our economy. The latest trends in vehicle automation are the predicted first signs of a (partially) autonomous future of mobility. Whether this future will be with or without individual vehicle ownership will become apparent in the coming years. For the moment, all researchers can do is to work on new subjects to make the future of mobility faster, more efficient, quieter and safer. Detailed knowledge of state-of-the-art vehicle automation systems is essential in order to gain further insights into their effects, e.g. on traffic, the travel behaviour of people, the security blanks caused by these systems, and passenger comfort.

Background and research objectives

Vehicle automation is introduced at six different levels. Nowadays, level 2 automation is widely spread with the introduction of Adaptive Cruise Control (ACC) and Lane Centering Assistant (LCA) systems by vehicle manufacturers. Since the introduction of these systems, vehicles have been able to drive themselves, even if only for short periods of time. The driver is partly out of the active control- but still inside the monitoring-loop, supervising the system. Some Advanced Driver Assistance (ADA) systems provide autopilot functions. These systems execute both the longitudinal and lateral vehicle control task together.

Vehicle dynamics, in terms of lateral and longitudinal vehicle movement, have a significant impact on traffic. Especially longitudinal vehicle dynamics play an essential role in the occurrence of congestion situations due to the effect on traffic density. Lateral vehicle dynamics generally stand for the vehicle movement in its lane, e.g., the interaction of the vehicle with surrounding infrastructure, in the case of this thesis with the road. The individual vehicle movement in its lane marks just the start of a causal chain, which will lead to further effects by the vehicles surrounding. Therefore, lateral vehicle movement plays a crucial role in driver and passenger safety and interaction with other vehicles. The detailed knowledge of how these ADA systems work and in what way they control the movement of the vehicle gets increasingly essential in the field of transportation science. The conclusions can help scientists to investigate possible ways to increase the capacity of roads by the introduction of ADA systems with varying degrees of market penetration. Traffic prediction models can be calibrated with real-world experimental data results. Road authorities can use the findings to improve infrastructure to meet future demands of automated vehicles. Likewise, engineers can use the results to invest in technologies to fill knowledge blanks in the security of automated driving. Since vehicle manufacturers neither use the same hardware and algorithms to realize automated driving or ADAS nor publish extensive information about the controlling scheme, scientists have to make predictions and assumptions for their models. Design and control strategies of ADA systems are closely guarded secrets of Original Equipment Manufacturers (OEM) and their developers, resulting in a lack of detailed insight results for re-

searchers in other institutions.

For these reasons, accurate insights in the way automated vehicles drive will help to fill research gaps. Therefore, the main objective of this research is to describe the automated vehicle movement as precisely as possible. To achieve this objective, the following main research question is proposed.

How do Automated Vehicles (AVs) drive interacting with different infrastructure and other vehicles on the road?

This rather unspecific research question is broken down into secondary questions (subquestions) in this work. Longitudinal and lateral vehicle movement is distinguished fundamentally in this research. This distinction enables the possibility to break down automated driving into its components and to examine the state-of-the-art systems involved individually. To answer the research question, firstly the theoretical backgrounds of the considered ADA systems is discussed. This investigation reveals degrees of freedom of vehicle control systems and helps to understand their principle. Furthermore, the examination of basic ADA system principles helps to find suitable data sets for the later evaluation of field tests.

Research methodology

The methodology of this research is to find values for the degrees of freedom identified in the theoretical study of ADA systems. By focusing on the literature study and the examination of ADA systems, potential driving situations in Field Operational Test (FOT) are identified which can deliver values for the degrees of freedom.

For longitudinal vehicle dynamics the data sources are searched for situations which we define as *stable, sustained stable, accelerated* and *decelerated* car-following. All driving conditions are specified by uniform definitions that are applied to all data sources. These driving conditions all serve a specific purpose, *stable* car-following to estimate the general time-headway in between the vehicles, *accelerated* car-following to predict how the time-headway changes when the vehicle in front accelerates and finally *sustained stable* car-following to predict if the time-headway remains constant over speed. Starting from this rather loose evaluation of the longitudinal driving conditions, a transition is made to prescribed acceleration and deceleration manoeuvres. The introduced manoeuvres consist of an acceleration or deceleration part followed by a stable driving part. The acceleration situations thus corresponds to a change in speed leading to an unaccelerated vehicle movement. The characteristics of the velocity signal and the time-headway of the following vehicle are recorded for these manoeuvres and evaluated. Of particular interest are time delays, settling times, overshoots, and initial errors. The acceleration and deceleration manoeuvres found are further suitable for the estimation of transfer functions, which consider the speed of the leading vehicle as input and the speed of the following vehicle as output and thus describe a Single Input Single Output (SISO) system. The basics for this transfer function estimation are explained in the detailed description of ADA systems aforementioned. During acceleration manoeuvres, a second-order time lag transfer function shows the best adaptation results within an appropriate calculation time. For deceleration manoeuvres, additional poles and zeros in the transfer function must be used to accommodate the increased dynamics in the reaction of the following vehicles to a decrease in velocity.

The methodology for investigating lateral vehicle dynamics follows a more descriptive

approach. Since the Lane Keeping Assistant (LKA) system has various inputs and degrees of freedom that are not causally related and the experiments considered were not intended to develop these systems backwards, we concentrate only on phenomena caused by the activation of LCA systems. The evaluation of lateral vehicle dynamics should help to gain a better insight into how AVs interact with different infrastructures, in the case of this research, with different curves. Therefore, curve identification and classification are essential. For this purpose, a map-matching algorithm is developed to match the GPS measuring points recorded during the test drives with the GPS points describing the driven road network. This methodology also provides ground truth. The driving path thus determined is used together with the recorded speed of the vehicle to calculate the lateral acceleration during the test drives. Since international standards regulate the functionality of LCA systems by limiting the maximum lateral acceleration under which they can be activated, the lateral acceleration is used to classify curves. Using the lateral acceleration has the advantage that the results are uniform and transferable. When using, e.g. the curve radius, this would not be possible. Two different levels of lateral acceleration are introduced to characterize curves of different sharpness. In conclusion, the following scenarios are distinguished for lateral vehicle movement. *Straight* driving, *light* and *sharp* right and left curves. Afterwards, the lateral position of the vehicle in its lane is linked to these scenarios.

Considered data sources

The approach followed in this research is data-driven. Therefore, real road and test track data is taken into account. Research institutes conducted all experiments used. For the longitudinal vehicle dynamics, four ACC data sources and one Cooperative Adaptive Cruise Control (CACC) data source is used. Only one suitable data source is evaluated for lateral vehicle dynamics.

Results: Longitudinal vehicle movement

During *stable* and *sustained stable* driving the following vehicle keeps a constant time-gap to its leader in all considered experiments. The considered CACC data-set shows the smallest time-headways for all driving conditions. A dependence of time-headway and velocity is found in all experiments. High velocities cause the time-headways to be smaller than low velocities. For *accelerated* following, with acceleration greater than $0.5\,{}^{m}/_{s^2}$, the time-headways are extended as the follower tries to maintain the speed profile of the leader. For deceleration phases where the acceleration is below a threshold of $-0.5\,{}^{m}/_{s^2}$ time-headways stay in the same range as for *stable* and *sustained stable* following. The estimated transfer functions for deceleration manoeuvres further confirm this result and show increased dynamics for input jumps. The system response of the CACC system to acceleration manoeuvres is of first-order, whereas it is of second-order for ACC systems. The differences in the way the CACC system controls the velocity in order to approach the speed of the leading vehicle during acceleration manoeuvres are obvious in comparison to the ACC system. In deceleration manoeuvres, the difference is less noticeable when comparing the ACC and CACC transfer functions. When comparing the frequency responses of the transfer functions of deceleration manoeuvres, it is striking that the critical frequencies at which the magnitude has a peak are in the same range as the critical frequencies for acceleration manoeuvres. Besides, these critical frequencies are in the same range as the oscillations of the space-headway signal around its mean for *sustained stable* following.

Results: Lateral vehicle movement

In the data sources for lateral vehicle movement regarded in this thesis, the vehicle tends to drive more on the left side of the lane in curves and on straight road segments. For *straight* sections, this effect was first shown by comparing the distances to the lane markings recorded on both sides of the vehicle. The effect could then be shown in curves as well. It is noticeable that the probability of the vehicle driving on the left side of the road in *sharp* left and right-hand bends is higher than in *light* curves. In all situations, whether they are classified as *straight* driving, *light* or *sharp* curves, a lateral oscillating movement of the vehicle in its lane is present. This oscillation especially applies in curves.

Main contributions

This research provides scientific and applied contributions concerning automated vehicle movement. It fills gaps in previous research by providing detailed insights into the behaviour of the Automated Vehicle (AV) in interaction with other road users and the infrastructure, which were obtained from real road tests.

The five main contributions of this research are the following:

- For ACC and CACC car-following, the time-headways at high speeds are shorter than at low speeds
- The longitudinal dynamics for braking are higher than for accelerating
- Statistical oscillation of the space-headway around its mean value does meet the critical frequencies of the system transfer functions in some cases
- On straight road sections and in curves, the vehicle shows a bias towards driving on the left roadside
- There is a lateral oscillating movement of the vehicle in its lane

All five main contributions are the subject of the present work and are elaborated and discussed in detail.

Research limitations and next steps

Given the nature of this study, the novelty of the methods used and other decisions made throughout the research, there are limitations to this thesis. The research aims to bring theory and practice together to fill research gaps, especially in the description of automated road traffic. The approach of this thesis is data-driven, which means that measurement errors occur, and each data set has its own structure. We tried to extract similar situations from the data sets to make them comparable. However, the influence of the human driver and the environment cannot be excluded completely. For this purpose, the considered ADA systems would have to be always tested with the same FOT under the same environmental conditions.

Recommendations for further steps are based on these limitations as well. Further research can focus on the testing of ADA systems under the same conditions to make detailed statements about the underlying control strategy of the systems.

Contents

List of Figures

List of Tables

1 Introduction

The importance of Automated Vehicles (AVs) and autonomous driving is expected to increase in the coming years gradually. The level of vehicle automation is classified into six different stages following the Society of Automotive Engineers (SAE). The scale reaches from level 0 no automation, meaning that the driving task is up to the driver at any time or the human is inside the control loop at any time, to level 5 full automation, standing for that the driving task is up to the Automated Vehicle (AV) at any time or the human is entirely outside the loop [63]. Nowadays, level 2 automation is distributed, while only a few commercially used cars can perform level 3 driving for more extended periods. Nevertheless, an increasing share of commercially used vehicles get delivered with Advanced Driver Assistance Systems (ADAS) to perform level 2 automation [49]. This increase signifies that vehicles are steadily taking over the driving task themselves. AVs control their throttle, brake, and the steering system, look ahead, plan to overtake, or warn the driver in case of a hazardous situation. Thus Advanced Driver Assistance (ADA) systems increasingly influence the vehicle dynamics.

Vehicle dynamics, in terms of lateral and longitudinal vehicle movement, have a significant impact on traffic. Longitudinal vehicle dynamics mainly describes the movement of a vehicle relative to the vehicle in front. Therefore, especially longitudinal vehicle dynamics play a role in the occurrence of congestion situations due to the impact on traffic density[46]. Besides, the precise knowledge of descriptive parameters of longitudinal vehicle dynamics is essential for the accuracy of simulation models replicating traffic behaviour on the road [40]. Lateral vehicle dynamics generally stand for the vehicle movement in its lane, i.e., the interaction of the vehicle with surrounding infrastructure, in the case of this thesis, with the road. Vehicle lateral movement, therefore, plays a crucial role in driver and passenger safety and interaction with other vehicles[71]. With the introduction of ADAS, mainly Adaptive Cruise Control (ACC), and its further developed system Cooperative Adaptive Cruise Control (CACC) as well as Lane Keeping Assistant (LKA), and its more sophisticated form Lane Centering Assistant (LCA) or *autosteer*, which continuously take over driving tasks from the driver, a description of the driving dynamics by these systems becomes increasingly important. Since vehicle manufacturers neither use the same hardware and algorithms to realize automated driving or ADAS nor publish extensive information about the controlling scheme, prediction models have to use new findings and theories for the driving behaviour of vehicles equipped with ADAS functions. Simulation studies comprehensively investigated the effects of the ACC and CACC systems on the traffic flow. The simulation studies use assumptions about the operation strategy and essential parameters such as time-headway and reaction time [66]. These parameters are currently still primarily estimated or anticipated from previous results

describing human driving behaviour. A comparison of results from different experiments for automated driving is currently unavailable. Design and control strategies of the systems under consideration are closely guarded secrets of Original Equipment Manufacturers (OEM) and their developers, resulting in that these insights could not be used by traffic scientists to calibrate their models in order to predict traffic events more accurately. The insights are also not available to vehicle engineers, for example, to improve their open-source control models for automated driving. Moreover, the fact that vehicle properties, when equipped with ADAS, differ widely, e.g., engine and brake power, aerodynamics, size, mass, and height, have a significant impact on the dynamic behaviour of vehicles, especially when car-following in ACC mode [15], [41]. ADAS systems are used across derivatives and must function properly under different loading conditions and system configurations. Dependence between the vehicle quantities, like loading conditions or wheelbase, and the quality of steering support by a LKA system is shown in [95]. Therefore, the automated lateral guidance of a vehicle with automated steering differs widely throughout makes and derivatives.

The functional scope and the system requirements for ADAS are only roughly regulated by international standards. ISO15622 contains the requirements for ACC functions. ISO11270 provides basic performance requirements and test procedures for LCA systems. Both standards rule the limiting values, e.g., lateral and longitudinal acceleration, jerk, and steering angle output, and provide test procedures to verify the system performance. The standards neither classify the vehicle space or time-headway distribution for ACC or CACC systems nor the distribution of the vehicle in-lane position for LCA system usage. They merely define the framework conditions for the operation of assistance systems and limit the interventions caused by the systems. The adjustment of the systems is a matter of the manufacturers.

Various scientific papers have been dealing with the prediction of market shares of autonomous vehicles in the future. Researchers agree that the number and market share of such vehicles will increase. The share of vehicles holding at least LKA and ACC will be above 20% in the US and the German vehicle marked in 2030, predicted by [105]. This increase implies that market penetration will be rising slightly, leading to a mixed vehicle population with various levels of automation[22]. For many years ahead, automated and man-operated vehicles will coexist. This coexistence raises the demands on modern traffic prediction models estimating situations of mixed traffic with higher marked penetration of ADAS equipped vehicles and the interaction with man-operated cars [9], [10]. However, to explore this interface, additional detailed knowledge of the driving dynamics of automated vehicles is required. Afterwards, the interface can be modelled by traffic scientists, psychologists, and vehicle engineers to make vehicles even safer, more efficient, and greener.

1.1. Research objectives & questions:

The main research objective of this thesis is the better understanding of the longitudinal driving behaviour of AVs when following each other with activated ACC/CACC and the lateral vehicle movement when driving with activated LCA.

This work will provide descriptive and generic values for the system behaviour of driver assistance systems. Besides that, it is evident that different types of ADAS systems presented by various manufacturers show differences in their behaviour in similar situations. Therefore, this thesis will show the extend of these differences. According to this, the following research questions are discussed in this thesis.

The main research question (RQ) is:

- How do AVs drive interacting with different infrastructure and other vehicles on the road?

The following sub-research questions (SRQ) are related to this topic and specify the steps necessary to meet the main research question:

- SRQ1: What previous research is available, and what methods were used to investigate vehicle dynamics?
- SRQ2: How do the considered ADAS work, and what are their degrees of freedom?
- SRQ3: How to describe the lateral and longitudinal vehicle dynamics objective and generic?
- SRQ4 What is the impact of different driving manoeuvres on the movement of the vehicle?
- SRQ5: How does the vehicle drive interacting with various infrastructure?
- SRQ6 What are the differences between the investigated data-sets for longitudinal and lateral driving?

The research questions are listed top-down, arranged by order of processing in the following chapters.

1.2. Research methodology:

Firstly, a literature research is carried out, according to SRQ1, SRQ2, and SRQ3, to identify research potentials and clarify the approach used later in this thesis. This literature research is focusing on the driving characteristics and quality of ADAS systems like ACC and LCA. The literature review should gain insight into measurable values describing the vehicle dynamics. The overall impact of ADA systems on traffic flow and density is examined. Furthermore, the dynamic behaviour of car-following under ACC/CACC use is focused on, in particular, the impact of different driving manoeuvres. Besides that, the prior mentioned international standards for ACC systems are presented and discussed regarding their applicability for this research. For LCA use, literature regarding the characteristics and quality of lateral vehicle movement is presented. Especially the interaction of the vehicle when driving in various infrastructure is considered. The field of focus is the AV behaviour in curves and on straight road segments. Based on the literature review, research gaps are identified, and the research questions, sub-research questions and the methodology of this thesis are adjusted accordingly. This thesis is using a data-driven approach to investigate vehicle dynamics in automated traffic. Therefore, the literature review is used as find data-sets that are beneficial and linked to the research topic for evaluation. The thesis outcome describes the AVs movement while driving in automated mode following a target vehicle or, in case of the evaluation of LCA use, driving free. The outcome of this thesis is generic, experimental based, and scalar, to make predictions Afterwards. Therefore, this thesis uses real road or test track driving data and renounces simulation-based data-sets.

The topic of research is divided into two classes: longitudinal car-following and lateral vehicle movement. This classification is used throughout the thesis and for all considered data-sets. Furthermore, longitudinal car-following is classified in the two following subtopics, a

stable driving or an accelerating target vehicle, presented in Figure 1.1. The left side of the figure, *longitudinal car-following*, describes the interaction of the vehicle with other road participants. The right side, *lateral vehicle movement*, describes the interaction of the vehicle with surrounding infrastructure.

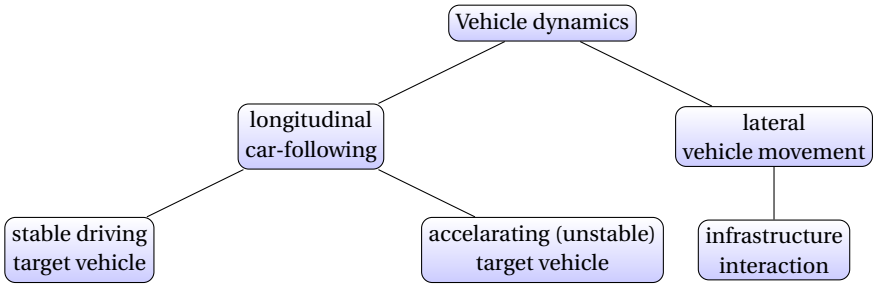

Figure 1.1: Classification of vehicle dynamics in this thesis

A separate chapter of this thesis is dedicated to the description of ACC and LCA systems. This chapter is related to SRQ2 and SRQ3 and serves to show the influences and degrees of freedom to reproduce vehicle motion in models. Different control approaches are presented, and simulations of driving manoeuvres are performed to illustrate the effects of changes in the degrees of freedom. This analysis leads to a simplified model that takes all essential parameters into account which can be provided by the evaluation of various experimental data.

For the evaluation of longitudinal vehicle dynamics, the data should describe the ACC/CACC car-following behaviour of at least two vehicles. The use of platooning experiments with more than two vehicles following is suitable as well. The used data sets should contain information about vehicle movement, e.g., vehicle speed and acceleration, as well as light detection and ranging (LIDAR) or radar information for the determination of relative velocity and distance between the vehicles. Furthermore, GPS signals, steering wheel angle, video material, break, and acceleration pedal signals and the yaw-rate can be used but are not necessarily needed. The acquisition of data, in particular the following and target vehicle velocity, acceleration, and the status of automated driving (human in or outside the loop) should be provided as in [54] for longitudinal vehicle movement. Data for lateral vehicle movement should be acquired as in [7]. These sets of data where present at the start of this thesis project and will be used for first investigations, while the use of other data-sets is foreseen. Data sources can be data-sets collected by universities or organizations recording the movement of a commercial vehicle like defined above. Especially the use of data from thesis or scientific work is foreseen since OEMs are usually not willing to share the results of internal evaluations. A significant part of this research is the search for and the selection of sufficient data-sets complying to the set conditions.

For longitudinal vehicle dynamics, an algorithm is created whether the target vehicle is stable driving or accelerating. Limiting motion quantities for this classification are investigated in the literature review. The relative acceleration and the velocity of the following vehicle are used to estimate the vehicle state. The vehicle's motion is classified in four different situations, depended on motion quantities. Afterwards, the evaluation of the dynamics of the following vehicle is done according to the identified situation. The evaluation takes space-headway between the vehicles and the time-headway derived from the space-headway through division by velocity into account. The expected results for longitudinal car-following could be increasing time-headways between the vehicles under a specific distribution when

driving at different velocities as well as oscillating frequencies around the median space-headway. For the evaluation of dynamic car-following, an assessment of the acceleration behaviour of the following vehicle is carried out. Time delays and overshoots of speed are taken into account as well as an estimation of transfer functions linking velocity of leading and following vehicle. For an accelerating target vehicle, the forming of distance hysteresis is possible as well as a variation of the velocity overshoot for different Field Operational Tests (FOTs) and between singe test runs.

The evaluation of the lateral vehicle movement does need an explanation of the infrastructure it is interacting with while driving. This research defines how this infrastructure can be described and what infrastructure is considered. Besides, an algorithm is created which determines the infrastructure with which the vehicle interacts during data recording. For a first approach, the behaviour of the AV in curves is regarded. An algorithm to detect curves, based on GPS and map matching is created. Then the data is screened for situations in which the vehicle is interacting with the detected infrastructure. The lateral vehicle position for these situations is tracked. Expected results are an asymmetric distribution of the distance to the lanes centre line when driving through curves, e.g., in right turns, the distance to the lane centre is higher than in comparable left turns. A rising distance to the lane centre when driving curves of different curvature and under different speed is also an expected result.

1.3. Research scope:

This thesis covers the vehicle dynamics of automated vehicles. It focuses on longitudinal and lateral vehicle movement clustering it in the vehicle's interaction with other road users and its interaction with the surrounding infrastructure. The research is covering the movement of the automated vehicle on the stabilization level according to [20], as explained in more detail below.

This research does use existing data only. Therefore, the comparability of different data-sets needs to be evaluated. Intersections between the data-sets have to be found and described. The used data must meet the following criteria. For the ACC/CACC evaluation: captured on public roads or test tracks, a minimum of two vehicles following each other, information of acceleration, velocity and distance, and the status of the assistant system. For the evaluation of LCA, driving information about the system activation and the absence of the driver in the control loop as well as the distance to the lane boundaries and GPS information is essential. This research only considers continuous vehicle control by the LCA system and not by the driver or by the combination of driver and assistance system. For the longitudinal and lateral dynamics of vehicles, three different data-sets each are foreseen for evaluation. Further, this research uses assumptions to make data comparable. Due to the assumptions made, some variables influencing the experiments cannot be considered. Examples of these unconsidered parameters are the surrounding temperature and time of the day, whereby most data-sets are captured during the daytime.

It is crucial to indicate that this thesis focuses on LCA and ACC functions above a level1 automation. This research describes the vehicle dynamics of a vehicle driving itself and not the driver support by these systems. Therefore, driver influence should be avoided at any time.

1.4. Scientific & Societal relevance:

Within the scientific literature, abundant research on the impact of ACC and LCA on traffic flow and stability can be found as well as effects on traffic safety [34] [39]. The differences in the inter-vehicle headway between a human driver and an AV has been estimated by [25]. An evaluation of lane change effects of ACC vehicles in mixed traffic has been done by [43]. Overall lesser research on the actual impact of ACC and LCA on vehicle dynamics based on experiments can be found. Also, most existing research focuses on phenomena in one data-set or comparing results to a model. The minority of scientific work used different data sources to be compared under the same aspects.

Modern traffic prediction models are used for planning and managing mobility in the future. The upcoming trends in, e.g., automation, smart vehicles, urbanization, rural exodus, and ecology, to name a few, set new or raise the existing requirements for the accuracy of traffic prediction models [73]. The effective use of existing infrastructure can provide a solution for upcoming mobility issues [27]. Level 2 ADAS systems can contribute to the effective use of existing infrastructure. Since driving headway and capacity flow on a lane segment are dependent variables, positive effects by ACC systems on the traffic flow can be measured by [45] and simulated by [12]. Both agree in the rising demand for network performance for increasing penetration of ACC/CACC. Therefore, a new description of vehicle dynamics with ADAS functions can help improve traffic prediction models and will make future mobility more efficient and ecologic.

1.5. Thesis outline

The outline of this thesis is drawn in Figure 1.2. Hereinafter, a short declaration about the content and the sense of each chapter (CH) is given. CH1 is focusing on the research questions previously asked as well as on the actual background and motivation of the subject. CH2 gives an overview of the current research regarding the topic of this research. Focus-fields are the driving quality of ADAS systems in real traffic. In addition to that, the interaction of the vehicle with different infrastructure and other road participants is estimated. The literature review identifies the research gaps as well as determine statements that should be proven or debunked. The results are used to plan the evaluation and to file the expected results in existing literature and scientific findings. Additionally, suitable data-sets can be acquired by the literature review. CH3 gives a summary of the controlling systems to understand important parameters, control variables, and system stability. In this chapter, the degrees of freedom of the regarded ADA systems are elaborated. CH4 describes the used methods according to the elaborated degrees of freedom for the evaluation of the data. The methodology development and implementation are carried out with the help of literature research. The described methodology is used to answer the previously proposed research questions. CH4 describes the used data-sets shortly according to their origin. CH4 gives additional information on what kind of vehicles are present in the Field Operational Test (FOT). CH5 addresses the data analysis, assessment, and the comparison between different data-sets. CH6 concludes the research results. In this conclusion, a discussion is followed by debating the results and the limitations of this research. The research questions presented above are answered in summary. Finally, recommendations for future research are given.

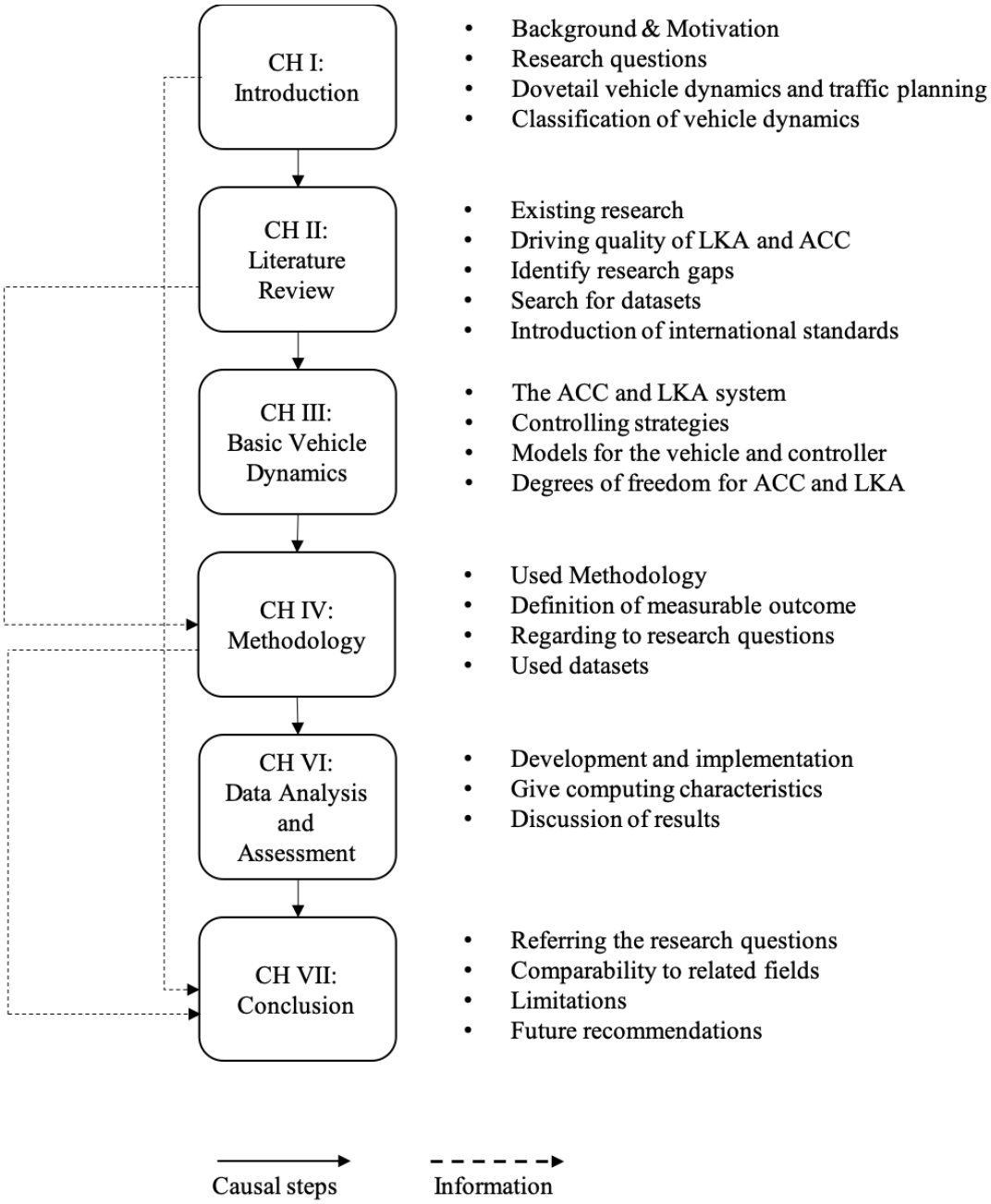

Figure 1.2: Thesis Outline

2

Literature Review

This chapter contains literature regarding vehicle dynamics in automated traffic. The chapter is separated into longitudinal and lateral vehicle dynamics as introduced previously. For longitudinal vehicle dynamics, the driving quality of ADAS systems like ACC and CACC is reviewed. After that, lateral vehicle dynamics are focused on, especially the use of LCA and its impact on the road-following accuracy of automated vehicles. Attention is paid to the question of what the potential impacts on traffic of these systems are. Earlier in this thesis mentioned research is deepened, and results are presented and discussed. The purpose of this chapter is, besides assuming literature and giving essential insight to the topic, to find comparable results regarding the research topic and methods to apply in this thesis. Besides, the literature review is used to identify suitable data-sets for comparative analysis. This chapter only presents current research on the topic of vehicle dynamics in automated traffic. The theoretical foundations of vehicle dynamics are then described separately in Chapter 3.

In general, scientists agree that the market penetration of AVs will increase in the next years. Forecasts predict that in 2035 over 80% of the sold vehicles are equipped with level 3 ADAS systems regarding [56] and [101]. A similar rise of vehicles equipped with ADAS systems is forecasted by [105] and [70]. The market penetration of AVs will, therefore, increase, albeit slower than the sale rates. Automated and non-automated vehicles will be present at the same time. Therefore, the estimation of vehicle dynamics and the behaviour between automated and not automated vehicles have to be investigated further. As Chapter 3 will show, vehicle dynamics and inter-vehicle movement have a significant impact on traffic and traffic flow. OEM design their ADA systems to provide maximum comfort for the driver, i.e., to imitate human driving behaviour [33], to avoid unfavourable points in the engine map [93] or to increase vehicle safety [50], effects on traffic flow are of secondary interest for OEM.

2.1. Longitudinal vehicle dynamics

The impact on traffic for a rising market penetration of ACC or the more recent and cooperative form CACC systems was investigated using microscopic simulations by various researchers. Research about the impact of ACC systems on traffic flow had been carried out by [18] and [50]. The impact on traffic by the introduction and rising shares of the more cooperative CACC systems has been investigated by [94],[12] and [108].

For rising ACC penetrations in traffic networks, the research agrees in the potential increase of free- and dynamic-capacity on highways, which leads to a reduction of traffic con-

gestion [94]. The used simulation models pay attention to string stability, and research mentions that real-world ACC systems may have a negative influence on traffic network performance when their market penetration is extensive. Due to the user-oriented design of the ACC systems by the OEM mentioned before, string stability is not guaranteed, which can cause traffic flow to collapse. For CACC systems, it turned out that they provide the chance to increase the traffic flow and stability drastically. The increase is predicted much higher than for ACC systems.

Moreover, real-world and state of the art insights into the phenomena and effects caused by ADA systems are becoming increasingly important, due to the prior mentioned rise of ADA systems. Microscopic traffic simulations include sub-models, e.g., for car-following during acceleration or in steady conditions. The sub-models for microscopic traffic simulation are mostly based on assumptions or estimated values. Overall, lesser research could be found regarding real road and real vehicle test environments giving the actual behaviour of ADA systems [65]. Carrying out a great FOT with multiple vehicles equipped with ACC or CACC systems is cost-intensive on the one hand and highly highway and time demanding, on the other hand[37]. Sub-models for microscopic traffic simulation like Intelligent Driver Model (IDM), Gipps model, and the Newells model are based on theories rather than on experimental results or phenomena [66]. However, feedback from real vehicle experiments can be used to calibrate these models and help to make them more accurate, as it was done in [84].

Milanés and Shladover [68] investigated in the development of CACC and ACC control models based on real experiment data from driving tests. In their research, they compare the two mentioned systems and, additionally, the IDM. The main findings are that the IDM does not perceptibly follows the speed changes of its leading vehicle. The ACC controlled vehicle is amplifying the speed changes of its leader and the traffic flow is not stable. The use of a CACC system promises noticeable improvements. The authors model the responses of the following vehicle, while exactly knowing the movement of the leading vehicle, using **TFs!** (**TFs!**). They found that for CACC car-following, the speed response of the following vehicle can be approximated with a first-order transfer function. For ACC car- following a second-order transfer function with time delay is suggested by Milanés and Shladover to model the behaviour of the following vehicle on speed changes. The comparison between IDM, ACC, and CACC shows that the IDM is producing a smooth car-following behaviour but slow responses to speed changes and large clearance gap variations. Besides, it shows that string stability is not reachable for multi-consecutive vehicles equipped with ACC, even for mild speed variations. This problem is solved with the implementation of CACC systems. These are suitable to improve highway capacity and stability significantly.

Calvert and van Arem [11] analysed a real road driving experiment on an urban arterial road, including CACC and ACC test data in the region of North Holland, The Netherlands. The authors found that both ACC and CACC systems can platoon at lower time-headways than human-driven vehicles do. Further, they found that the spread of time-headway measurements for ACC systems is narrower than for manual driving, and the spread for CACC is even smaller compared to the ACC distribution. Alkim et al. have done similar, in a FOT, they investigated the effects of ADA systems in traffic situations of varying density [2]. They have found more stable time-headways around the median for all traffic conditions in comparison to a human driver.

Makridis et al. [66] investigated on the response time, the time-headway, and its distribution for two vehicles while following with activated ACC. They performed a real road experiment with two commercial passenger vehicles. The authors found that the time-headway between the vehicles when using an ACC system has its mean around 1.5 seconds, and the distribution is not symmetric since there is a minimum acceptable time-headway. The time-headway for the use of ACC systems is slightly higher than the values of human drivers reported in the literature. For the system response time, defined as the time in between the moment of the leader's action until the moment of the follower response, Makridis et al. found that the values are between 0.8 and 1.2 seconds.

Gunter et al. [36] carried out an extensive field test with seven ACC equipped vehicles that are available widely in the US. They collected data from over 1900 kilometres of test driving. They aimed to clarify whether the used commercial on-board ACC systems are string stable or not. It turned out that no commercial implemented ACC system is string stable. The authors investigated on a linear second-order differential equation model that can approximate the ACC system behaviour. They showed that a homogeneous platoon of vehicles, all the same year, make and model, is not string stable. An initial disturbance is amplified to a value that is four times as large as the initial disturbance.

Bareket et al. [5] introduced methods for characterising the longitudinal performance of vehicles equipped with ACC systems. They describe the experimental setup as well as driving manoeuvres for measuring the ACC performance. The median time-headway for ACC car-following in their experiment is 1.33 s. They also found significant overshoots in the velocity of the following vehicle when keeping up with an accelerating leading vehicle.

The potential benefits of Vehicle to Vehicle (V2V) communication, therefore, the benefits of CACC, have been subject in the *Grand Cooperative Driving Challenge* in Helmond, The Netherlands in 2011 [109]. Nine teams from all over the world did participate. Participating teams were able to reduce the time-headway during test driving to 0.6 seconds due to V2V communication [29]. The Grand Cooperative Driving Challenge also showed that it is possible to drive in cooperation with heterogeneous systems. The benefits of connected driving had been shown by Ploeng et al. in a FOT. The authors showed theoretically and by experiment that CACC, which is built on conventional ACC sensors and a radio communication link across the vehicles, allows time-headways of significantly less than 1 second while maintaining string stability.

The international standard ISO 15622:2018 (Intelligent transport systems. Adaptive cruise control systems. Performance requirements and test procedures) and ISO 15622:2018 (Intelligent transport systems. Adaptive cruise control systems. Performance requirements and test procedures) restrict the system output of ACC systems. The restrictions are as follows.

$$-3.5\frac{m}{s^2} \leq a_x \leq 2\frac{m}{s^2} \tag{2.1}$$

$$|\gamma_x| \leq 2\frac{m}{s^3} \tag{2.2}$$

$$|a_{y,I}| \leq 2\frac{m}{s^2} \tag{2.3}$$

$$|a_{y,II}| \leq 2.3\frac{m}{s^2} \tag{2.4}$$

where a_x is the vehicles longitudinal acceleration, γ_x is the longitudinal jerk and $a_{y,I}$ and

$a_{y,II}$ are the vehicles lateral accelerations, differ only in the performance class[1] introduced by the standard. For more information please consider the norm.

2.2. Lateral vehicle dynamics

The automated lateral vehicle movement performed by LKA/LCA systems has additional degrees of freedom. In contrast to longitudinal vehicle control, lateral vehicle control must take the surrounding infrastructure into account. While for longitudinal vehicle dynamics, only the longitudinal position and the headway to the leading vehicle was descriptive for the vehicle dynamics, now two sizes have to be respected. The lateral lane deviation and the yaw rate error, for more detailed insights, please refer to Chapter 3. The LCA system has as control input the current track deviation and a feed-forward track estimate recorded by cameras [85]. The output of the LCA system is the steering angle or, to be more precise, the steering wheel torque [106]. The system of LCA controller and the controlled vehicle has more dynamic input parameters that the ACC controller and a simple model for the longitudinal movement of the vehicle. Especial driving dynamic quantities are identified by [95] to have a high impact on the lateral driving performance of passenger vehicles.

Research regarding lateral driving performance dates back to 1982 [77]. As a primary parameter, the lateral deviation from the lane centre is used to assess lateral driving performance. Possible performance indicators are the standard deviation of lateral position (SD), the Mean Lane Position (MLP), and the Steering Reversal Rates (SRR). Concerning only the lane-keeping performance, this thesis assumes that the introduced lane-keeping performance indicators of human driving are also suitable to describe the driving of LCA systems. The mentioned measures are used in research, and they had been proved to be useful for describing driving performance [38]. The focus of this thesis is to evaluate the performance of the LCA system interacting with the surrounding infrastructure. The mentioned measures do not pay attention to road characteristics and the ego vehicle state. For example, a high standard deviation around the lane centre following a straight road is different from a high standard deviation in a sharp curve in terms of, e.g., safety or comfort. Infrastructural influence on the lane-keeping task by the LCA system is therefore additionally taken into account in this thesis.

Shubham Bhusari [8] performed a field test with an electrified vehicle under the use of its LCA and ACC functions. This work contains a road test regarding vehicle and driver behaviour as well as a questionnaire about the driver comfort while using the automated driving functions. The thesis sums up the data and introduces a risk measurement metric. Outstanding is the inconsistent performance of the LCA for the same test-routes and the vehicle bias driving more on the left roadside rather than to the right. Furthermore, it was observed that the mean lane positions are further away from the lane centre in urban environments compared to the highway sections. Significant differences in lane-keeping performances across different test days was observed as well.

Benine-Neto et al. [6] performed a simulation-based study on controller design. They build a stable lateral vehicle control system by placing the eigenvalues of the closed-loop system on the negative real side of the $\Re - \Im$ plane. For more detailed insights, please refer to Chapter 3. Moreover, they could show that the lateral deviation to the lane canter could be minimised to zero for paths of constant curvature even on wet roads. For abrupt changes

[1] Full Speed Range Adaptive Cruise Control (FSRA) or Limited Speed Range Adaptive Cruise Control (LSRA)

in curvature, deviations still occur and rise with increasing driven speeds. Therefore, the vehicles speed and the shape of the road influences the lateral driving accuracy, albeit only in situations these values do change. This finding implies that commercially available LCA systems do similar.

The international standard ISO 11270:2014 (Lane-keeping assistance systems (LKAS) - Performance requirements and test procedures) specify the for LKA systems minimum functional requirements, basic Human Machine Interface (HMI) elements and test methods for passenger cars, buses, and commercial vehicles on highways and equivalent roads[2]. Additionally, the standard UN ECE R-79 and a guideline of the Japanese Ministry of Land, Infrastructure, Transport and Tourism (MLIT) apply to the function of LKA systems. The system boundaries of LKA systems, according to ISO 11270:2014, UN ECE R-79, and the technical guideline of MLIT, are the following.

$$-3\frac{m}{s^2} \leq a_{yint} \leq 3\frac{m}{s^2} \tag{2.5}$$

$$|\gamma_{yint}| \leq 5\frac{m}{s^3} \tag{2.6}$$

$$|a_{y_I}| \leq 2\frac{m}{s^2} \tag{2.7}$$

$$|a_{y,II}| \leq 0.5\frac{m}{s^2} \tag{2.8}$$

where a_{yint} is the vehicles lateral acceleration due to an intervention of the system, γ_{yint} is the maximum lateral jerk caused by system intervention. $a_{y,I}$ and $a_{y,II}$ are the vehicles lateral accelerations under that the system is active. a_{y_I} rules the maximum lateral acceleration of driving through curves while $a_{y_I I}$ specifies the acceleration for straight driving.

[2]These standards were introduced for LKA systems but also apply to LCA systems

3

Theoretical Principles of ADA systems

The following chapter describes the ADA systems considered in this thesis and presents the fundamental principles of the used vehicle dynamics. The chapter refers to SRQ2 (How do the considered ADAS work and what are their degrees of freedom?) and SRQ3 (How to describe the lateral and longitudinal vehicle dynamics objective and generic?) and gives measurable values describing the vehicle dynamics and the parameters influencing the movement of the vehicle. The chapter considers lateral and longitudinal vehicle motion separately. This chapter aims to show the variable input values for the controlling system that influence the automated movement of the vehicle, either lateral or longitudinal. In the next chapter, the approaches on how to determine these identified variable inputs from experimental data is focused. Theoretical estimation of the vehicle's behaviour in different driving manoeuvres, regarding SRQ4 (What is the impact of different driving manoeuvres on the vehicle's movement?), is derived in this chapter by multiple simulations of a simple vehicle model and the respective ADA controller. This estimation is used later to evaluate the dynamic behaviour, e.g., accelerated car-following under the use of ACC systems. This chapter reveals the link between the field of vehicle dynamics and the field of traffic flow and transportation science.

For a structured analysis of vehicle movement, a model of the three levels of vehicle guidance (navigation, manoeuvre planning, and stabilisation), given for human-driven vehicles in [21] and extended in [30] for highly automated vehicles[1], is used. The model consists of an environment, a driver and a vehicle area as well as the linked system information, presented in Figure 3.1.

[1] Automation level 2 regarding the SAE definition

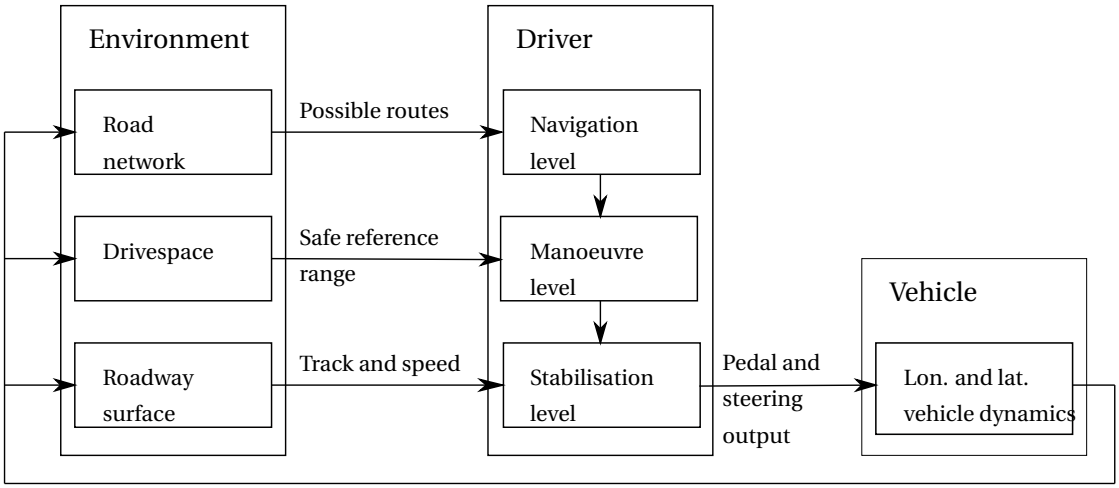

Figure 3.1: Levels of vehicle guidance. Derived from [75] [31]

More detailed information on the tasks included in all three areas - environment, driver, and vehicle - are found below.

- Vehicle Environment
  - **Traffic network**: all roads in a road network.
  - **Traffic state**: congestion or free driving etc.
  - **Road network geometry**: different curvature, tunnels or bridges.
  - **Roadway surface**: lane marking or potholes.
  - **Speed limits**
  - **Time of the day**: and other secondary boundary conditions .
- Driver/ Assisted driving system
  - **Navigation task**: find the way to your desired destination.
  - **Lane guiding task**: set the desired speed, overtaking other cars, drive in the desired lane of the road or keep the desired distance to target vehicles and the lane markings.
  - **Vehicle stabilisation task**: adjust the vehicles steering wheel, use a break and acceleration pedals so that the prior defined desired target sizes are fulfilled.
- Vehicle
  - **Vehicle dynamics**: longitudinal and lateral movement of the vehicle, due to inputs from the Driver/ Assisted driving system level.
  - **Driving dynamic quantities**: body shape, wheelbase used tires.
  - **Vehicle loading**

This thesis regards all three areas: Vehicle environment, Driver and Vehicle, but not all tasks or information they include. We assume a driver completely outside the loop therefore the ADA system is driving at any time. Therefore, the driving task is due to the system and not to the driver on the *Stabilisation level*. For the description of the automated longitudinal vehicle dynamics, the *stabilisation* level is in focus since ADA systems control the longitudinal

acceleration. The *drivespace* level at the environmental area is used to track the movement of the preceding vehicles and link interventions of the ADA system to them. For lateral vehicle dynamics, the *roadway surface* and the *roadway network* is additionally taken into account to describe the surrounding infrastructure. The ADA system output on the *stabilisation level* remains in focus.
This thesis does not examine the navigation and manoeuvre level in the driver area since route and manoeuvre planning are not the aim of this research and part of the driver's responsibility [76]. The following list illustrates the areas of importance for the evaluation.

Longitudinal vehicle dynamics	Lateral vehicle dynamics
• Drivespace	• Road network
• Stabilisation level	• Roadway surface
• Lon. and lat. vehicle dynamics	• Stabilisation level
	• Lon. and lat. vehicle dynamics

3.1. Longitudinal vehicle dynamics: ACC and CACC

In this section, information on and the function of adaptive cruise control systems is presented. ACC describes a method of controlling a vehicle's speed to adapt traffic situations using the throttle and brakes of the vehicle. The ACC system inputs are radar sensor signals providing relative velocity and distance to a target vehicle. The longitudinal control task for the cruise control is designed hierarchical, containing an upper-level controller and a lower level controller[58]. The upper-level controller calculates the torque demands to accelerate or brake the vehicle. In contrast, the lower-level controller calculates the throttle angle and brake pressure that is sent to the engine and the brake control. This thesis will discuss the ACC on the *stabilisation* level, as mentioned above. Lower-level controller functions will not be subject to this work. ACC systems incumbent the international standard ISO 15622:2018 (transport information and control systems, adaptive cruise control systems, performance requirements, and test procedures). The limiting values are given in Chapter 2.

This section first describes the basic principles of ACC systems, followed by a description of the system's control scheme. A vehicle model is presented afterwards to describe the longitudinal vehicle movement. The combination of ACC control and vehicle model is afterwards simulated with an acceleration manoeuvre to investigate on the descriptive parameters for the whole system.

3.1.1. The principle of ACC

The ACC system sets the vehicles speed so that the headway to a target vehicle is in between a particular range. In situations of free driving, the ACC behaves like a speedometer and sets the vehicles speed to a value desired by the driver.

A constant space-headway control rule between the vehicles is not suitable for autonomous control regarding [85], [98]. Because of the loss of string stability, to be introduced later, and the inefficient use of the road. Therefore, a Constant Time Gap (CTG) spacing policy is followed [85]. The controller adopts the velocity of the following vehicle to meet the target vehicle's speed, respecting the desired headway, which is calculated with the current velocity. The constant time-gap spacing is also taught as a rule of thumb for spacing in manually operated passenger vehicles. Let $V1$ and V_2 be two vehicles driving behind each other in the same lane, Figure 3.2. Moreover, let x_{i-1} and x_i be the distances of the vehicles from a fixed global coordinate system. Vehicle V_1 will be called leader or target vehicle. Vehicle $V2$ will

just be called following vehicle, ego vehicle, or follower. The headway to the target vehicle can be defined in terms of space- or as a time-headway. Space-headway describes the actual distance in meter from the front bumper of the following vehicle to the rear end of the target. In Figure 3.2, R_n is the space-headway between the vehicles. A time-headway is the time interval of two vehicles passing the same point on a lane. The time-headway for the following vehicle $h_i^t(t)$ is defined as

$$h_i^t(t) = \frac{x_{i-1}(t) - x_i(t) - l_{i-1}}{\dot{x}_i(t)}, \tag{3.1}$$

where $\dot{x}_i(t)$ is the velocity of the following vehicle and l_{i-1} is the leading vehicles length.

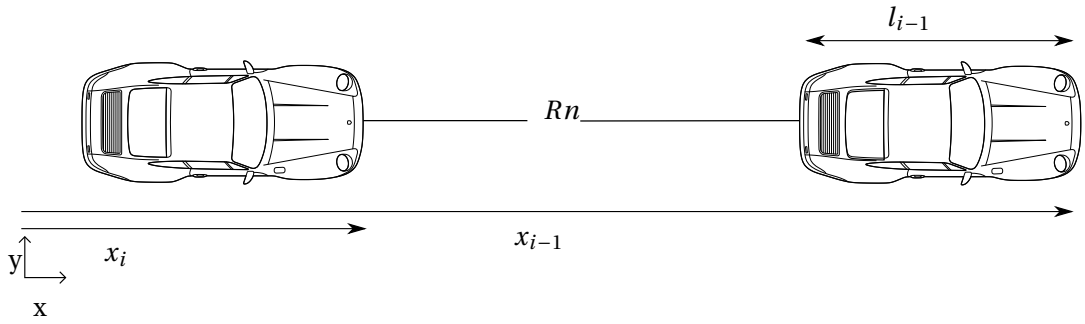

Figure 3.2: Sting of ACC vehicles in a lane

3.1.2. The ACC controller

The control architecture of ACC controllers is designed to be hierarchical [58]. An upper-level controller to determine the desired acceleration needed to keep track of the target vehicle and a lower level controller to determine the throttle or brake commands required to keep track of the desired accelerations. The objective of the upper-level controller is to determine the desired acceleration concerning a natural human behaviour of acceleration and to the individual stability of the vehicle so that it can asymptotically achieve and maintain the desired headway [85]. The lower level controller then calculates throttle and brake commands to achieve the desired acceleration paying respect to engine maps and vehicle dynamic thresholds [93], [89] using non-linear control synthesis techniques [59]. The upper level controller uses the actual headway R_n and the difference in velocity between the vehicles $\frac{dx_{i-1}}{dt} - \frac{dx_i}{dt}$ as control inputs. As prior mentioned, not a Constant Space Gap (CSG) spacing rule is pursued. Instead, a CTG spacing rule is used. Applying a CTG spacing policy implies that the space-headway between the vehicles is not constant but varies linearly with the velocity of the following vehicle. For a vehicle V_i following a target, the CTG spacing policy relates the desired space-headway $h_{i,des}^s$ to a constant time-gap and the driven speed, regarding [78].

$$h_{i,des}^s = \tau_h \dot{x}_i + L \tag{3.2}$$

The parameter τ_h is the time-gap between the vehicles in seconds, $\dot{x}_i$ is the following vehicle velocity, and L is a constant space offset at a standstill. The standstill distance will be omitted hereinafter for the sake of clarity. The headway spacing error can be defined as

$$\delta_i = \epsilon_i + \tau_h \dot{x}_i, \tag{3.3}$$

with $\epsilon = x_i - x_{i-1} + l_{i-1}$ seen as the space-headway R in Figure 3.2 with a changed sign[2]. A control law to estimate the desired acceleration of the following vehicle and ensures that the

[2]The length of the leading vehicle l_{i-1} is neglected in the following because in general $l_{i-1} \ll x_{i-1} - x_i$

error in spacing δ_i converges to zero is is presented in [42] and [17] as

$$\ddot{x_i} = -\frac{1}{\tau_h}(\dot{\epsilon_i} + \lambda\delta_i). \tag{3.4}$$

With λ a dynamic scaling parameter. Other strategies to determine the desired acceleration of ACC systems are presented by Kesting et al. [51] for the IDM, Fancher et al. [23] for combining human factors psychology as well as by Wang and Rajamani [112] for a new Variable Time Gap (VTG) approach. However, this thesis assumes that all test vehicles are controlled with the less complex CTG spacing policy to gain insights into the control strategy. At this point, the difference between the time-gap and the time-headway should be pointed out. In the following, time-gap is always used as a synonym for the parameter τ_h, while time-headway refers to a measure in experiments denoted by h^t in equation (3.1).

Remark. *Discussion of the emergence of positive accelerations for system analysis. Visible in equation* (3.4) *is that positive accelerations appear whenever the following applies*

$$\dot{\epsilon_i} + \lambda\delta_i < 0. \tag{3.5}$$

Using the previous given definitions for spacing error (3.3) *and space-headway, rearranging the terms and using* $\epsilon_2 = -R$ *as well as* $\dot{x_i} - \dot{x_{i-1}} = \Delta v$ *leads to*

$$\begin{aligned} &\dot{x_i} - \dot{x_{i-1}} + \lambda(\epsilon_i + \tau_h\dot{x_i}) < 0 \\ \Leftrightarrow\ &\Delta v + \lambda(-R + \tau_h\dot{x_i}) < 0. \end{aligned}$$

The control law generates positive accelerations whenever the velocity of the leader $\dot{x_{i-1}}$ *is grader then the followers* $\dot{x_i}$ *or the present space-headway* R *is greater than the desired* $\tau_h\dot{x_i}$*. The control law shows no acceleration in situations where the velocity of the leader* $\dot{x_{i-1}}$ *is grader than the followers* $\dot{x_i}$*, but the real space-headway is smaller than desired and vice versa.*

Applying the matrix notation of the control law, equation (3.4), leads to

$$\mathbf{X}_i^*(t) = \boldsymbol{A}_i\mathbf{X}_i(t) + \mathbf{R} \tag{3.6}$$

where $\mathbf{X}_i^* = \begin{bmatrix} s_{des}(t) \\ v_{des}(t) \\ a_{des}(t) \end{bmatrix}$, $\boldsymbol{A} = \begin{bmatrix} 0 & 0 & 1 & 0 \\ 0 & 0 & 0 & 1 \\ \frac{\lambda}{\tau_h} & \frac{1}{\tau_h} & -\frac{\lambda}{\tau_h} & -(\lambda + \frac{1}{\tau_h}) \end{bmatrix}$, $\mathbf{X}_i = \begin{bmatrix} x_{i-1} \\ \dot{x_{i-1}} \\ x_i \\ \dot{x_i} \end{bmatrix}$ and $\boldsymbol{R} = \begin{bmatrix} 0 \\ 0 \\ \lambda * l_i \end{bmatrix}$.

Laplace transforming equation (3.4) leads to the open-loop transfer function for the ACC controller[3]

$$G_c(s) = \frac{\mathbf{X}_{i-1}}{\mathbf{X}_i} = \frac{s + \lambda}{\tau_h s^2 + (1 + \lambda\tau_h)s + \lambda}. \tag{3.7}$$

This transfer function is presenting a second-order system with one zero. The step response of the system, for values of $\lambda = 1$ and $\tau_h = 1$, is similar to a first-order system response with decreased dynamics and approaches the static value from below asymptotically.

[3] Assuming $l_{i-1} = 0$ for the sake of clarity

3.1.3. The CACC controller

For CACC systems also a CTG spacing policy is applied regarding [82] and [19]. The design of the CACC controller is additionally dependent on the information flow topology between the vehicles forming a platoon [74]. The topology defines the wireless connection between the vehicles, [119]. Commonly a predecessor following topology is used where the follower receives signal only from the vehicle right in front [60] and [114]. Different other topology approaches are introduced, e.g., a bidirectional topology or two predecessors following topology are introduced in[119] and [32].

The controlling system for the predecessor following topology communication is basically the addition of two controllers: a feedback ACC and a feed-forward CACC controller [74]. Both the CACC and the ACC outputs are acceleration signals [19]. Since the CACC input does not have to be sensed, like the ACC inputs, the controller can react faster to input changes. This decreased reaction time results in a more precise regulation of the longitudinal headway and minor overshoot, e.g., in the velocity of the following vehicle when driving an acceleration manoeuvre [68]. In case information loss or general communication failures occurs, the CACC systems degrade back to a ACC system. This degrade diminishes platoon performance related to stability and safety [81].

The introduction and implementation of CACC systems [37], string stability of the used controllers [74] and their impact on traffic flow [108] had been research subject in the last years. Various research on CACC systems has been carried out in the last years by multiple researchers and organisations. This thesis will not go into detail on CACC systems any further. Instead, this research assumes a similar behaviour like the above introduced ACC systems and asses CACC systems like ACC systems to work out differences and similarities.

3.1.4. A vehicle model for longitudinal movement

The simple ACC controller output is not representative of the vehicle movement. To describe the longitudinal motion of a vehicle, a state-space model is used

$$\frac{d}{dt}\mathbf{X}_i(t) = \boldsymbol{A}_i\mathbf{X}_i(t) + \mathbf{B}_i u_i(t) \tag{3.8}$$

where $\mathbf{X}_i = \begin{bmatrix} x_i \\ v_i \\ a_i \end{bmatrix}$, $\mathbf{A}_i = \begin{bmatrix} 0 & 1 & 0 \\ 0 & 0 & 1 \\ 0 & 0 & 0 \end{bmatrix}$, $\mathbf{B}_i = \begin{bmatrix} 0 \\ 1 \\ 0 \end{bmatrix}$ and $u_i(t) = \ddot{x}_{des}(t)$ the desired acceleration as a signal from the controller. This model can achieve the desired acceleration from equation (3.4) instantaneously. Due to delays in the vehicle dynamics caused by the powertrain or the brake system, an instantaneously achieving the desired acceleration is not possible. Reasons could be engine gas dynamics [4], rotation inertia masses, pressure reduction by ADAS [47] or the hydraulic damping in the braking system. The following transfer function has been introduced by [116], [83] [80] to describe the vehicles response on e.g. acceleration inputs

$$G_L(s) = \frac{1}{\tau s + 1}. \tag{3.9}$$

We assume that the vehicle acceleration depends on the by the ACC controller commanded acceleration as

$$a_i(s) = G_L(s)\,\ddot{x}_{des} \Rightarrow \tau\dot{a}_i(t) + a_i(t) = \ddot{x}_{des}(t). \tag{3.10}$$

This equation implies that the vehicle can follow the controller's commands at any driven velocity and in any driven scenario with a first-order time lag. Therefore, the vehicles state-

space model, given in equation (3.8), is enhanced that it satisfies equation (3.10). This leads to the following

$$\frac{d}{dt}\mathbf{X}_i(t) = \boldsymbol{A}_i\mathbf{X}_i(t) + \mathbf{B}_i u_i(t)$$

where $\mathbf{X}_i = \begin{bmatrix} x_i \\ v_i \\ a_i \end{bmatrix}$, $\mathbf{A}_i = \begin{bmatrix} 0 & 1 & 0 \\ 0 & 0 & 1 \\ 0 & 0 & -\frac{1}{\tau} \end{bmatrix}$, $\mathbf{B}_i = \begin{bmatrix} 0 \\ 0 \\ \frac{1}{\tau} \end{bmatrix}$. The matrix $\mathbf{A}_i$ has two eigenvalues of zero and one on the negative $\Re$-axis dependent of the parameter τ. Therefore, the system is unstable[4]. Figure 3.3a shows the system response for velocity and distance in a phase space diagram. In Figure 3.3 the y-axis represents the velocity v_i and the x-axis represents the distance travelled x_i. The black lines are phase spaces for a specific initial velocity. Visible is that for any given positive velocity, the values for the travelled distance blow up while the velocity remains unchanged. This behaviour is not representative for a passenger vehicle since we would exact the vehicle to slow down over time until standstill.

Therefore, the equation system of longitudinal vehicle motion must take additional energy dissipation like rolling resistance, tire forces as well as aerodynamic drag into account[44]. The equilibrium of forces on the vehicle chassis is given as

$$m\ddot{x} = ma_{des} + F_R + F_{aero} \tag{3.11}$$

where m is the vehicle mass, F_R is the rolling resistance, and F_{aero} is the air drag force as a function of velocity. F_{aero} will be hereinafter written as $C\dot{x_i}^2$, where C is the summed-up coefficient, including the resistance coefficient, the shadow-casting of the flowed-around area, and the density of air. When applying the air drag force definition to equation 3.8 we obtain the following equation system

$$\frac{d}{dt}\mathbf{X}_i(t) = \boldsymbol{A}_i\mathbf{X}_i(t) + \mathbf{B}_i u_i(t) + \mathbf{C}_i \tag{3.12}$$

where $\mathbf{X}_i = \begin{bmatrix} x_i \\ v_i \\ a_i \end{bmatrix}$, $\mathbf{A}_i = \begin{bmatrix} 0 & 1 & 0 \\ 0 & 0 & 1 \\ 0 & 0 & -\frac{1}{\tau} \end{bmatrix}$, $\mathbf{B}_i = \begin{bmatrix} 0 \\ 0 \\ \frac{1}{\tau} \end{bmatrix}$, $\mathbf{C}_i = \begin{bmatrix} 0 \\ 0 \\ \frac{C}{m}\dot{x_i}^2 \end{bmatrix}$.

This non-linear system of differential equations does present the response of the vehicle to an acceleration command, given by the upper-level controller while paying respect to the actual driven velocity and the appearing aerodynamic drag force. The system response to different initial velocity is shown in Figure 3.3b. Visible is the decreasing speed over time. The solutions in the figure do not reach zero speed due to the absence of a rolling resistance term and approach the x-axis asymptotically.

[4] Solutions grow indefinitely. There is no stable or asymptotically stable behaviour

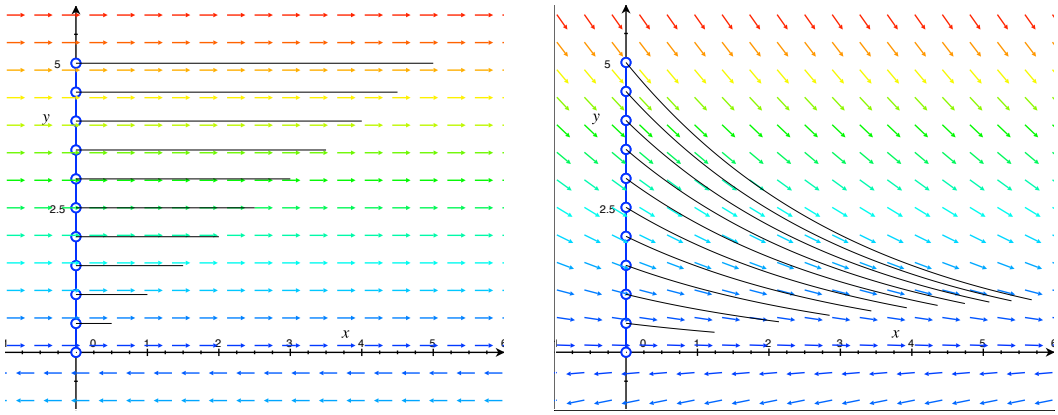

(a) Model without aerodynamic drag, phase space with $t \in [0,1]$

(b) Model with aerodynamic drag, phase space with $t \in [0,3]$

Figure 3.3: Vehicle state-space model

The combined transfer function for the system consisting of the ACC controller and the non-linear vehicle model cannot be found due to the non-linear term for air resistance, which cannot be Laplace transformed. In addition, when introducing a term for rolling resistance, it is also impossible to apply the Laplace transformation to it. Therefore, in the following, composite system considerations, consisting of ACC controller and vehicle model, are performed based on simulations.

In Figure 3.4 a block diagram of the controller and the vehicle model is given, representing the combination of equation (3.6) and (3.12). The controller **C** uses the system inputs x_{i-1} and $\dot{x}_{i-1}$ from an integrated distance and velocity sensor tracking the leading vehicle and the velocity of the considered vehicle $\dot{x}_i$. The Vehicle Model (VM) has as system input the calculated desired acceleration from the controller (C) as well as the vehicles current velocity looped back from its output for the air drag forces. The degrees of freedom of the controller and the vehicle model are shown as system inputs from above. Typical values regarding [85] are given as $\lambda = 1\,\frac{1}{s}$, $\tau_h = 1\,s$ and $\tau = 0.5s$ by [116].

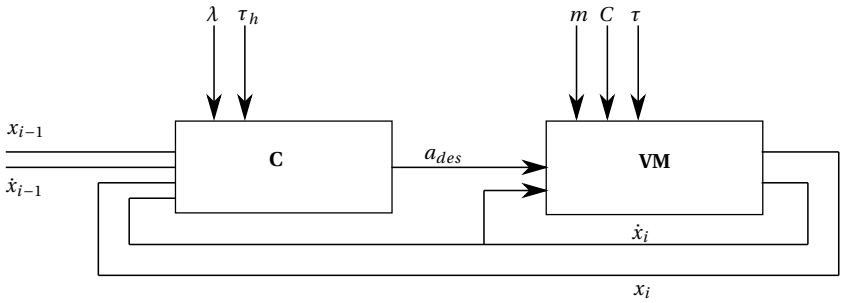

Figure 3.4: Block diagram ACC controller

A simulation of a simple acceleration manoeuvre of the leading vehicle from 0 to $33\,^{m}/_{s}$ in 20seconds, is carried out. The system output is drawn in Figure 3.5a. Noticeable is the overshoot in the velocity of the second vehicle while following the acceleration manoeuvre.

For better insight in the response of the ACC system, when variate the constant input values for λ and τ, a parameter variation is performed for the prior described acceleration

manoeuvre. The acceleration manoeuvre of the leading vehicle is maintained, the values for λ and τ are changed in between rational boundary. The results of this simulation are presented in Figure 3.5. Noticeable is the system's instability for values greater than $3\,{}^{1}/_{s}$ and $3\,s$ for λ and τ, due to rising velocity overshoots and the expanded settling time for the variation of τ and the unsteady mesh shape for the variation of λ. Since the vehicle mass and the air resistance coefficient are well known for passenger vehicles and the shadow-casting of the flowed-around area as well as the density of air could be determined easily, a variation of these parameters is not performed here. The principle of behaviour, while following a velocity ramp, could be described as follows. When increasing the vehicle aerodynamic drag coefficient C, the system response will be a decreasing overshoot. With increasing vehicle mass, the vehicle inertia does increase as well. Therefore, a higher overshoot is expected. Due to acceleration saturation by the controller and the international ruling standards, a mass variation is beside the point.

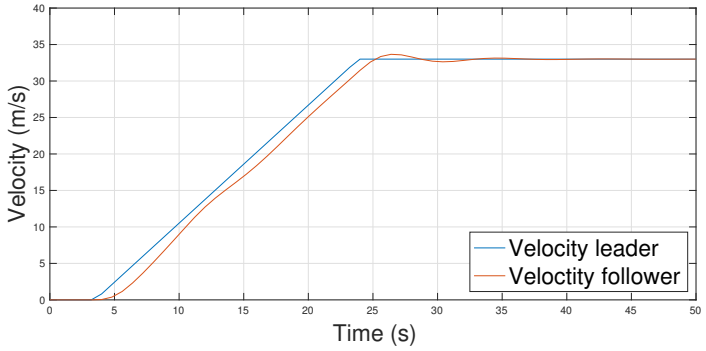

(a) System response for $\tau_h = 1s$, $\tau = 0.5s$, $\lambda = \frac{1}{s}$, $m = 1500kg$ and $C = 0.45\frac{kg}{m}$

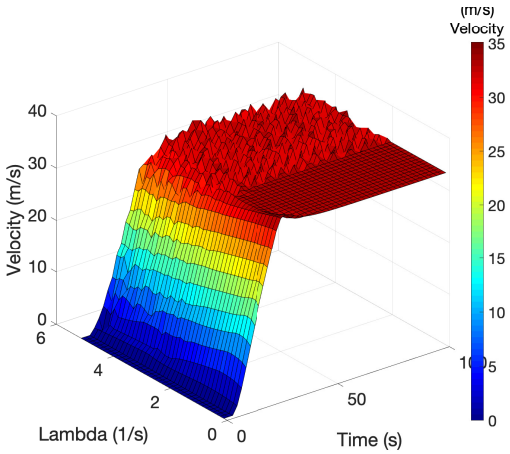

(b) Variation of λ

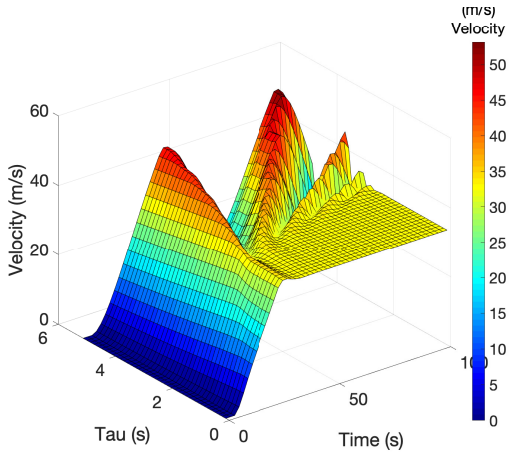

(c) Variation of τ

Figure 3.5: Simulation of a acceleration manoeuvre

In summary, the simulated behaviour of the following vehicle to the system input is similar to a second-order system respond with damping. Due to the velocity overshoot and the subsequent settling time. Therefore, we assume that the system response of controller and vehicle in real road experiments can be expressed as a simple second-order response with damping as well. This assumption is also done by [68] and [36]. The following transfer function is adequate to describe the dynamics of the following vehicle sufficient accurate

$$G_i(s) = \frac{k}{s^2 + 2\theta\omega_n s + \omega_n^2} e^{-T_d s} \tag{3.13}$$

with k the static gain, θ damping factor, ω_n natural frequency and T_d the time delay.

Because vehicles generally show increased dynamics during braking, with other words, the acceleration and deceleration capability are different, stated by [55] and [1]. We expect a different system behaviour during deceleration manoeuvres. The system behaviour is not to be derived at this point, but the possibility of inserting additional poles and zeros in the transfer function should be mentioned. Previous research assumed mostly a second-order response for deceleration manoeuvres carried out by the ACC system [94] and [68]. However, since different FOTs are compared in this work, the aim is to reproduce the system's reaction as accurately as possible.

3.1.5. String stability of platoons of ACC or CACC vehicles

String stability of either ACC and CACC systems was subject to various recent research. String stability does play an essential role in the usage of ACC and CACC systems on public roads [113]. Systems that are not string-stable tend to support the formation of congestion when the penetration rate of these systems in a traffic network is high enough [100]. Therefore, the previously presented CTG spacing rule is examined for string stability hereinafter.

As mentioned in equation (3.10) we assume that the desired acceleration could not be obtained instantaneously. We use the control rule given in (3.4) and substitute for $\ddot{x}_{des}$ in (3.10), so we obtain

$$\tau \dot{a}_i + a_i(t) = -\frac{1}{\tau_h}(\dot{\epsilon}_i + \lambda \delta_i). \tag{3.14}$$

Using the second derivative of (3.3) substituting $\dot{a}_i$ from equation (3.14) and the first derivative to substitute for a_i we find the following

$$\ddot{\epsilon}_i = \ddot{\delta}_i + \frac{1}{\tau_h}(\dot{\delta}_i + \lambda \delta_i). \tag{3.15}$$

The spacing error differences of following vehicles is given as

$$\delta_i - \delta_{i-1} = \epsilon_i - \epsilon_{i-1} + \tau_h \dot{\epsilon}_i. \tag{3.16}$$

By deriving equation (3.16) twice, substituting $\ddot{\epsilon}_i$ and $\ddot{\epsilon}_{i-1}$ from equation (3.15) and transferring it in the frequency domain using the Laplace transformation we obtain the following

$$\mathcal{L}\{\dot{\delta}_i + \lambda \delta_i + \tau_h(\ddot{\delta}_i + \lambda\, \dot{\delta}_i) + \tau_h \tau \dddot{\delta}_i\} = \mathcal{L}\{\dot{\delta}_{i-1} + \lambda \delta_{i-1}\}. \tag{3.17}$$

Rearranging the terms leads to the transfer function for spacing errors between the vehicles of a platoon

$$G(s) = \frac{\delta_i(s)}{\delta_{i-1}(s)} = \frac{s + \lambda}{\tau_h \tau s^3 + \tau_h s^2 + (1 + \lambda \tau_h)s + \lambda}. \tag{3.18}$$

String stability means uniform limitation of all the states, here the vehicles spacing errors of the system for all times. A system is considered stable if the following applies regarding [97], [116], [96]

$$||G(jw)||_\infty \leq 1, \forall w > 0, \tag{3.19}$$

where $G(jw)$ is derived from equation (3.18) by substituting s by the complex frequency jw. The string stability of the CTG control policy is proven by [85] and [116] to be stable, whenever for the time-headway $\tau_h \geq 2\tau$ does apply.

String stability of either ACC and CACC systems was subject to various research. This thesis does not deal with the subject any further. Nevertheless, it could be shown that string stability of either ACC and CACC system has an impact on traffic and, therefore, on other vehicles following. For further information the interested reader is referred to [82], [83] and [96].

3.1.6. ACC systems and impact on traffic flow

As mentioned before, the ACC system's performance has a major impact on the inter-vehicle distance in terms of space- and time- headways. Whenever a spacing error occurs as defined in equation (3.3), this leads to uncertainty in the inter-vehicle distance that the controller is trying to pull down to zero. For steady car-following[5], only the controller input parameter τ_h is responsible for the inter-vehicle spacing. For a general platoon of vehicles, referring Treiber and Kesting [104], traffic density ρ is defined as the number of vehicles NV per unit length of the road L.

$$\rho = \frac{NV}{L} \tag{3.20}$$

The inverse of ρ is the inter vehicle space-headway s

$$\rho = \frac{1}{s}. \tag{3.21}$$

The default time-headway τ_h therefore has a direct influence on the traffic density as $s = \tau_h v_i$. Traffic flow Q can be defined as the number of vehicles passing a reference point per unit of time T or as the product of traffic density ρ and velocity.

$$Q = \frac{NV}{T}. \tag{3.22}$$

In traffic jams, the unit time T remains constant while the number of vehicles NV passing a reference point decreases, and the traffic flow tends to be zero. The inverse of traffic flow is time-headway h^t, which describes the time-span between two vehicles passing a reference point, and it is equal to the introduced time-gap τ_h for steady car following. In congestion, h^t remains constant. As a traffic jam forms, h^t approaches infinity, since $NV \rightarrow 0$.

The variables ρ and Q can be measured for real traffic with road detectors and be drawn in a density flow diagram. This Fundamental Diagram (FD) of traffic flow describes the relation between flow and density of traffic, which is in equilibrium. An abstracted model of such real road experiment data is drawn in Figure 3.6. The FD can be divided into two parts one is the stable and one the unstable region. The stable region is classified as it is capable of taking more road participants. In contrast, the unstable region is classified as if one traffic participant brakes unexpectedly, the flow will collapse. The diagram's basic statement is that there is a connection between traffic density and vehicle velocity (flow rate). It points out that there is a configuration so that the flow Q maximises for a specified traffic density ρ_{crit} called the critical density. For points to the right of the critical density, this means, the more vehicles are on a road segment, the slower their velocity (flow rate) will be. Therefore, an improvement in traffic-flow efficiency is assumed when the time-headway decreases and the flow rates therefore increase [108], [94] and [118].

[5] Without acceleration

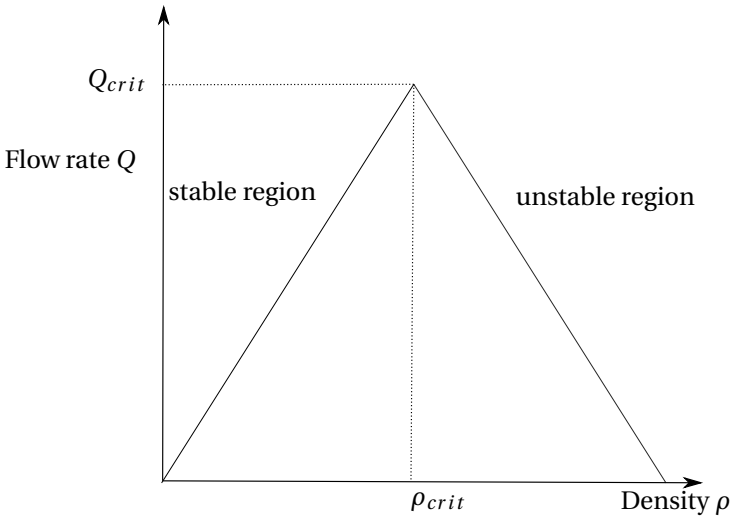

Figure 3.6: Fundamental diagram of traffic flow

[112] and [16] state that traffic flow is stable when the following condition is met.

$$\frac{\partial Q}{\partial \rho} > 0 \tag{3.23}$$

We claim that the CTG spacing policy does not lead to a stable traffic.

Proof. We use the headway definition (3.2) to define the density of traffic flow out of (3.21).

$$\rho = \frac{1}{\tau_h \dot{x_2} + L} \tag{3.24}$$

Solving for $\dot{x_2}$ in terms of ρ

$$\dot{x_2} = \frac{1}{\rho \tau_h}(1 - \rho L) \tag{3.25}$$

and applying the definition of traffic flow $Q = \rho \dot{x}$ gives

$$Q = \frac{1}{\tau_h}(1 - \rho L). \tag{3.26}$$

Calculating the gradient $\frac{\partial Q}{\partial \rho} = \frac{-L}{\tau_h} < 0$ □

It is proven that ACC systems, using the CTG spacing policy, drive the vehicle on the right side, the unstable region, of the fundamental diagram of traffic flow. Considering a section of a motorway on which only ACC vehicles drive, this means that if a vehicle is unexpected or abrupt braking, the flow of traffic will collapse.

3.2. Lateral Vehicle dynamics: LCA systems

In this section, general information and the function of lane-centring systems is given. A LCA system automatically controls the steering system of a vehicle to follow a road as it curves around. The LCA adjusts the vehicle steering angle so that the desired yaw rate is achieved, and the vehicle is driving in-between the lane markings. The used system inputs are sensor signals, either optical or inductive, providing the position of the vehicle in its lane, a look forward curvature estimation as well as yaw-rate provided from an on-board gyroscope, [64] and [107]. LCA incumbent the international standard ISO 11270:2014 (Intelligent transport systems - Lane-keeping assistance systems (LKAS) - Performance requirements and test procedures). The LCA can perform the lane-keeping task jointly with a ACC system so that the driver is completely outside the control loop for a short time. In this section, first, the principle of LCA is presented. After, a vehicle model for lateral dynamics is introduced, which takes into account the steering angle, hence the LCA output and curvature parameters. Then the control scheme of LCA is presented, followed by a simple steering test for a practical demonstration of a steering manoeuvre performed by the LCA. All this preliminary work then leads to the degrees of freedom for LCA, which can be determined from driving tests after.

3.2.1. The principle of LCA systems

Figure 3.7 shows a vehicle driving around a curve in a single-track lane. The solid curve line marks the lane boundary, the dotted line the imaginary lane centre. A vehicle fixed coordinate system is used. The abscissa describes the vehicle movement tangential to the road, the ordinate the deviation around the lane centre. The yaw-angle ψ represents the coordinate transformation around the height axis from an initial global coordinate system I to the vehicle fixed coordinate system. The LCA tries to minimise the lateral distance to the lane centre with paying respect to the desired yaw-rate given by the curve radius and the vehicles speed [85]. The controlling strategy is developed by vehicle manufacturers and not published to the public. The control strategy pays attention to a smooth steering [79], a robust and stable system behaviour [57] as well as to a brand-typical steering feel [92].

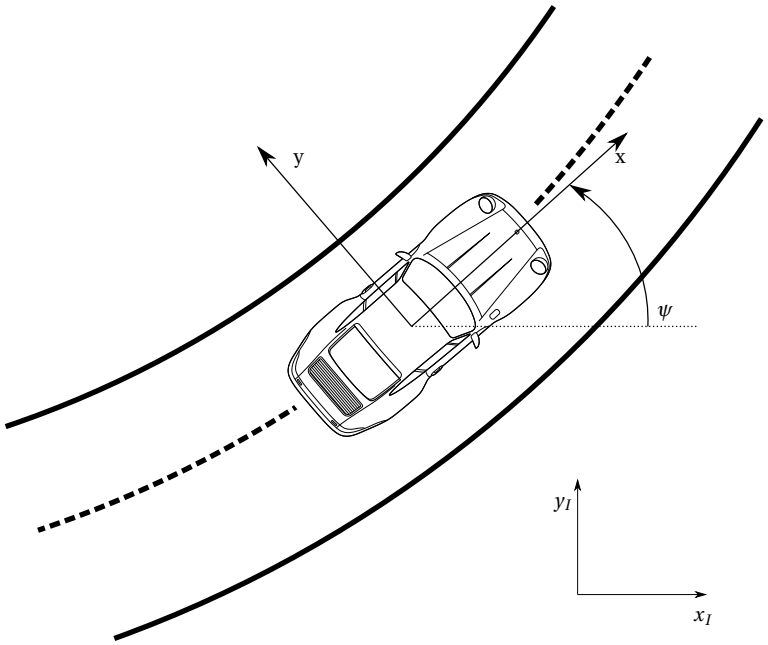

Figure 3.7: Vehicle in its lane

3.2.2. A vehicle model for lateral movement

To describe the lateral motion of a vehicle, a state-space model can be used. First applying Newtons law to the vehicles body referring [35],

$$ma_y = F_{yf} + F_{yr}. \tag{3.27}$$

Where m is the vehicle mass, a_y is the vehicles lateral acceleration, F_{yf} and F_{yr} are the tire forces at the front and rear axle. Using $a_y = \ddot{y} + V_x\dot{\psi}$ leads to

$$m(\ddot{y} + V_x\dot{\psi}) = F_{yf} + F_{yr}. \tag{3.28}$$

When applying the definitions from [85] to substitute F_{yf} and F_{yr} by introducing the steering angle δ in the equation mentioned above, the vehicles state-space model can be derived as

$$\frac{d}{dt}\begin{bmatrix} y \\ \dot{y} \\ \psi \\ \dot{\psi} \end{bmatrix} = \begin{bmatrix} 0 & 1 & 0 & 0 \\ 0 & -\frac{2C_{\alpha f}+2C_{\alpha r}}{mV_x} & 0 & -V_x - \frac{2C_{\alpha f}l_f + 2C_{\alpha r}l_r}{mV_x} \\ 0 & 0 & 0 & 1 \\ 0 & -\frac{2C_{\alpha f}l_f + 2C_{\alpha r}l_r}{I_z V_x} & 0 & -\frac{2C_{\alpha f}{l_f}^2 + 2C_{\alpha r}{l_r}^2}{I_z V_x} \end{bmatrix} \begin{bmatrix} y \\ \dot{y} \\ \psi \\ \dot{\psi} \end{bmatrix} + \begin{bmatrix} 0 \\ \frac{2C_{\alpha f}}{m} \\ 0 \\ \frac{2C_{\alpha f}l_f}{I_z} \end{bmatrix} \delta(t). \tag{3.29}$$

Where $C_{\alpha r}$ and $C_{\alpha f}$ are the tire oblique stiffens of the rear and front tire, I_z is the vehicles moment of inertia around the z-axis, l_r and l_f are the distances from the vehicle's centre of gravity to the axles.

Remark. *When considering a vehicle driving with constant longitudinal velocity V_x through a curve of a defined radius R. We define the desired change-rate of the orientation of the vehicle as*

$$\dot{\psi}_{des} = \frac{V_x}{R}. \tag{3.30}$$

We assume further a scenario where a vehicle drives at a certain speed through a curve of known radius. Using (3.30) *to determine the desired yaw-rate $\dot{\psi}_{des}$. By definition the yaw-rate does not change, therefore is $\ddot{\psi}_{des} = 0$. The lateral acceleration is given as*

$$\ddot{y}_{res} = \frac{m{V_x}^2}{R}. \tag{3.31}$$

Applying the definitions to the vehicles state space model defined in (3.29) *which leads to*

$$\begin{bmatrix} \dot{y} \\ \ddot{y}_{res} \\ \dot{\psi}_{des} \\ 0 \end{bmatrix} = \begin{bmatrix} 0 & 1 & 0 & 0 \\ 0 & -\frac{2C_{\alpha f}+2C_{\alpha r}}{mV_x} & 0 & -V_x - \frac{2C_{\alpha f}l_f + 2C_{\alpha r}l_r}{mV_x} \\ 0 & 0 & 0 & 1 \\ 0 & -\frac{2C_{\alpha f}l_f + 2C_{\alpha r}l_r}{I_z V_x} & 0 & -\frac{2C_{\alpha f}{l_f}^2 + 2C_{\alpha r}{l_r}^2}{I_z V_x} \end{bmatrix} \begin{bmatrix} y \\ \dot{y} \\ \psi \\ \dot{\psi} \end{bmatrix} + \begin{bmatrix} 0 \\ \frac{2C_{\alpha f}}{m} \\ 0 \\ \frac{2C_{\alpha f}l_f}{I_z} \end{bmatrix} \delta(t). \tag{3.32}$$

Considering the third line of the equation system, the given identity $\dot{\psi} = \dot{\psi}_{des}$ does simplifies this line drastically. Reducing the equations system by the identities in line one and three the system can be rewritten as

$$\begin{bmatrix} \ddot{y}_{res} \\ 0 \end{bmatrix} = \begin{bmatrix} -\frac{2C_{\alpha f}+2C_{\alpha r}}{mV_x} & -V_x - \frac{2C_{\alpha f}l_f+2C_{\alpha r}l_r}{mV_x} \\ -\frac{2C_{\alpha f}l_f+2C_{\alpha r}l_r}{I_zV_x} & -\frac{2C_{\alpha f}{l_f}^2+2C_{\alpha r}{l_r}^2}{I_zV_x} \end{bmatrix} \begin{bmatrix} \dot{y} \\ \dot{\psi} \end{bmatrix} + \begin{bmatrix} \frac{2C_{\alpha f}}{m} \\ \frac{2C_{\alpha f}l_f}{I_z} \end{bmatrix} \delta(t). \tag{3.33}$$

We assume that the vehicle can follow the curve proper and $\dot{y} = 0$ for the first moment when driving through the curve. So, the steering angle δ can be written as

$$\delta = \frac{2C_{\alpha f}{l_f}^2+2C_{\alpha r}{l_r}^2}{2C_{\alpha f}l_fV_x}\dot{\psi}_{des} \tag{3.34}$$

to solve the system of equations. A small diverge of the steering angle will lead to deviation of the term $\begin{bmatrix} \dot{y} \\ \dot{\psi} \end{bmatrix}$ in the following time steps and hence leads to a change in lateral acceleration and further to a lateral position change, due to $\dot{y} \neq 0$. It is therefore not simple to perform steady state cornering, i.e. to meet the conditions for both the yaw-rate and the lateral track deviation.

3.2.3. The LCA controller

When the objective is to build a lane-keeping system, the prior defined coordinates in the vehicles state-space model are not useful. However, a more viable approach is to use the position and orientation error instead of the global lane departure y and global orientation change (ψ). Hence the vehicle state-space model developed earlier is re-defined with the introduction of error variables regarding [35].

$$\dot{e_1} = \dot{y} + V_x(\psi - \psi_{des}) \tag{3.35}$$

$$e_2 = \psi - \psi_{des} \tag{3.36}$$

The state-space model in error variables is now given by

$$\frac{d}{dt}\begin{bmatrix} e_1 \\ \dot{e_1} \\ e_2 \\ \dot{e_2} \end{bmatrix} = \begin{bmatrix} 0 & 1 & 0 & 0 \\ 0 & -\frac{2(C_{\alpha f}+C_{\alpha r})}{mV_x} & \frac{2(C_{\alpha f}+C_{\alpha r})}{m} & -\frac{2(C_{\alpha f}l_f+C_{\alpha r}l_r)}{mV_x} \\ 0 & 0 & 0 & 1 \\ 0 & -\frac{2(C_{\alpha f}l_f+C_{\alpha r}l_r)}{I_zV_x} & \frac{2(C_{\alpha f}l_f+C_{\alpha r}l_r)}{I_z} & -\frac{2(C_{\alpha f}{l_f}^2+C_{\alpha r}{l_r}^2)}{I_zV_x} \end{bmatrix} \begin{bmatrix} e_1 \\ \dot{e_1} \\ e_2 \\ \dot{e_2} \end{bmatrix} + \begin{bmatrix} 0 \\ \frac{2C_{\alpha f}}{m} \\ 0 \\ \frac{2C_{\alpha f}l_f}{I_z} \end{bmatrix} \delta(t) + \begin{bmatrix} 0 \\ -\frac{2(C_{\alpha f}l_f+C_{\alpha r}l_r)}{mV_x} - V_x \\ 0 \\ -\frac{2(C_{\alpha f}{l_f}^2+C_{\alpha r}{l_r}^2)}{I_zV_x} \end{bmatrix} \dot{\psi}_{des} \tag{3.37}$$

This can be rewritten as

$$\frac{d}{dt}\dot{\vec{\mathbf{x}}} = A\vec{\mathbf{x}} + \mathbf{B}_1\delta(t) + \mathbf{B}_2\dot{\psi}_{des}, \tag{3.38}$$

with $\vec{\mathbf{x}} = [e_1\ \dot{e}_1\ e_2\ \dot{e}_2]^T$ $\mathbf{A}$, $\mathbf{B}_1$ and $\mathbf{B}_2$ are the matrices out of equation (3.37).
Considering the open loop system $\frac{d}{dt}\vec{\mathbf{x}} = \mathbf{A}\vec{\mathbf{x}}$. Let ($\lambda_1$,...,$\lambda_4$) be the eigenvalues of matrix $\mathbf{A}$. It can be shown that matrix $\mathbf{A}$ has two eigenvalues at the coordinate origin, $\lambda_1 = 0$ and $\lambda_2 = 0$.

Moreover, matrix **A** is unstable, due to $\Im\{\lambda_3,\lambda_4\}=0$ and $\Re\{\lambda_3,\lambda_4\}>0$ for rational assumptions for the vehicle dynamic quantities. This shows that the system has to be stabilized by feedback. Hence, using the control law for the steering angle δ

$$\delta = -K\vec{\mathbf{x}} = -k_1 * e_1 - k_1 * \dot{e}_1 - k_2 * e_2 - k_4 * \dot{e}_2. \tag{3.39}$$

The feedback by the controller $\frac{d}{dt}\vec{\mathbf{x}} = (\mathbf{A}-\mathbf{B}_1\mathbf{K})\vec{\mathbf{x}} + \mathbf{B}_2\dot{\psi}_{des}$ allows to place the eigenvalues of the system at any desired location on the real-imaginary plain. At this point it should be noted that the desirable location of all eigenvalues is on the negative real axis. A simulation of a curve manoeuvre is conducted. For the simulation the following values for the vehicle dynamic quantities are used. The values are representative for an average passenger vehicle. $m = 1500kg$, $I_Z = 2800kgm^2$, $l_f = 1.1m$, $l_r = 1.58m$, $C_{\alpha f} = 80000^N/_{rad}$ and $C_{\alpha r} = 80000^N/_{rad}$. The choose manoeuvre is driving to a clothoid shaped curve with a curve radius of 1000 meter driven with a velocity of $30\frac{m}{s}$. The maximal yaw-rate is reached after 6 seconds of driving, after the curve has a constant radius. Figure 3.8 gives the results of the Simulation. The eigenvalues are placed as followed $[-5-3j\ -5+3j\ -10\ -7]^T$ to determine the share values of K.

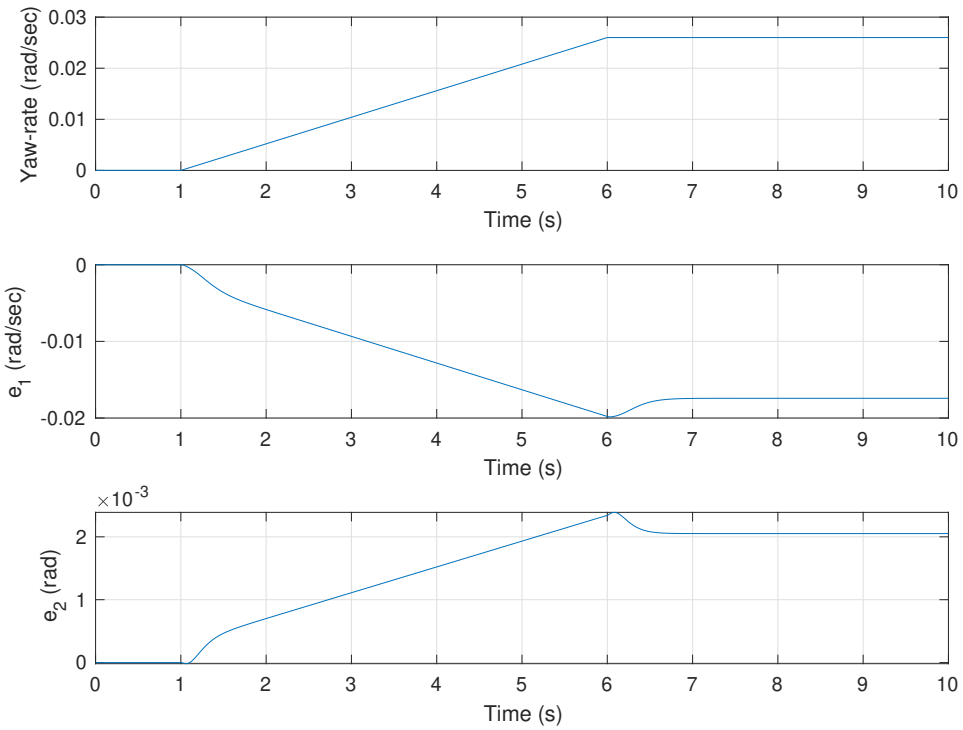

Figure 3.8: System response for LCA curve driving. (top) Yaw-rate input. (middle) Yaw-rate deviation. (bottom) Lane-centre deviation

Noticeable is the linear increase of yaw-rate during the first six seconds of the manoeuvre like expected from a clothoid shaped curve. The yaw-rate remains at a constant value after 6 seconds. The error with respect to the centre of the lane first increases and then remains at a steady value for constant yaw rates. The same behaviour can be seen for the yaw-rate error. Noticeable is the yaw-rate overshoot at the beginning and the end of the clothoid shaped road segment. The error values $\vec{\mathbf{x}}$ do not fall to zero due to the input of road curvature $\dot{\psi}_{des}$

and the non-predictive control strategy.

In modern LCA systems a slightly different control rule is applied [103], [90]. Modern LCA systems use a feed-forward term to estimate the yaw-rate demand on the driven path in front of the vehicle. So the controller can be described as a state feedback and a feed-forward controller, leading to the assumption that the actual steering angle contains a share for the in-lane position error minimisation $-K\vec{\mathbf{x}}$ and a share for the curve compensation δ_{ff}

$$\delta = -Kx + \delta_{ff}. \tag{3.40}$$

It can be shown that the lateral position error e_1 can be reduced to zero for an appropriate choice of the feed-forward term δ_{ff} [85]. The yaw-rate error will remain no matter which values are chosen for the feed-forward steering angle[6]. The steady-state yaw-angle error can be written as

$$e_{2_{ss}} = -\frac{l}{R} + \frac{l_f}{1 * C_{ar}(l_f + l_r)} \frac{mV_x^2}{R}. \tag{3.41}$$

The steady state position error e_1 can be made zero for the following choice of the feed forward steering angle

$$\delta_{ff} = \frac{L}{R} + K_V a_y - k_3 e_{2_{ss}}, \tag{3.42}$$

where a_y is the lateral acceleration and K_V the under-steer gradient. Due to the fact that stationary cornering (position error and yaw rate error equal to zero) is not possible because of various vehicle quantities such as length and tyre oblique stiffness, the vehicle control strategies pursue a compromise between both objectives [85]. This implies that the fulfilment of one of the error term conditions leads to different distances to the road markings than the fulfilment of the other requirement.

A block diagram for the in this section introduced vehicle model and LCA controller is given in Figure, referring 3.9 [102] and [48]. The following nomenclature is used Feed Forward Controller (FFC), State Feedback Controller (SFC), VM. The *Nominal trajectory* is the by the sensing unit calculated position of the vehicle in its lane. This unit is sensing the environmental signals dependent on $\vec{x}$ and calculates the by the controller used error terms in $\vec{x}_{norm}$.

From the position of an external observer, only the vehicle movement could be measured, e.g., the lateral lane deviation and yaw-rate errors. Unfortunately, there is no insight into the control loop. The algorithmic used for the controllers, the precision of the sensing units, the share inputs of the controllers, and some vehicle quantities are unknown. Due to these uncertainties, a detailed description of the lateral control law, like for longitudinal vehicle dynamics, is not possible in this research. Nevertheless, by observing the vehicle movement in defined situations, the parameter y_{off} can be estimated. It should be noted at this point that the evaluation of the lateral vehicle movement needs more insight in the control loop as well as comprehensive measurements on the vehicle outputs and the position estimation within its lane. Therefore, the evaluation of lateral automated driving is phenomena orientated. This phenomenon orientated approach allows the derivation of the parameter y_{off} from real driving tests.

[6] For a specified vehicle-dependent speed, this is possible but will be not considered

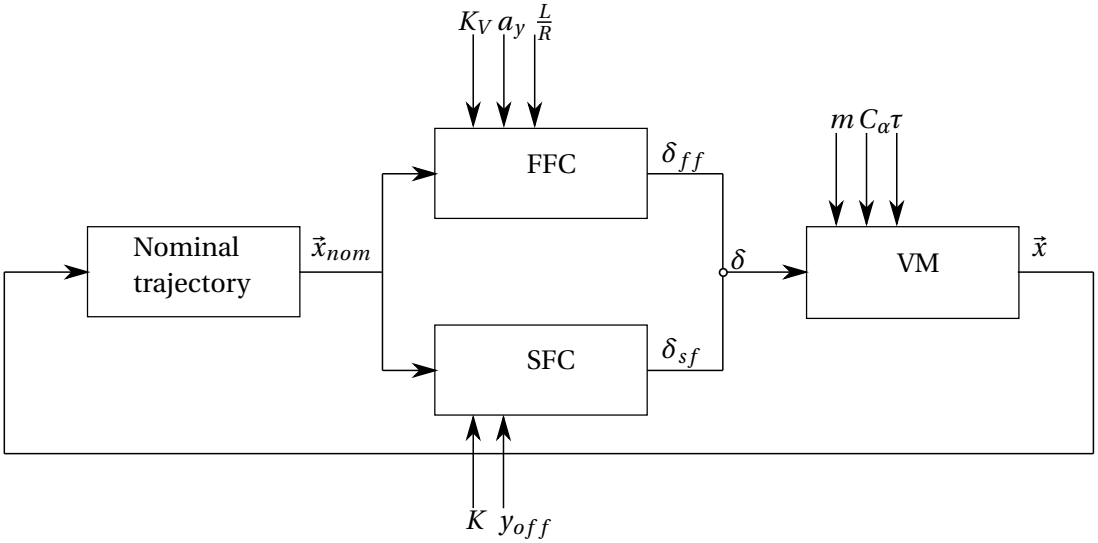

Figure 3.9: Block diagram LCA controller

3.2.4. LCA systems and their impact on traffic

For human-operated vehicles without any assistance, the driver collects information about the surrounding infrastructure and other road participants to fulfil the driving task [20]. The driver can rely on rule-, skill-, and knowledge-based techniques to estimate the best interaction with the vehicle for different driving situations [87]. However, the surrounding vehicles play a significant role in the driving capacity of humans [86]. In particular, the lateral lane deviation of the surrounding vehicles leads to a situation assessment, which results in the driver maintaining greater distances. Mullakkal-Babu et al. [71] assessed the use of safety indicators for vehicle trajectories on highways. Lateral safety indicators are used for the risk measure in lane change controllers and lane-keeping systems for the safety assessment of lateral vehicle driving manoeuvres [64]. Mullakkal-Babu et al. stated that the vehicle's lateral position in its lane influences the safety indicator and, therefore, the behaviour of successors.

AVs estimate the states and the movement of the surrounding vehicles [117]. To guarantee safe driving in dynamic traffic, automated vehicles have to be able to anticipate the surrounding traffic in the near future and respond to these estimations appropriately. Methods to predict surrounding vehicles trajectory are presented by Xin et al. [117] and by [53] as well as from [3]. However, all these models can be improved by feedback of test data for lateral vehicle movement to enhance the quality of prediction. Moreover, better prediction leads to a more precise vehicle guidance for longitudinal movement because of the omission of unclear situation, causing heavy brake, steering, or throttle interventions by the system.

3.3. Summary and degrees of freedom

The controlling and driving dynamic concepts introduced in this chapter should gain insight in automated driving and derive SRQ2 and SRQ3.

The vehicle dynamics for automated longitudinal driving could be described by the state vectors, containing acceleration, velocity, and distance of two vehicles following each other. The time-headway proved to be an appropriate value for linking the state vector variables and making situations comparable. Therefore, the vehicle velocity and the inter-vehicle headway are essential values. For unaccelerated driving, the time-headway can be used to describe the distance between the vehicles relative to their leader. The control variable τ_h can be esti-

mated by evaluating the time-headways of FOTs. For accelerated driving, overshoot and settling time of the following vehicle velocity can be used to describe the dynamics. A simplified second-order response model was derived from the equation of motion that describes the following vehicle's movement respecting the accelerating motion of its leader. The parameters of this model can be estimated by evaluating experimental data. Therefore, the dynamic model parameters θ and ω_n can be used to describe the vehicle's behaviour. For deceleration manoeuvres, the additional use of further poles and zeros for transfer function estimation was introduced. Furthermore, the transfer functions derived from the experiments can be used to compare data-sets in the time or frequency domain.

For automated lateral vehicle control, the yaw-rate $\dot{\psi}$, the deviation around the lane centre y, and the steering angle δ are identified as descriptive for the lateral movement of the vehicle in its lane. For the measurement of δ, the test vehicle has to be equipped with additional measurement equipment. The used data-sets do not contain this information. Due to the unknown system architecture and inputs, an approach is used that is focusing on the phenomena caused by the LCA systems. Analysing a system response, like for longitudinal car-following, is not suitable. Nevertheless, the independent parameter y_{off} can be derived from experimental data to gain insights into the LCA system

The control systems presented here are used because they provide a simple approach and sufficient system insight for the use in this thesis. For ACC systems, there are various other approaches, such as the VTG spacing policy [26]. However, the aim of this research is not to develop a new spacing policy. CTG and VTG spacing policy share the approach that not space-headway, but time-headway is the systems target size. Therefore, essential system inputs such as time-gap adjustment and dynamic quantifiers are suitable to derive basic knowledge about the longitudinal motion of the vehicle, regardless of the control approach followed.

For lateral vehicle control, various approaches for the controller design were introduced as well. Extended to the feed-forward controller discussed in this research, more advanced control approaches using system identification or trajectory prediction were developed by [14] and [52]. However, since the described simple feed-forward controller has several system inputs and the measurement of the system response is very cost-intensive and was not carried out in the experiment under consideration, we follow the approach of concentrating on the phenomena caused by the system rather than on the precise system inputs and outputs. The results can, therefore, also be transferred to other control strategies.

4

Methodology

With regard to the research sub-questions SRQ4 (What is the impact of different driving manoeuvres on the movement of the vehicle?) and SRQ5 (How does the vehicle drive interacting with various infrastructure?) of this thesis, this chapter introduces the methodology which is used to answer them in the next chapter. As shown in the previous chapter, the theoretical description of automated vehicle dynamics has specific inputs that are unknown, and it is expected that these input parameters will differ between vehicles, derivatives, and brands and, therefore, between the data-sets used in this research. This chapter aims to identify driving manoeuvres in existing data-sets suitable for an estimation of the input parameters. The described methodology is followed to identify capable sequences in all used data-sets to evaluate. In the following, a sequence or a situation describes a period within the data-set that meets specific requirements. The distinction between lateral and longitudinal vehicle movement introduced earlier in this research is maintained, due to the unique content of data-sets describing either lateral or longitudinal vehicle motion.

In order to evaluate the longitudinal dynamics of vehicles, uniform definitions of the driving situations are firstly presented for evaluation purposes. These definitions are applied to the used data-sets to identify comparable situations between them. Subsequently, this chapter describes the evaluation of the found sequences to find the already presented dependent quantities of the vehicle movement models.
Finally, this chapter introduces a method to classify curves using the lateral-acceleration and a map-matching algorithm to generate ground truth for lateral vehicle movement. Afterwards, this chapter describes the necessary steps to evaluate the vehicle's position in its lane for driving through different infrastructures.

4.1. Longitudinal vehicle dynamics

This section describes the synthesis of data sequences out of the data-sets with ACC or CACC use. The longitudinal vehicle movement is divided in *stable*, *sustained stable*, *accelerated* and *decelerated* car-following. From now on, we will use italics when talking about the defined driving situations. A presentation of this classification is shown in Figure 4.1. The area *Data-Set* represents the whole data-set, including human driving interventions, emergency braking, and vehicles cutting in the platoon. Subset *Stable* contains situations in which the acceleration of the considered vehicle is in between a certain acceleration limit, and the ACC system is in control of the vehicles longitudinal movement. The acceleration boundaries used are defined in Subsection 4.1.1. The subset *Sustained Stable* contains situations in which

the acceleration and speed of the flowing and target vehicle meet certain requirements for a defined period, given in Subsection 4.1.2. Subset *Accelerated Driving* contains situations in which the ACC system is activated, and the vehicle is thus accelerating, Subsection 4.1.3[1]. The last subset *Acceleration manoeuvre* consists of situations where the target vehicle performs a specified acceleration or deceleration manoeuvre, defined in Subsection 4.1.4.

This hierarchical definition makes it possible to conclude from general to specific driving situations and allows comparisons with existing research. In addition, the more restrictive definitions of *accelerated* and *stable* car-following situations, represented by the subsets *Sustained Stable* or *Acceleration manoeuvre* in Figure 4.1, allow novel possibilities for evaluations to gain a deeper understanding of the longitudinal vehicle movement by matching the velocities of the two vehicles by transfer functions or consider the time-headway under different velocities. The subsets *Accelerated Driving* and *Stable* car-following do not have intersections and are used for the evaluation of time-headways. The subset *Acceleration manoeuvre* is used for the estimation of transfer functions and not for the evaluation of time-headways. This sharp division cuts out the double use of data.

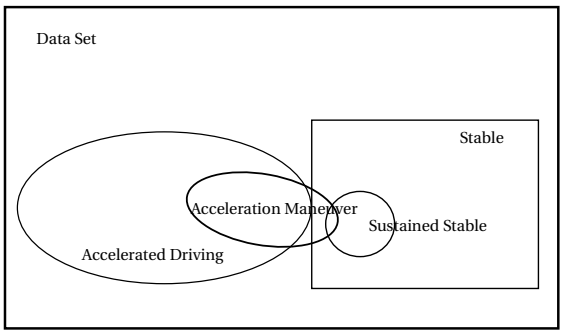

Figure 4.1: Different quantities in a data-set

As noted in Section 3.1 and presented in Figure 3.4, *stable* car-following can be described by the time-headway spacing parameter τ_h, which sets the time-gap between the following and the target vehicle. Therefore, sequences that could be claimed as *stable* or *sustained stable* car-following are suitable to derive this parameter. Acceleration manoeuvres can derive the parameters θ and ω_n as described in Section 3.1.

A schematic representation of the data processing followed in this research is shown in Figure 4.2. The figure shows the necessary steps and the order to be followed to get from the raw data to a summarized evaluation of comparable driving situations. The steps to be performed during data evaluation are as follows.

- Structure
- Find patterns
- Pattern processing
- Evaluate

In the task *Structure*, different data-sets are made comparable by transforming them into a similar data structure, for shared evaluation code use. This procedure is used as well for

[1] For decelerated car-following the same approach is used but has been omitted here for the sake of clarity

filtering and outlier removal. Afterwards, patterns for *stable* and *accelerated* car-following are identified in procedure *Find patterns*. These steps are described in Subsection 4.1.2 for *stable* and 4.1.4 for *accelerated* car-following. The task *Pattern processing* describes how the found patterns are further processed. Finally, the found segments are evaluated under the same circumstances in procedure *Evaluate*. The methods used are presented in this chapter, the comparative evaluation, and a comparison between the data-sets is the subject of Chapter 5.

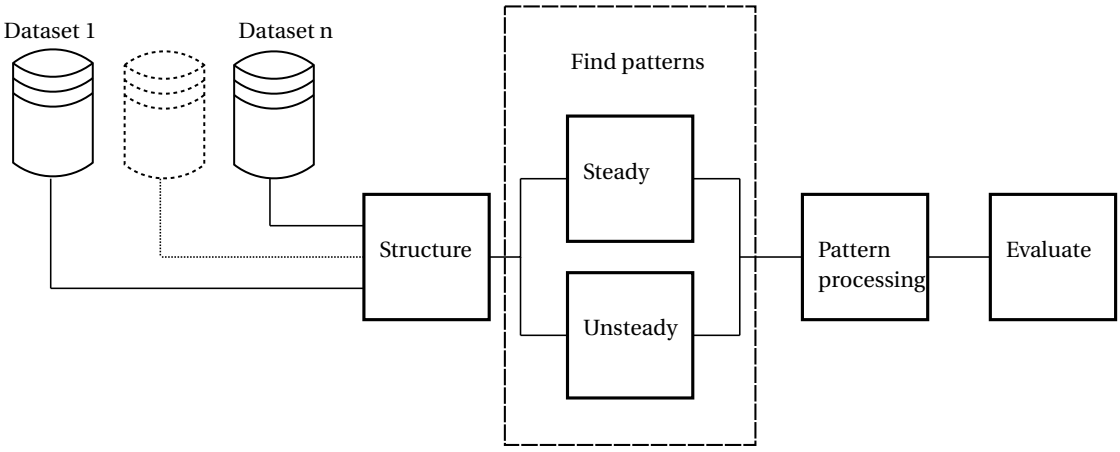

Figure 4.2: Processing longitudinal vehicle dynamics

4.1.1. Stable car-following under ACC/CACC control

The in this research used definition for *stable* car-following is that the acceleration and deceleration of the following vehicle remains within the bandwidth of $0.5^{m}/_{s^2}$ to $-0.5^{m}/_{s^2}$. This definition is used in [11]. The evaluation of *stable* car-following segments is carried out in the same way as the evaluation of *sustained stable* car-following segments, which is described in the following paragraph. The time headways for *stable* car-following are evaluated with histograms subsequently.

4.1.2. Sustained stable car-following under ACC/CACC control

For the evaluation of *sustained stable* car-following with ACC/CACC system use, firstly a rule is designed when a situation inside the data is defined as *sustained stable* car-following. We use the following definition and comply with the guidelines from [62] and [11]. Let $v_i(t)$ be the velocity of the following vehicle and $v_{i-1}(t)$ the velocity of the leader. Henceforth, a situation of *sustained stable* car-following is given if the speed of the successor vehicle and the leading vehicle is according to the following conditions.

(i)
$$|v_{i-1}(t+n) - v_{i-1}(t)| \leq \Delta V, \quad \forall n\{n \in \mathrm{N} | n \leq 20\} \quad \Delta V = 0.75\frac{m}{s}$$

(ii)
$$v_{i-1}(t) \geq V_{min}, \quad V_{min} = 10\frac{m}{s}$$

(iii)
$$|{}^{d}/_{dt}\, v_{i-1}(t+n)| \leq a_{max}, \quad \forall n\{n \in \mathrm{N} | n \leq 20\} \quad a_{max} = 0.5\frac{m}{s^2}$$

(iv)
$$|v_{i-1}(t+n) - v_i(t)| \leq \Delta V_1, \quad \forall n\{n \in \mathrm{N} | n \leq 20\} \quad 1.5\frac{m}{s} \quad \Delta V_1 = 1.5\frac{m}{s}$$

The variable t represents an independent time in the data, while n is the time horizon in seconds. Condition (i) defines the minimum length of a *sustained stable* car-following sequence and the maximum change of velocity starting from the first assumed element. Condition (ii) filters out data points when the vehicle velocity is under the set velocity threshold since ACC/CACC systems, in general, can only be activated at a minimum velocity. Condition (iii) excludes situations with abrupt acceleration starting from the first assumed element. Condition (iv) defines the maximum difference in the velocities of the following and the leading vehicle regarding [28]. In data-sets where the vehicles ACC assistant state is specified inside the data, e.g., ACC is activated or not. This information is taken additionally into account. Situations that meet the given definition without the active assistance system are not considered. In case the data specifies the target vehicle, it is essential that the leading vehicle is part of the experiment and no other vehicles are cutting in.
Figure 4.3 presents a data sample from the North-Holland experiment data-set (Appendix A). Noticeable is that there are nine segments where the prior given definition does apply to. These segments are marked green. The found segments are visually checked for correctness by the author for all experiments. All n found data segments out of the p-th trace are stored in matrices $\mathbf{X}_{m,p}$ with $m \in \{1,2,...,n\}$ containing all information provided by the on board sensors of the vehicles as vectors $\mathbf{X}_{m,p} = [\vec{a}_{m,i}\ \vec{v}_{m,i}\ \vec{h}_{m,i}\ \vec{a}_{m,i-1}\ \vec{v}_{m,i-1}\ \vec{h}_{m,i-1}]^T$. With $\vec{h}$ the space-headway to the vehicle driving ahead.

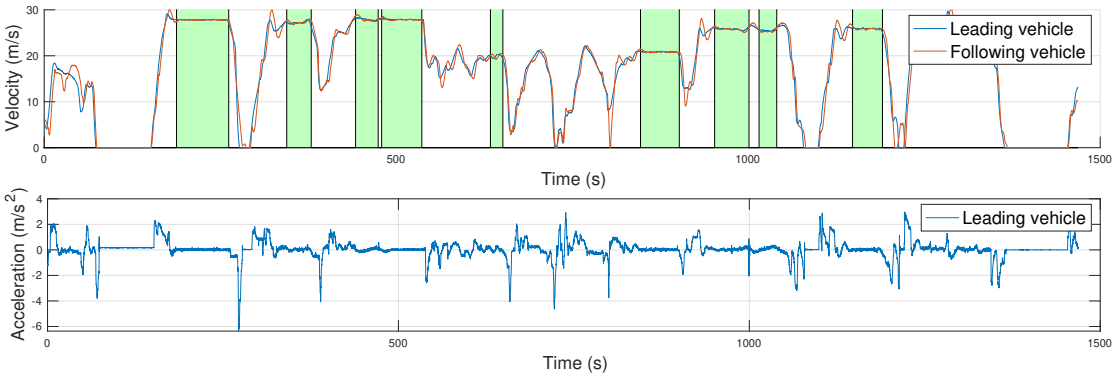

Figure 4.3: Sustained stable car-following under ACC use

The entirety of the found segments is evaluated with different graphs. Firstly, all segments $\mathbf{X}_{m,p}$ are drawn in a space-headway (m) - velocity (m/s) plot in order to get an overview of the driven speeds and the given space-headway. For a situation identified as *sustained stable* car-following, the average velocity of the segment is calculated, and all values of the space-headway are drawn for this average value in a space-headway (m) - velocity (m/s) graph. Since the applied definition of *sustained stable* car-following restrict the deviation of velocity for a segment, condition (i), the velocity error for every segment of the leading vehicle is smaller than $\pm 0,75^{m}/_{s}$.

Secondly, the time-headways are presented in a histogram to determine the parameter τ_h according to the frequency of its occurrence. To determine differences in the value of τ_h for different velocities, a velocity dependent breakdown of the found segments is carried out in the following chapter. This help to identify differences in the time-headway and its distribution for different speeds. Splitting the range of velocity in three equal parts for every regarded experiment. Let $\vec{v}_{m,i-1}$ be the velocity data of the leading vehicle out of a segment that fulfils the definition of *sustained stable* car-following. The velocity intervals are defined as follows $I_{slow} = [min\{\vec{v}_{m,i-1}\}, min\{\vec{v}_{m,i-1}\}+\Delta)$, $I_{medium} = (min\{\vec{v}_{m,i-1}\}+\Delta, max\{\vec{v}_{m,i-1}\}-\Delta)$ and $I_{high} = (max\{\vec{v}_{m,i-1}\}-\Delta, max\{\vec{v}_{m,i-1}\}]$. With Δ the step size defied as

$$\Delta = \frac{max\{\vec{v}_{m,i-1}\} - min\{\vec{v}_{m,i-1}\}}{3}.$$

As the last step of the *sustained stable* car-following evaluation, the containing frequencies in the time and space-headway around the mid-range are considered. Since the ACC/CACC system controls the vehicle acceleration, oscillations around the median values for space-headway h_i appear because the headway is the target value of the controller [85]. This behaviour is observed during the previous evaluation of segments of *sustained stable* car-following. As already mentioned, ACC systems tend to amplify speed disturbances. The estimation of the frequencies contained in the space-headway signal should help to decide whether these occurring frequencies can be considered as input disturbances for the following vehicles. To extract the oscillation frequencies around the average space-headway, an Fast Fourier Transformation (FFT) is used.

Let $h_i(t)$ be the space-headway between the i and the $i-1$ vehicle in meter out of $\mathbf{X}_{m,i}$ for a found segment of *sustained stable* car-following. The space-headway is normalized to its average value.

$$h_{iNorm}(t) = h_i(t) - \emptyset h_i(t) \tag{4.1}$$

To avoid the influence of the FFT by the initial headway $h_i(0)$ biased by previous acceleration manoeuvres the start time t_{start} for the FFT has to be adjusted. The start time is set to the first change of sign of $h_{iNorm}(t)$. Therefore t_{start} is defined as the minimum time index for the first sign change

$$t_{start} = min\{t_{pm}, t_{mp}\}. \tag{4.2}$$

With the following definitions for the times of the first change of sign from plus to minus t_{pm} and minus to plus t_{mp}. The variable e is the smallest time step represented in the data, assuming that the experiment is recorded with 10 Hz. e corresponds to 0.1 seconds.

$$\{t_{pm} \in Q | sgn(h_{iNorm}(t)) = 0, sgn(h_{iNorm}(t+e)) = 1\} \tag{4.3}$$

$$\{t_{mp} \in Q | sgn(h_{iNorm}(t)) = 1, sgn(h_{iNorm}(t+e)) = 0\} \tag{4.4}$$

The FFT is carried out with every data segment in $\mathbf{X}_{m,p}$ from the start time t_{start} to the end of the sequence. Figure 4.4 represents the evaluation of a found segment in the North-Holland experiment data-set A. The upper graph shows the normalized space-headway, equation (4.1), for a time-span of 13 seconds. The lower graph illustrates the frequency spectrum of the upper printed signal derived by a FFT. A peak in the frequency spectrum at ≈ 0.1 Hz is clearly visible. All smaller deflections are due to noise in the space-headway signal and of no interest for further evaluation.

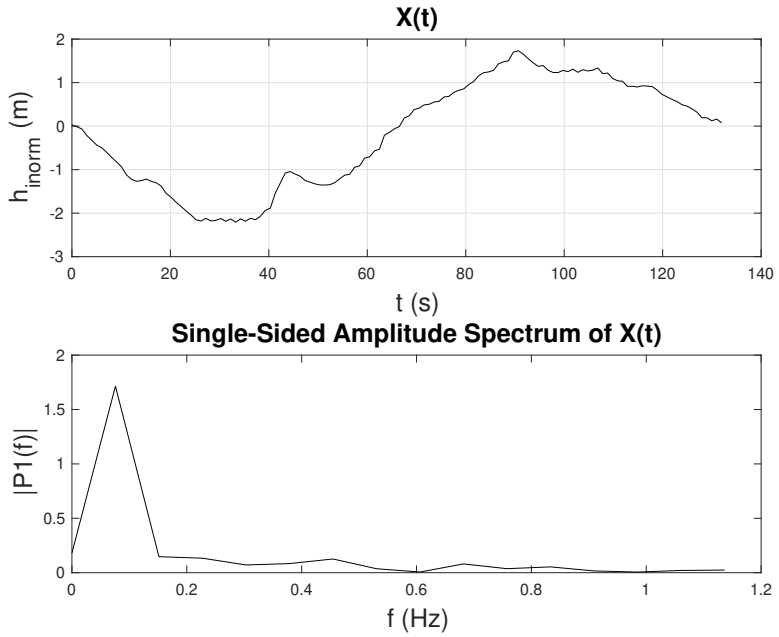

Figure 4.4: Frequency spectrum of space-headway signal

4.1.3. Acceleration and deceleration under ACC control

Acceleration situations are defined in this thesis when the acceleration of the following vehicle is above $0.5^{m}/_{s^2}$. The ACC/CACC system has to be activated. This definition is used with regards to [11]. Deceleration situations are defined when the following vehicle's acceleration undercuts $-0.5^{m}/_{s^2}$. The time headways for accelerated and decelerated vehicle following are evaluated with histograms subsequently.

4.1.4. Accelerating and decelerating manoeuvres under ACC/CACC control

For the description of driving manoeuvres in which the vehicle is accelerating, a strict definition of the manoeuvres must be used to find comparable situations, as there is an infinite number of acceleration situations in the data. In contrast to *sustained stable* car-following, where only a limitation of the acceleration of the leading vehicle in a certain time is used, the shape of the driven velocity ramp of the leader has to be specified for accelerating driving manoeuvres. The classification of acceleration and deceleration manoeuvres is considered separately, due to the large differences in the occurring speed changes for acceleration and deceleration in the data. We follow the definitions of acceleration manoeuvres in [68], [69] and [36] to identify comparable acceleration manoeuvres in this research.

Acceleration manoeuvres:
The following definition is used to find standardized acceleration manoeuvres inside the data.

(i)
$$\int_{t}^{t+20} a_{i-1}(t)\,dt \geq \Delta V_{min}, \quad \Delta V_{min} = 10\frac{m}{s}$$

(ii)
$$\int_{t+20}^{t+40} a_{i-1}(t)\,dt \leq \epsilon_v, \quad \epsilon_v = 2\frac{m}{s}$$

(iii)

$$|\frac{d}{dt}v_{i-1}(t+n)| \leq \epsilon_a, \quad \forall n\{n \in \mathrm{N}|20 \leq n \leq 40\} \quad \epsilon_a = 0,5\frac{m}{s^2}$$

(iv)

$$v_i(t+n) - \frac{1}{20}\int_{t+20}^{t+40} a_{i-1}(t)dt \leq \epsilon_{v1} \quad \forall n\{n \in \mathrm{N}|20 \leq n \leq 40\} \quad \epsilon_{v1} = 0,5\frac{m}{s}$$

Condition (i) is used to search for situations where the velocity is rising over a specified level in a time of 20 seconds. Condition (ii) defines the stable driving phase immediately after the acceleration phase. Condition (iii) limits the maximum acceleration in the stable driving phase after accelerating, regarding the definition of steady driving. Condition (iv) ensures that the velocities of boot vehicles are sufficiently equal in the stable driving phase after accelerating. In data-sets where the vehicles ACC state is specified inside the data, e.g., ACC/CACC is activated or not. This information is introduced as an additional condition. Sequences that meet the previously given definition without an activated assistance system are not considered. In case the data specifies the target vehicle we do also pay attention that the leading vehicle is part of the experiment and no other vehicle cutting in.

Figure 4.5 presents data out of the North-Holland experiment data-set (Appendix A). In the green area marks segments inside the data that meet the above-given definition of acceleration manoeuvres under ACC use. When comparing Figure 4.5 with Figure 4.3, it is noticeable that there are fewer situations in which the conditions for the acceleration manoeuvre apply than for steady car-following. Besides that, not all shown acceleration manoeuvres in the data do apply the given definition. Especially the downstream phase with constant travel velocity of the leading vehicle, proposed by condition (iv), cannot be satisfied in several cases.

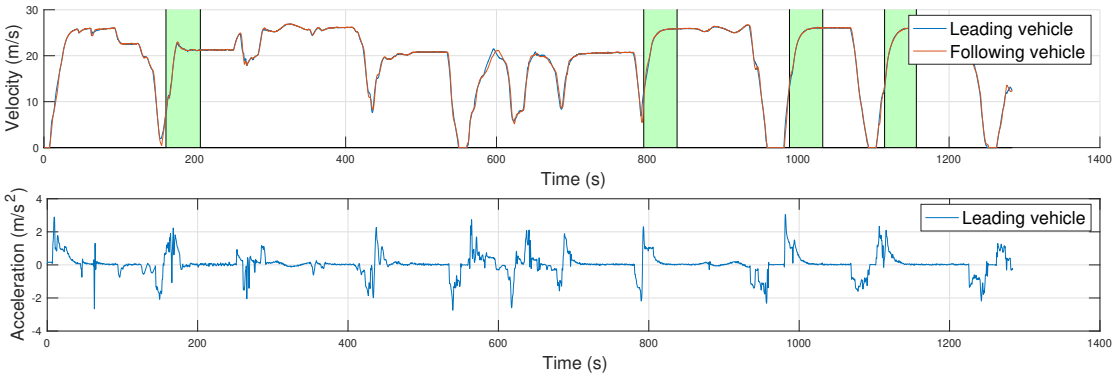

Figure 4.5: Accelerated car-following under ACC use

The segments found are checked visually and stored in indexed matrices, which contain information about the followers' and leaders' velocity, the acceleration, and the space and time-headway between the two vehicles.

As the acceleration segments are identified, the following parameters are introduced to describe the phenomena caused by the acceleration manoeuvres, as shown in Table 4.1. Since the relationship between acceleration manoeuvres using a ACC system and analogous transfer functions was introduced in the Section 3, the following terms are used to describe phenomena caused by the acceleration manoeuvre.

Table 4.1: Parameter definition for acceleration manoeuvre

Formula symbol	Description	Unit
$\hat{v}$	Velocity overshoot between leader and follower	$^m/_s$
T_{SH}	Settling time for time-headway	s
$\hat{h}$	Time-headway inertial error	m
Δt_{vh}	Time difference between $\hat{v}$ and time-headway minimum	s

For the sake of clarity, Figure 4.6 shows a graphic illustration of the introduced parameters in Table 4.1. Parameter $\hat{v}$ describes the velocity overshoot of the following vehicles concerning the mean speed of the leading vehicle in the stable driving phase. T_{SH} specifies the required time for the headway to fall back to a constant value in between a boundary of $0.05s$. The parameter $\hat{h}$ is the initial error for the time-headway, so the time difference between the initial and the mean value in the stable driving phase. Parameter Δt_{vh} is the time between the velocity overshoot and the resulting minimum time-headway between the vehicles. In addition, the evaluation shows the order of the system response for velocity and time-headway. In Figure 4.6, a second-order response for the following vehicle velocity is present, due to the overshoot over the leader's constant velocity. For the time-headway also a second-order system response is present. Starting at the end of the acceleration manoeuvre of the leading vehicle, the time-headway falls below the average value for the stable car-following segment, last third of the graph, and then slowly approaches it from a lower level. A red marking indicates the peak of the undershoot.

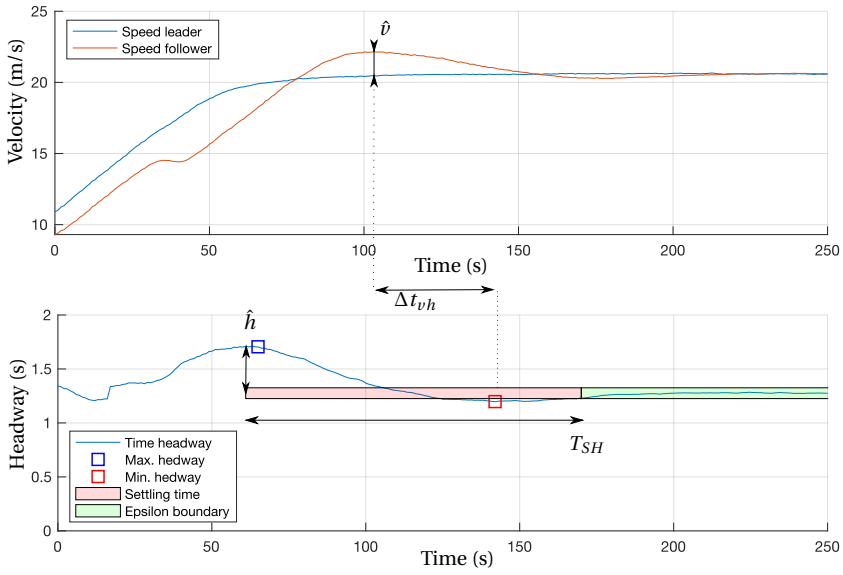

Figure 4.6: Definition of dynamic parameters

In addition to the descriptive evaluation of phenomena caused by acceleration manoeuvres, the transfer function of the Single Input Single Output (SISO) system, taking the vehicle velocities into account, is estimated. The systems transfer function is given as

$$G_i(s) = \frac{\mathbf{X}_i}{\mathbf{X}_{i-1}}. \tag{4.5}$$

Where $\mathbf{X}_i$ and $\mathbf{X}_{i-1}$ are defined as the vehicle outputs, in the considered case, the velocities. The System Identification Toolbox provided by MATLAB is used to obtain the second-order transfer functions $G_i(s)$ in the frequency domain. In Figure 4.6, a second-order system response without static gain is shown, as the efforts in Chapter 3 have already indicated. This choice is on account of the following vehicle overshooting the velocity of the leader after the leader's velocity already settles down to a constant value. This typical second-order system response was also observed by [68] and [69] for acceleration manoeuvres. The System Identification Toolbox permits a whole variety of possible transfer functions. The chosen transfer function representing the behaviour of the vehicle was selected as a compromise between simplicity, because of the second-order model, and accuracy. The second-order transfer functions with time delay are identified out of the found data sequences with the following form

$$G_i(s) = \frac{k}{s^2 + 2\theta\omega_n s + \omega_n^2} e^{-T_d s}. \tag{4.6}$$

Where k is the static gain, θ damping factor, ω_n natural frequency, and T_d the time delay. This transfer function has two poles and no zeros.

In total, one transfer function is generated for every found segment of data, which means that the number of transfer functions equals the total number of segments. Step inputs assess all estimated transfer functions and their behaviour in the frequency domain is studied for evaluation purposes.

Deceleration manoeuvres:
Usable deceleration manoeuvres appear less frequently in contrast to acceleration manoeuvres in the data. The change of the road speed limit from a higher to a lower value along a street does not lead to an instant deceleration or breaking of a leading vehicle. Moreover, sharp deceleration manoeuvres appear when approaching a traffic light that turns red or shows red already. For most experiments, it turned out that in these situations, the observing test driver takes over the control from the system. Besides that, deceleration to a standstill is not suitable when performing the prior mentioned evaluation for accelerating vehicle movement. Overshoots in velocity cannot appear while time-headways between vehicles reaching infinity. For this purpose, the data-sets are searched for deceleration manoeuvres for which the following definitions apply. Take note that the velocity deltas are smaller than for the acceleration manoeuvres defined above.

(i)
$$\int_t^{t+8} a_{i-1}(t)\,dt \leq \Delta V_{deacc}, \quad \Delta V_{deacc} = -2\frac{m}{s}$$

(ii)
$$\int_{t+13}^{t+25} a_{i-1}(t)\,dt \leq \Delta V_{stead}, \quad \Delta V_{stead} = 1\frac{m}{s}$$

(iii)
$$|\frac{d}{dt} v_{i-1}(t+n)| \leq a_{max}, \quad \forall n\{n \in \mathrm{N} | 13 \leq n \leq 25\} \quad a_{max} = 0.25\frac{m}{s^2}$$

(iv)
$$v_i(t+n) - \frac{1}{20}\int_{t+20}^{t+30} a_{i-1}(t)\,dt \leq v_{max}, \quad \forall n\{n \in \mathrm{N} | 20 \leq n \leq 30\} \quad v_{max} = 0.25\frac{m}{s}$$

The requested velocity delta of $2^{m}/_{s}$ is due to the fact that this research wants to consider changes in the set speed and not emergency braking situations. Because of the manoeuvres included in the data-sets, only the evaluation of slight declaration manoeuvres can be done. Condition (i) is used to search for situations where the velocity is reducing under a specified level in a specific time of 8 seconds. Condition (ii) defines the stable driving phase immediately after the acceleration phase. Condition (iii) limits the maximum acceleration in the stable driving phase after accelerating, regarding the definition of steady driving. Condition (iv) ensures that the velocities of both vehicles are sufficiently equal in the stable driving phase after accelerating. Figure 4.7 presents data out of the Southwest experiment. The above-given definition applies to the red coloured areas.

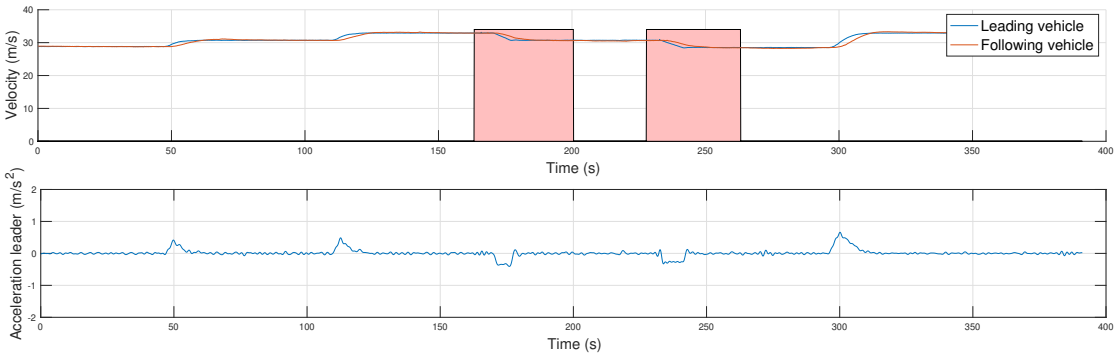

Figure 4.7: Decelerating under ACC use

As Chapter 5 will show, the dynamic reactions of the following vehicle to deceleration manoeuvres are faster than for acceleration manoeuvres. In order to estimate transfer functions with suitable fitting accuracy, additional poles and zeros must be inserted into the transfer functions. The system responses between the individual experiments are therefore more different than for acceleration manoeuvres. Thus, a description of the phenomena caused by the deceleration manoeuvres is not given as it is done for the acceleration manoeuvres. Instead, the estimated transfer functions from the different data-sets are compared.

4.2. Lateral vehicle dynamics

In the previous section, the vehicle's velocity and the inter-vehicle distance are used to describe the vehicle's dynamics. When driving through different road geometries, e.g., curves of different curvature, an additional variable must be introduced for the considered geometry to adapt to different infrastructures and make data comparable. The speed of the vehicle alone is not sufficient for this. In Chapter 3, the validity of the lateral acceleration to link velocity and curve radius has been presented. Hereinafter the lateral acceleration will be used to compare the lateral vehicle movement while curving around.

Since the lateral acceleration measurements in the regarded data are unsuitable for detailed evaluation, due to high noise, changing position of the sensor in the vehicle, and change of orientation of the sensor, the vehicle lateral acceleration has to be calculated differently. For the evaluation, an acceleration estimation algorithm is introduced, which uses map matching to determine the curve radius and combines the measured vehicle speed to deliver the lateral acceleration.

A prior approach by Carlson et al. [13] uses GPS, and differential wheel speeds of a vehicle and Kalman filtering to derive a stable yaw-rate[2] measurement. Because of the absence of odometry data in the considered data-set, a different approach using GPS positioning and velocity is followed. The simultaneous use of GPS positioning and velocity data makes the generation of ground truth indispensable to cut out stochastic and system-based biases [67]. The approach uses the following nomenclature presented in equation (4.7). *Origin* describes the origin of the data, for example, from the GPS measurement or road map data sources. *System* specifies the coordinate system the data is given in. This subsection will distinguish between the geographical coordinate system P, using latitude and longitude, and introduce a Cartesian coordinate system I and its geometric transformation K. The small set suffix n indexes the measuring point in the data.

$$ {}^{Origin}_{System}\boldsymbol{\chi}_n \tag{4.7} $$

4.2.1. Map matching algorithm

The on-board Global Positioning System (GPS) measurement shows high noise and fluctuations when projecting the data on an open street map. The measuring points scatter randomly around the driven road with no predictable error. When connecting the measured data points with lines, no steady spline is generated. Instead, this procedure leads to sharp turns of the recorded vehicle trajectory, which is inadmissible for evaluation. To match the measured data points to the real driven road and to generate ground-truth the following approach for a simple map matching algorithm is used.

Let ${}^{GPS}_{P}\vec{\mathbf{x}} = [{}^{GPS}_{P}x_1\ {}^{GPS}_{P}x_2 \cdots {}^{GPS}_{P}x_N]^T$ and ${}^{GPS}_{P}\vec{\mathbf{y}} = [{}^{GPS}_{P}y_1\ {}^{GPS}_{P}y_2 \cdots {}^{GPS}_{P}y_N]^T$ be the measured GPS coordinates for the longitudinal and latitudinal position on the globe. Furthermore, let ${}^{RN}_{P}\vec{\mathbf{x}} = [{}^{RN}_{P}x_1\ {}^{RN}_{P}x_2 \cdots {}^{RN}_{P}x_M]^T$ and ${}^{RN}_{P}\vec{\mathbf{y}} = [{}^{RN}_{P}y_1\ {}^{RN}_{P}y_2 \cdots {}^{RN}_{P}y_M]^T$ be the longitudinal and latitudinal points for the regarded road network infrastructure from an open street map shape-file. Only necessary primary, secondary, and tertiary types of roads are taken into account. For a driven road segment in the experiments, the number of measured GPS data points is larger than the number of data points in the open road map source, therefore $N > M$. The open street map data does not show many data points in these segments due to interpolation for straight road sections or curves of a constant curve radius. To match all measured points ${}^{GPS}_{P}\vec{\mathbf{x}}$ and ${}^{GPS}_{P}\vec{\mathbf{y}}$ to points represented in the road network ${}^{RN}_{P}\vec{\mathbf{x}}$ and ${}^{RN}_{P}\vec{\mathbf{y}}$ the zones in which few data points lie must be refined. We refine the vectors ${}^{RN}_{P}\vec{\mathbf{x}}$ and ${}^{RN}_{P}\vec{\mathbf{y}}$ linear by factor 100 which causes $N \ll M$.
For any given point ${}^{GPS}_{P}P_n$ with $({}^{GPS}_{P}x_n, {}^{GPS}_{P}y_n)$, where $n \in [1, N]$, out of the GPS measurement we define $\vec{\mathbf{e}}_n$ as the vector of position error as follows.

$$ \vec{\mathbf{e}}_n = \begin{bmatrix} e_1 \\ e_2 \\ \vdots \\ e_M \end{bmatrix} = \begin{bmatrix} \| {}^{GPS}_{P}P_n - {}^{RN}_{P}P_1 \|_2 \\ \| {}^{GPS}_{P}P_n - {}^{RN}_{P}P_2 \|_2 \\ \vdots \\ \| {}^{GPS}_{P}P_n - {}^{RN}_{P}P_M \|_2 \end{bmatrix} = \begin{bmatrix} \sqrt{({}^{GPS}_{P}x_n - {}^{RN}_{P}x_1)^2 + ({}^{GPS}_{P}y_n - {}^{RN}_{P}y_1)^2} \\ \sqrt{({}^{GPS}_{P}x_n - {}^{RN}_{P}x_2)^2 + ({}^{GPS}_{P}y_n - {}^{RN}_{P}y_2)^2} \\ \vdots \\ \sqrt{({}^{GPS}_{P}x_n - {}^{RN}_{P}x_M)^2 + ({}^{GPS}_{P}y_n - {}^{RN}_{P}y_M)^2} \end{bmatrix} \tag{4.8} $$

In other words $\vec{\mathbf{e}}_n$ is the $\mathbb{R}^{M\times 1}$ vector with entries that represent the Euclid norm for the tuple $({}^{GPS}_{P}x_n, {}^{GPS}_{P}y_n)$ to any other given point ${}^{RN}_{P}P_m$ with $({}^{RN}_{P}x_m, {}^{RN}_{P}y_m)$ in the street map data base.

[2] Yaw rate and lateral acceleration are related variables

Let $e_{i,n}$ be the smallest element in $\vec{\mathbf{e}}_n$ so that $min\{\vec{\mathbf{e}}_n\} = e_{i,n}$ with $i \in \mathbb{N}$. The best matching point in a given road network for a given tuple of GPS measurement $({}^{GPS}_{P}x_n, {}^{GPS}_{P}y_n)$ is the tuple $({}^{RN}_{P}x_i, {}^{RN}_{P}y_i)$. This derives a new map matched position vector which is used hereinafter.

$$[{}^{MM}_{P}\vec{\mathbf{x}} \quad {}^{MM}_{P}\vec{\mathbf{y}}] = \begin{bmatrix} {}^{RN}_{P}x_{i,1} & {}^{RN}_{P}y_{i,1} \\ {}^{RN}_{P}x_{i,2} & {}^{RN}_{P}y_{i,2} \\ \vdots & \vdots \\ {}^{RN}_{P}x_{i,N} & {}^{RN}_{P}y_{i,N} \end{bmatrix} \tag{4.9}$$

Figure 4.8 gives a visual representation of the map matching procedure. Figure 4.8a shows the imported road network for the city of Amsterdam. The considered experiment was carried out in this area. The blue lines represent all roads in the network. The cyan coloured represents the primary, secondary and tertiary roads that are crucial for the evaluation. Figure 4.8b shows how the algorithm matches GPS measurement points on the existing refined road network.

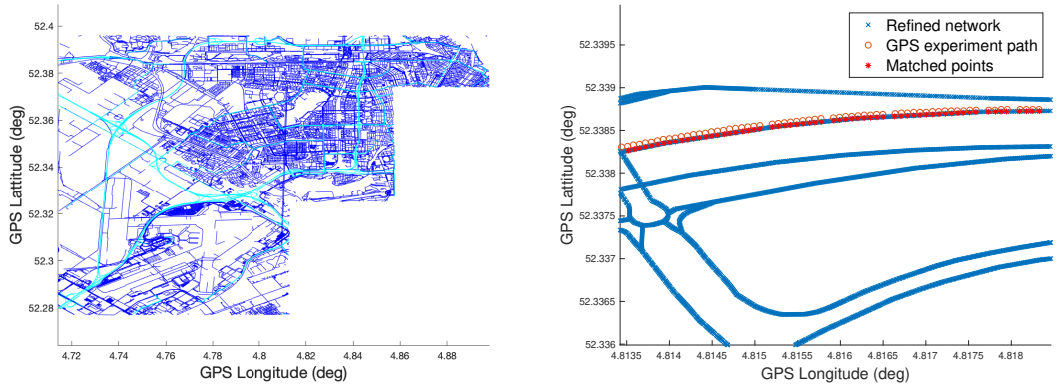

(a) Road network of Amsterdam

(b) Matched GPS points

Figure 4.8: Map matching procedure

4.2.2. Curve radius estimation

Although open street map data derives high accuracy and rich data, it provides no information about the curvature of roads in the network. For the estimation of lateral acceleration, this factor is highly essential. In order to estimate the curve radius, the selected approach is described in this subsection.

Instead of the spherical coordinate system P in which GPS measurements are specified, a Cartesian coordinate system I is used because it is easier to estimate curve radii on a plane than on a sphere. The coordinate transformation between the polar coordinate system of the GPS measurement in longitude and latitude $({}^{GPS}x_n, {}^{GPS}y_n)$ to a Cartesian coordinate system with the centre of the earth as the origin of coordinates can be performed as follows

$${}_{I}\vec{\mathbf{r}}_n = \begin{bmatrix} {}_{I}x_n \\ {}_{I}y_n \\ {}_{I}z_n \end{bmatrix} = R_m \begin{bmatrix} cos({}^{GPS}_{P}x_n)\, cos({}^{GPS}_{P}y_n) \\ cos({}^{GPS}_{P}x_n)\, sin({}^{GPS}_{P}y_n) \\ sin({}^{GPS}_{P}x_n) \end{bmatrix}. \tag{4.10}$$

Where R_m is the median earth radius at a given position on the globe. Since the Earth is not perfectly spherical, but rather an ellipsoid of revolution with an equatorial radius greater than

the radius to the poles, the earth radius R_m must be adjusted depending on the latitude.

$$R_m = \frac{1}{N}\sum_{i=1}^{N}\sqrt{\frac{(a^2\,cos({}^{GPS}_{P}x_n))^2 + (b^2\,sin({}^{GPS}_{P}x_n))^2}{(a\,cos({}^{GPS}_{P}x_n))^2 + (b\,sin({}^{GPS}_{P}x_n))^2)}} \tag{4.11}$$

Where a is the equatorial earth radius in meter and b is the polar earth radius in meter set to 63781370 and 63567523 meter.

Assumption: The area under consideration for the FOT is perfectly flat. This allows to project the 3D data vector ${}_I\vec{\mathbf{r}}$ from the initial Cartesian coordinate system I to twisted coordinate system K. Figure 4.9 shows how the coordinate system is rotated around the y-axis and z-axis so that the z-axis points to the regarded area on the sphere surface in our case The Netherlands.

To transform the vector ${}_I\vec{\mathbf{r}}$ from the initial coordinate system I to the rotated System K the following transformation is used. The rotation angle around the y-axis α is set to $-38°$ since the experiment is performed on a latitude of 52°. The rotation angle around the z-axis is set to $-85°$ since the experiment is performed on a longitude of 4°.

$${}_K\vec{\mathbf{r}} = \boldsymbol{A}_{KI}\,{}_I\vec{\mathbf{r}} = \boldsymbol{R}_z\boldsymbol{R}_y\,{}_I\vec{\mathbf{r}} = \begin{bmatrix} cos(\beta) & -sin(\beta) & 0 \\ sin(\beta) & cos(\beta) & 0 \\ 0 & 0 & 1 \end{bmatrix}\begin{bmatrix} cos(\alpha) & 0 & sin(\alpha) \\ 0 & 1 & 0 \\ -sin(\alpha) & 0 & cos(\alpha) \end{bmatrix}\begin{bmatrix} {}_Ix \\ {}_Iy \\ {}_Iz \end{bmatrix} \tag{4.12}$$

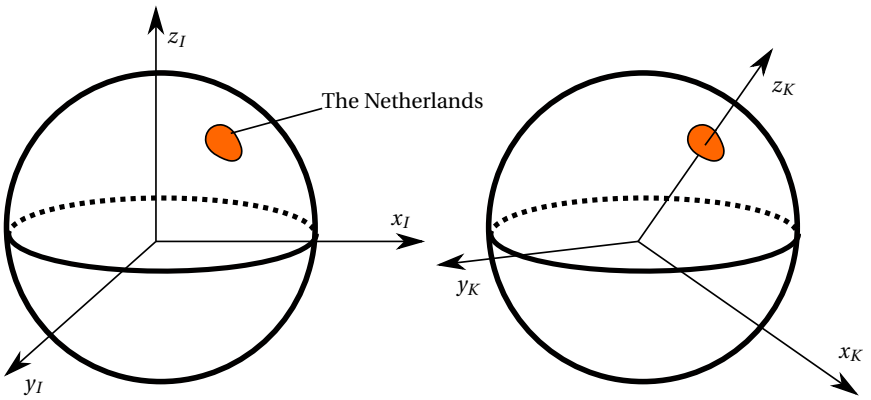

Figure 4.9: Coordinate transformation

Remark. *When transforming points located on a sphere into a square plane that tangentially touches the sphere at the centre of the considered area, the largest height errors are expected at the side edges of the plane. The error in height is* 0 *for the point where the plane is touching the sphere. For the side edges, the error in height can be calculated from simple geometric correlations as*

$$E = R - \sqrt{R^2 - (\frac{b}{2})^2}.$$

Where R is the radius of the sphere, and b is the plane width. We assume the plane to be 10 *km wide, and the earth radius is set to* 6378,1370 *km. The error in height at the side edges of the plane is less than* 1 *meter. This estimate is sufficiently accurate for our application. A*

height difference of 1 *meter has no noticeable effect on the curve radii in the plane with orders of magnitude of several* 100 *meters.*

To determine the curve radius of a driven path the map matched points transformed to the K coordinate system given by ${}^{MM}_{K}\vec{\mathbf{x}} = [x_1\, x_2 \cdots x_N]^T$ and ${}^{MM}_{K}\vec{\mathbf{y}} = [x_1\, x_2 \cdots x_N]^T$ are regarded. The z-axis coordinates ${}^{MM}_{K}\vec{\mathbf{z}}$ are not considered since the evaluation of the curve radius is carried out in the x-y-plane of the K system.

To estimate the curve radius three points located on the vehicle trajectory are used. To three points, exactly one circle can be found on which exactly these three points lie. For a general point on a circle (x, y) with radius r and the circle centre at (x_m, y_m) the following equation applies

$$(x - x_m)^2 + (y - y_m)^2 = r^2 \tag{4.13}$$

expanding the terms leading to

$$(x_m^2 + y_m^2 - r^2) + (-2x_m)x + (-2y_m)y = -x^2 - y^2. \tag{4.14}$$

Defining $A = x_m^2 + y_m^2 - r^2$, $B = -2x_m$ and $C = -2y_m$ resulting in

$$A + Bx + Cy = -x^2 - y^2. \tag{4.15}$$

For a circle with three points $P1(x_a|y_a)$, $P2(x_b|y_b)$ and $P3(x_c|y_c)$ this leads to a equation system the following appearance

$$\begin{bmatrix} 1 & x_a & y_a \\ 1 & x_b & y_b \\ 1 & x_c & y_c \end{bmatrix} \begin{bmatrix} A \\ B \\ C \end{bmatrix} = \begin{bmatrix} -x_a^2 - y_a^2 \\ -x_b^2 - y_b^2 \\ -x_c^2 - y_c^2 \end{bmatrix}. \tag{4.16}$$

Solving the system of equations for A, B, and C delivers the values for x_m, y_m, and r. This procedure is applied to the GPS measuring points recorded in the experiment and map matched with the algorithm mentioned above. The selection of the points along the driven path is carried out as it follows

$$\begin{aligned} P1 &= {}^{MM}_{K}P_{n100} = ({}^{MM}_{K}x_{n100}|\,{}^{MM}_{K}y_{n100}) \\ P3 &= {}^{MM}_{K}P_{(n+1)100} = ({}^{MM}_{K}x_{(n+1)100}|\,{}^{MM}_{K}y_{(n+1)100}) \\ P3 &= {}^{MM}_{K}P_{(n+2)100} = ({}^{MM}_{K}x_{(n+2)100}|\,{}^{MM}_{K}y_{(n+2)100}) \end{aligned}$$

$\forall n\{n \in \mathrm{N}|n \leq \frac{N}{100}\}$. In simple words, only every 100th point of the measurement is used for the curve radius estimation. The algorithm delivers the curve radius without a sign. The sign must be introduced to determine the direction of rotation of the curve. To determine the sign the location of the centre of the circle $(x_m\ y_m)$ relative to the driven path is taken into account, for left curves, the sign is positive for right curves negative.

Assumption: The selected step size of 100 data points is proper for a reasonable estimation of the yaw rate. The distance between the GPS data points should be more than 10 meters to be accurate, regarding [72]. The frequency at which the GPS signals were recorded was 100 Hz. On motorway sections and for congestion-free driving in city traffic, the speeds were over $18\frac{m}{s}$, respectively. Therefore, the approximate distance between every 100th data point is 18 meters. A velocity-depended refining for the estimation is not implemented. Nevertheless,

for this particular experiment and the driven speeds, the estimation with a step size of 100 shows good results. The radius of randomly selected curves had been tested by the author using online map services.

The results of a test run are presented in Figure 5.28c in Chapter 5. It is visible that in elongated curves, the radius estimation shows constant values, while for straight road segments, the colour changes more often but remains at high values above $\pm 2000m$. Straight segments show high curve radius values as expected. Curve radii over ±5000 meter are set to a static value of ±5000 meter for clarity. This definition is because such large curve radii can be regarded as straight and a distinction does not provide any essential information nor influences the calculation of the lateral acceleration significantly.

4.2.3. Estimation of the lateral acceleration

After the map matching procedure to gain ground truth, smoothing the noisy GPS measurement points and the estimation of the curve radius using a geometric algorithm, the vehicles lateral acceleration can be calculated as

$$a_{lat} = \frac{{V_x}^2}{R}. \tag{4.17}$$

The result of the acceleration estimation of a test drive is given in Figure 5.28. Figure 5.28b shows the driven speed over the test route, representing V_x in equation (4.17). Together with the results shown in Figure 5.28c representing R, this leads to the estimated lateral acceleration given in Figure 5.28d. The higher lateral acceleration in curves is noticeable. The fluctuation of the radius on straight road segments aforementioned is no longer significant in the lateral acceleration estimation, due to medium-high driven speeds.

4.2.4. Curve classification

When driving around a bend with a car, there are at least three degrees of freedom, the bend radius, the driven speeds, and the road bank angle. The lateral acceleration can be used to link the first two, while the previously made assumption that the test road is perfectly flat cuts out the bank angle as the third degree of freedom. Along the driven experimental road, different curves appear, which are driven with different velocity. This thesis distinguishes between left as well as right curves and straight driving. The lateral acceleration can be used for this differentiation. Positive accelerations represent right curves while negative stand for left ones. The yaw-rate would also be suitable for distinguishing different curve types. However, LCA systems are subject to various restrictions by regulatory authorities, as described in Section 2. The driving environment in which the systems can be activated is restricted by maximum lateral acceleration and jerk. In addition, the lateral acceleration, in contrast to the yaw-rate, can be actively experienced by most drivers. According to Reymond et al. [88], the driver adjusts the vehicle speed in curves so that the lateral acceleration remains below a critical value for him. This critical value is determined individually by driving experience, the vehicle's handling, weather and road conditions, and a personal acceptance risk. ADA Systems, however, have fixed limit values under which they operate - there is no acceptance risk. However, these systems also strive to keep lateral acceleration below a critical limit while following the road. Therefore, a classification of the occurring curve types using the lateral acceleration is preferable to a classification by the yaw-rate.

Figure 4.10 represents the lateral acceleration in right curves depended on a vehicle's velocity and the driven curve radius. The area where lateral acceleration is above $2^{m}/_{s^2}$ and the LCA cannot be activated is marked and set to $0^{m}/_{s^2}$ for the sake of clarity[3]. For right curves, only the sign of the curve radius and the present acceleration has to be changed.

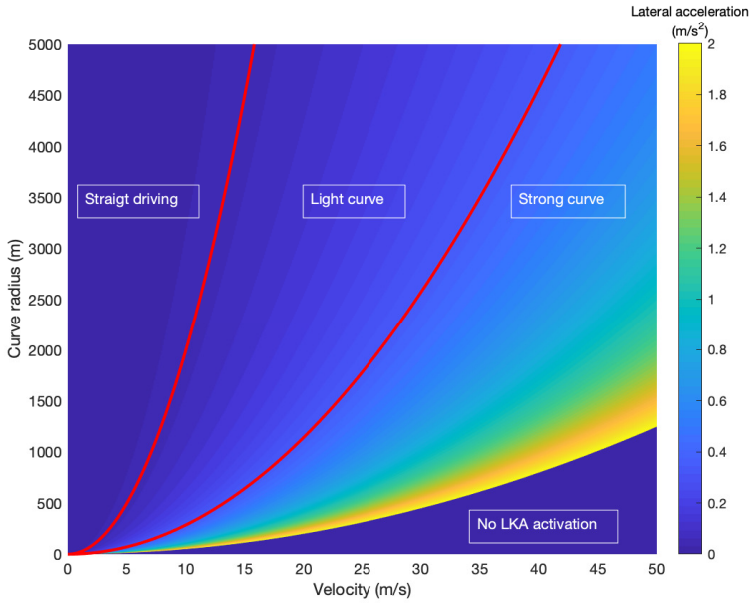

Figure 4.10: Lateral acceleration depended on velocity and curve radius

A distinction of a curve into its variable *sharpness*, e.g. which lateral accelerations appear, is made. This thesis makes a distinction between curves, depended on the lateral accelerations appearing in the sum of test drives and the performance limit of LCA systems of $2^{m}/_{s^2}$. The introduced borders represent hyperbolic lines of equal lateral acceleration also drawn in Figure 4.10.

- straight driving: $|a_{lat}| \leq 0,05\frac{m}{s^2}$
- light left curve: $0,05\frac{rad}{s} < a_{lat} \leq 0,35\frac{m}{s^2}$
- strong left curve: $0,35\frac{m}{s^2} < a_{lat}$
- light right curve: $-0,05\frac{m}{s^2} > a_{lat} \geq -0,35\frac{m}{s^2}$
- strong right curve: $-0,35\frac{m}{s^2} > a_{lat}$

After the distinction of curves appearing during the test drive, the captured LIDAR distance signals are evaluated. The aim is to determine the parameter y_{off}, the lateral offset to the lane centre, introduced in Chapter 3, in different driving situations. It is assumed that the behaviour of the vehicle interacting with road infrastructure is different for left and right turns as well as for straight driving. The results are presented in histograms to determine the distribution of the vehicle's position within its lane for different types of infrastructure.

[3] Down right in the figure

4.2.5. Evaluation of lateral vehicle dynamics

With the estimated lateral acceleration curves can be identified and classified. The vehicles position in its lane is evaluated using LIDAR sensors pointing down on the sides of the test vehicle to track the distance of the vehicle to the lane markings. The sensors are mounted right above the driver and co-driver doors on the top of the vehicle, for more information see [7]. In the following the LIDAR sensor mounted on the driver side is called left LIDAR and the one on the co-driver side is the right LIDAR.

There are two ways to describe the position of a vehicle in its lane. One is to indicate the distance to the centre of the lane. This value is called Distance to Centre Line (D2CL) hereinafter. The two sensor signals from the left and right sensor can be used to calculate the lane width L_L by adding the vehicle width to the signals. Then the value D2CL can be calculated as

$$D2CL = \frac{L_L}{2} - (\frac{L_V}{2} + L_r). \tag{4.18}$$

Where L_V is the vehicle width and L_r is the distance from the front wheel to the lane marking measured by the right LIDAR sensor. However, since the LIDAR signals are highly noisy, two valid signals from the two LIDAR sensors rarely appear simultaneously in the data-set. The estimation of the correct lane width is therefore not possible at any time. The road width is changing between urban and suburban roads as well as different lane types inside cities, e.g., at crossroads. Besides, the sensor signals are biased in curves due to the curvature of the street[4]. Therefore, D2CL cannot be specified, and instead, the raw sensor signals are used. The Signals are giving the distances to the lane markings on each side of the vehicle. Due to the dutiful execution of the underlying experiment, [7], the accuracy of the distance measurements of both sides can be considered sufficient.

[4] Theorem of Protagoras

4.3. Used Data-sets

This section addresses the used data-sets and their origin. Additional information to every experiment, e.g., the derived articles, documentation, contact persons, and detailed information to the data recording, is given in Appendix A.

4.3.1. Data-sets for longitudinal vehicle dynamics

Table 4.2 gives information of the used data-sets in a comparable way. Table 4.3 describes for what evaluation the single data-sets are used in the following. In this thesis, all investigated data-sets are designated according to their geographical origin.

Table 4.2: Data sources for the evaluation of longitudinal vehicle dynamics

Experiment	Nr. Veh.	Vehicle	Location of experiment	System status monitoring
North-Holland ACC experiment	2-7	Toyota Prius	The Netherlands	Yes
North-Holland CACC experiment	2-7	Toyota Prius	The Netherlands	Yes
Southwest US ACC experiment	2-7	Various	Southwest, USA	Yes
Ispra-Cherasco ACC experiment	2	BMW 530	Italy	No
Ispra experiment	2	BMW 530	Italy	No

Because of the fact that that some data sources specify the ACC and CACC system status[5] and others do not, the usability is limited. Data-sets that specify the system status can be used in most cases, while in data sets that do not specify the status, an additional data screening for capable situations has to be performed. In the Ispra experiment, this is done via GPS because the systems are only activated on straight sections of the test track. However, data sources that do not specify the system status are mostly used to evaluate the more general parameters, e.g., the time-headway and not for the estimation of descriptive transfer functions. This approach allows the possibly appearing human interventions to disappear behind the average values and to be less critical[6].

4.3.2. Data-sets for lateral vehicle dynamics

For the evaluation of lateral vehicle dynamics, only one data-set is used. Due to the high demands on the sensors used in the test, which include LIDAR measurements, GPS signals, and a classification of whether the LCA system is activated, only one data source could be found. Nevertheless, the entire evaluation is carried out on this data-set to support future research projects on the description of lateral dynamics.

[5] System status monitoring
[6] We assume that human intervention is very rare

Table 4.3: Use of the data sources for evaluation

	North-Holland CACC experiment	North-Holland CACC experiment	Southwest US ACC experiment	Ispra-Cherasco ACC experiment	Ispra ACC experiment
Stable car-following					
Suitained stable car-following					
Car-following under acceleration					
Car-following under deceleration					
Acceleration manoeuvre					
Deceleration manoeuvre					

5

Data Analysis and Assessment

This chapter illustrates the evaluation results of the data-sets introduced in Section 4.3 under the methodology described in Chapter 4. The chapter is divided into sections of vehicle longitudinal and lateral dynamics as every other chapter before.

Section 5.1 contains the results of the evaluation of longitudinal driving experiments. This section is divided in the prior defined four possible situations for longitudinal car-following: *stable, sustained stable, accelerated* and *decelerated*.

Section 5.2 presents the results of the evaluation of the experiment regarding lateral vehicle movement. This section shows the results for three different interactions with surrounding infrastructure: straight-ahead driving as well as driving through weak and strong curves.

5.1. Longitudinal vehicle dynamics

5.1.1. Stable car-following with ACC use

This section presents the results for *stable* car-following with ACC and accelerations during the experiment from below $0.5^{m}/_{s^2}$, as defined in section 4.1.1. Figure 5.1 presents the space-headways concerning the driven velocities for all experiments in one graph. Striking is that in the North Holland experiments, both ACC and CACC space-headways, show the highest bandwidth in velocity covering the entire range from low to high speeds. Noticeable in the Southwest experiment is the presence of four spatially limited point clouds. The gap in the space-headway is due to the default time-gap value in the experiment. The gap in velocity is because of the data acquisition with a fixed velocity profile. The two lower point clouds are captured with a smaller default time-gap, mentioned in the preceding of this thesis τ_h. In the Ispra-Cherasco experiment, there are essentially two point-clouds with a gap in velocity in between. This division is because of data acquisition on motorways and the resulting activation of the ACC system. Besides that, the Ispra experiment shows a smaller velocity bandwidth, covering only low and medium velocities, given the fact that it was captured on a test track. The original purpose of the Ispra experiment was the evaluation of dynamic car-following, which does not require high speeds. However, this thesis considers the results from the Ispra experiment hereinafter as well. It should be noted that the North-Holland, Southwest US and Ispra-Cherasco experiments are comparable due to the similar speed range. The Ispra experiment contains only low speeds so that comparability may be limited. Situation in the different experiments where the vehicle speeds up with equal space-headway or changes

its space-headway without adjusting the velocity will be cut out by the later introduced situation classification in *sustained stable* car-following. Therefore, comparability of the different FOTs will increase. Already at this point, an assumption can be made for the time-gaps τ_h, which is present in the different experiments. Since straight lines of positive gradient represent constant time-headways, and the gradient of these straight lines is proportional to the time-gap, one can assume that the time-headway in the Ispra experiment is the highest of all the experiments considered. If a regression line is drawn through all the points of the Ispra experiment, it is the one with the highest slope compared to the other FOTs.

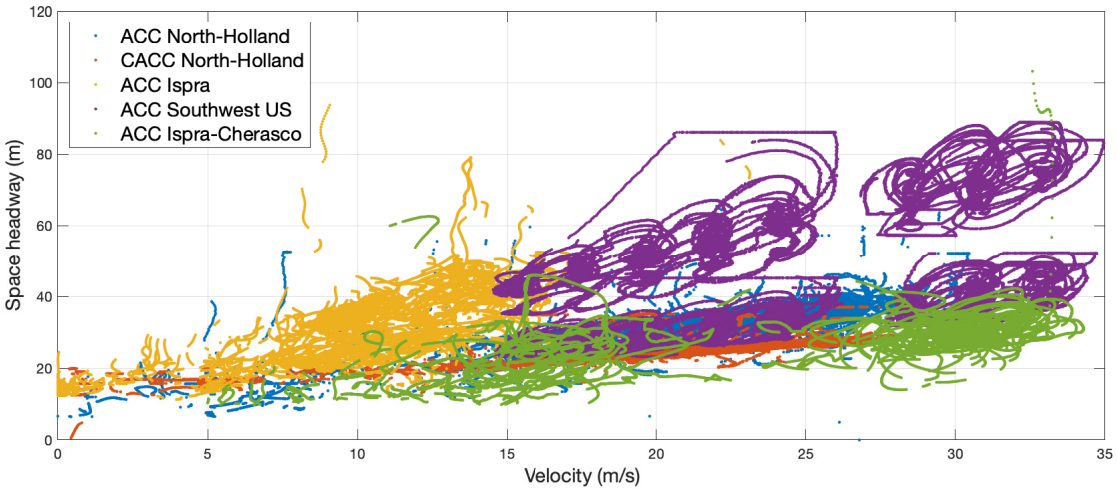

Figure 5.1: Overall space-headway for unaccelerated car-following

In the following, the time-headways, instead of the above-presented space-headways, and their distribution are considered for every experiment. Again, the use of the time-headway allows the comparison of ACC/CACC vehicle following with different speeds between experiments and between different default values with which the experiments were recorded.

The evaluation results of the North Holland experiment are presented in Figure 5.2. The left diagram represents the results from test rides with activated ACC and the right diagram with activated CACC system. Both results are compared using the median to avoid the effects of outliers. Noticeable is the symmetric distribution of the time-headway for activated ACC systems with values from 1 to 2 seconds with a median value of 1.44 seconds. When considering the activated CACC system, the values for the time-headway are more likely to be closer to the median, which means that the vehicle can follow more precisely because the time-headway does not scatter tremendously around the median. Time-headways beneath the median of 1,1 seconds are avoided while higher time-headways are not severely limited. Besides that, the median headway shrinks down to 1.12 seconds.

Figure 5.3 shows the results for the Southwest experiment. For the minimal time-gap setting, represented by the left diagram, the median time-headway is 1.38 seconds, which is about the same as in the previously described North-Holland experiment for ACC. The diagram on the right shows the results for the maximum time-gap setting. The broader distribution of the time-headway is striking. While in the left diagram, the time-headway was in the range of 1 second, the span in the right diagram is over 1.5 seconds. The larger default time-gap thus has a direct influence on the precision with which the vehicle follows the leading vehicle. Both graphs show the characteristic asymmetrical logarithmic normal dis-

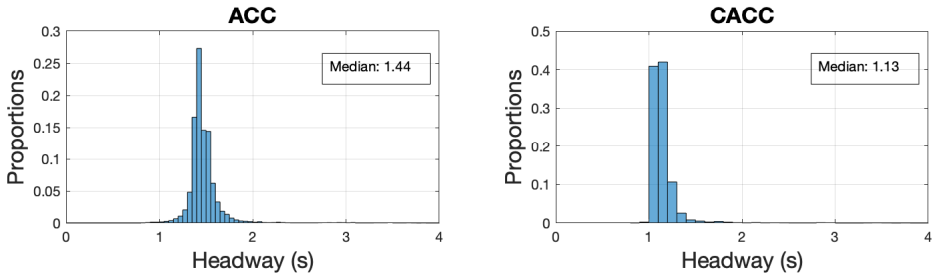

Figure 5.2: Overall headway North-Holland experiment for *stable* car-following

tribution of time-headways with fast-rising flanks at low values and flat ending flanks at high time-headway values, as it was mentioned earlier in the literature review in Chapter 2.

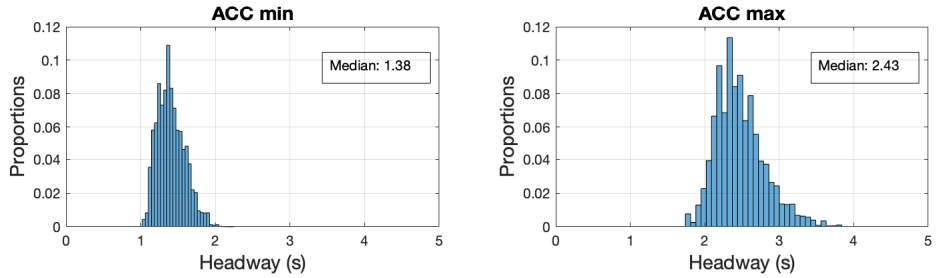

Figure 5.3: Overall headway Southwest experiment for stable car-following

Figure 5.5 includes the time-headway distribution solely from the Ispra-Cherasco experiment. None of the parameters, such as the time-gap, were changed in this FOT. The characteristic asymmetrical logarithmic normal time-headway distribution is present in this result as well. The median time-headway is the lowest of all experiments considered, while the range in which time-headway occurs is the largest with nearly 2 seconds. This increase may be due to the data acquisition on motorways with many other traffic participants and various road infrastructure.

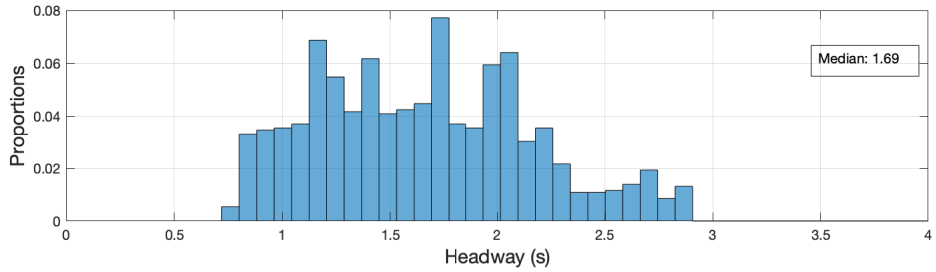

Figure 5.4: Overall headway Ispra-Cherasco experiment for stable car-following

The time-headway distribution for *stable* car-following in the Ispra experiment is shown in Figure 5.5. The median time-headway is, as previously suspected, the highest in all experiments and even higher than in the Southwest experiment with maximal default time-gap. Further, the results show a logarithmic normal distribution with more data points on the right side of the median than on the left side. The deviation of the values around the median is increased compared to all other experiments, and large outliers towards high values occur.

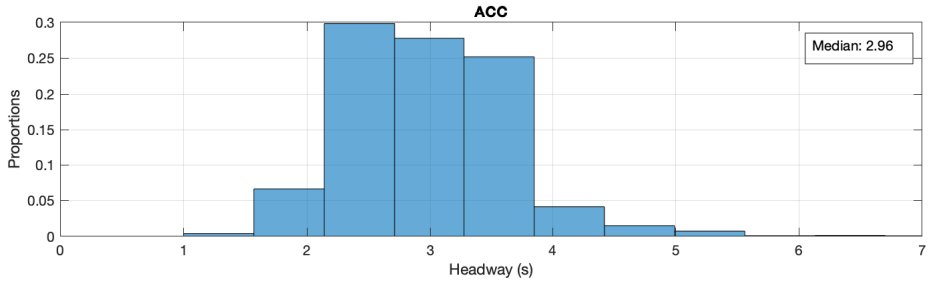

Figure 5.5: Overall headway Ispra experiment for stable car-following

5.1.2. Sustained stable car-following with ACC/CACC use

Besides the evaluation of *stable* car-following situations, the prior defined *sustained stable* driving situations are analysed. This change of perspective permits to change from the mere description of the occurring phenomena in the space- and time-headway to the description of generic and reproducible statements concerning the time-gap setting in the different FOTs. This conclusion is because a stricter definition of *sustained stable* car-following limits the potential situations and enables, therefore, deeper insight into the controlling strategy of the ACC/CACC system.

Estimation of the parameter τ_h for different velocities:
For *sustained stable* driving, the results for the space-headway of all regarded FOTs over the driven velocity is shown in Figure 5.6. Noticeable is, that in contrast to *stable* car-following for *sustained stable* car-following the results of the Southwest experiment cover the widest range of velocities from 15 to 32 $^m/_s$. The speed range covered by the North Holland and Ispra experiments is comparatively smaller. In the Southwest experiment, two different levels of space-headway can be identified for the same velocities. The appearance of these two levels is one again because of the default setting of the time-gap in the experiments. The experiment was performed once with the maximum time-gap and once with the minimal time-gap selectable by the driver. This variation of the default value leads to the two different levels of distance represented in the graph. The figure shows that the space-headways of the Southwest and North-Holland ACC experiments are almost on the same level when using data for the minimum adjustment of the time-gap in the Southwest experiment. However, in the Southwest experiment, the span of the space-headway increases most strikingly with increasing speed. The average space-headway values of the North-Holland ACC and the Southwest experiment with minimal default time-gap are almost equal for speed ranges from 17 to 27 $^m/_s$. This observation leads to the conclusion that the North-Holland ACC experiment was performed with the minimum settable value for the safe longitudinal distance as well. Visible is the small deviation of the space-headway in the North-Holland experiment for its CACC data. The space-headways in the CACC experiment for the same velocity range are also minimised compared to the ACC data. In the Ispra data-set, only two analysable situations are found. These two sequences are placed slightly higher than expected from the Southwest experiment with maximal time-gap setting at low speeds. Therefore, the Ispra experiment is not comparable to the other similar experiments. For the Ispra-Cherasco data-set, there are more analysable sequences than in the Ispra experiment. The speed range is similar to that of the Southwest experiment. The space-headways contained in the Ispra-Cherasco data-set are the smallest compared with the others. It is remarkable that the space-headways of the Ispra-Cherasco data-set even fall below the values of the North-Holland CACC experiment. Although the Ispra-Cherasco data-set contains information about the ACC system state due to the data acquisition on highways, cut-ins by other vehicles are possible, caus-

ing these small space-headways. These outliers are caused by other vehicles cutting in when the considered vehicle does not immediately engage and brakes. An abrupt braking would exclude the data points by definition from Subsection 4.1.2. Figure 4.3 contains lines of constant time-headway for 0.7, 1,5, 2 and 2,5 seconds with a standstill distance of 5 meter as well. It is noticeable that for the Ispra-Cherasco experiment, the time-headway falls below a value of 0.7 seconds. This low time-headway represents an uncertain driving situation in the data and further confirms the statement that these situations occur through interaction with other road users. For all other data-sets, this threshold is not undercut.

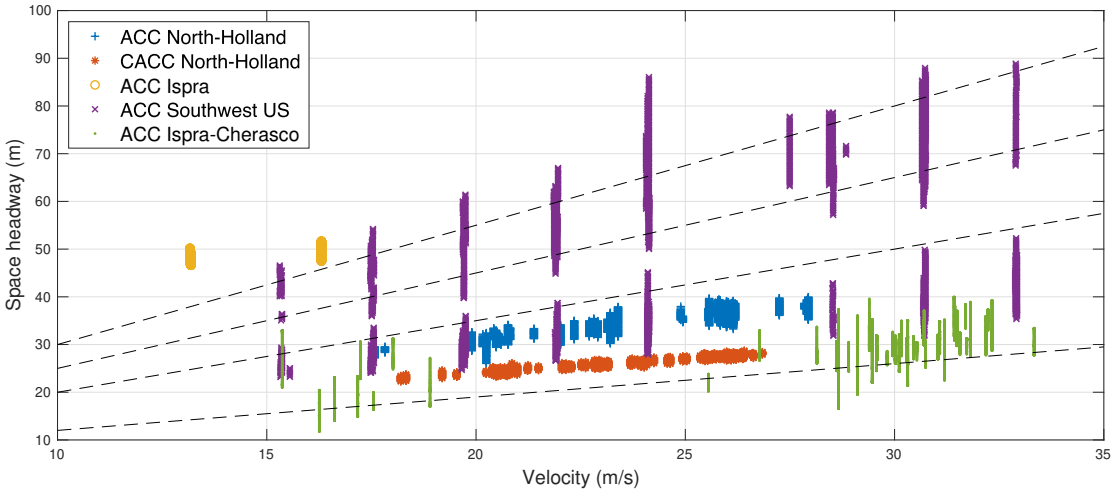

Figure 5.6: Space-headway for all data-sets

In the following the time-headways, instead of the above-presented space-headways, and their distribution are considered for every experiment.

The time-headway distribution of the North Holland experiment is shown in Figure 5.7 (top). Since the experiment regards ACC (left) and CACC (right) data, both are drawn. Time-headway distributions of either of ACC and CACC both show a major peak at lower and a minor second peak at larger values for the time-headway. For vehicles following under CACC usage, the major peak is found at smaller time-headway values. Furthermore, the CACC time-headway distribution shows a higher and less wide single peak for the major present time-headway. This single peak is suggestive for a more stable control strategy around the desired time-headway the CACC system is following. The found time-headway distribution does not fulfil the expectations for time-headways regarding [11], [110] and [91], presented in Chapter 2. As these authors describe the time-headway distribution in their work as single-peaked and logarithmic normally distributed, where the values for time-headways are bounded below. The fact that the distributions shown here have two peaks locally separated by a time-headway delta of about 0.2 seconds, while the area between the peaks has an almost constant frequency of appearance, leads to the assumption that two or more independent distributions underlie the graphs.

By dividing the data-set into three different independent velocity intervals, as explained in Subsection 4.1.2, it becomes clear that there are indeed three independent distributions for different velocities, see Figure 5.7 (bottom). The three velocity-dependent time-headway distributions now instead fulfil the expectations of a logarithmic normal distribution with a fast-rising flank for small time-headways and a slower falling flank for larger time-headways. This asymmetry implies that larger time-headways are more likely to occur than smaller ones. There is no remarkable difference in the speed-dependent time-headway for the use of ACC or CACC, respectively. Both FOTs show smaller time-headways for higher velocities.

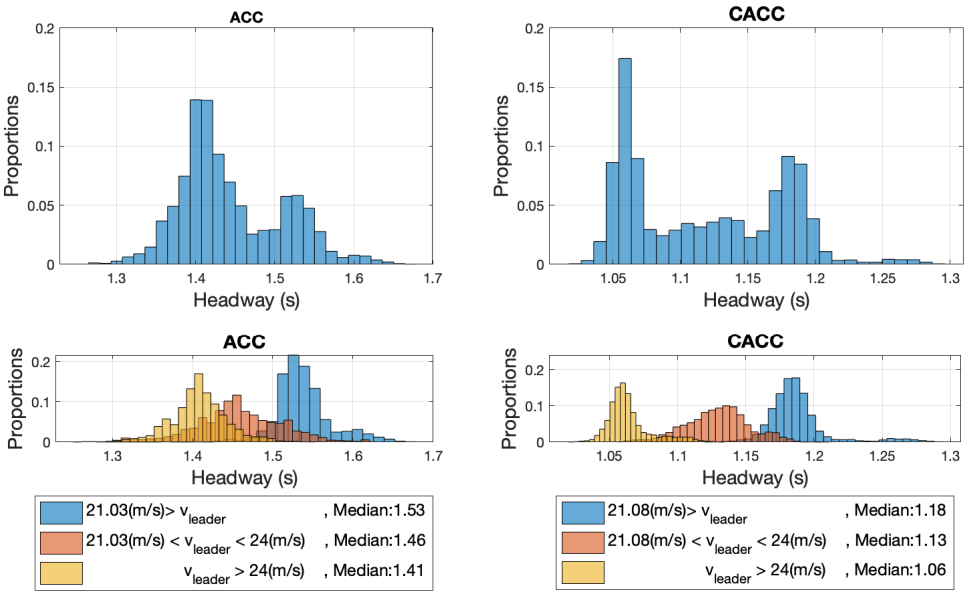

Figure 5.7: Time-headway North-Holland experiment *sustained stable* car-following

A similar behaviour is recognised in the Southwest ACC FOT. In this experiment, the single runs differ by the default setting of the default time-gap, as seen in Figure 5.6. Two default settings are displayed in the data, the minimum, and the maximum time-gap. Both settings are compared among themselves for the headway evaluation. In Figure 5.8 (top), a similar appearance of the total time-headways can be seen as in the North-Holland ACC experiment, see Figure 5.7 (top). The time-headway distribution for the maximum default value for the time-gap also shows two peaks. The higher peak is for small time-headway values and the smaller peak for larger ones. This behaviour cannot be clearly observed at the setting of minimal time-gap. An explanation for this phenomenon would be that due to the low default time-gap, the two peaks are so close together that they are indistinguishable in the graph. Therefore, are the two peaks standing out more clearly as they are further apart with maximal time-headway setting. When considering the time-headway distributions broken down by velocity in Figure 5.8 (bottom), we can observe the trend that at higher velocities, the vehicle remains a shorter time-headway from the leader. This effect is independent from the default time-gap setting in the FOT.

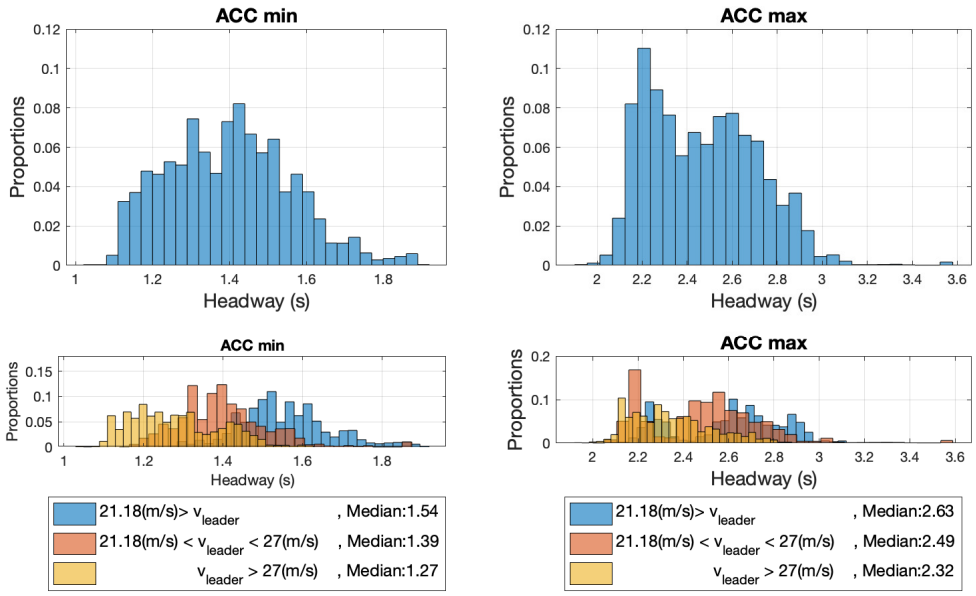

Figure 5.8: Time-headway Southwest experiment

In the Ispra-Cherasco experiment, the time-headways already seem logarithmic normal distributed around a median value of 1 second, Figure 5.9. When splitting up the data to the velocity intervals, a shift of the median time-headway is recognised. For slower velocities, the values spread over the whole range for time-headway from 0,9 to 2,2 seconds, where the median is 1,3 seconds. When the vehicle drives at a higher speed, the time-headway distribution stabilises at a median value of about 1 second. This distinction between three single speed ranges covers only two significant ones, as the steady driving sequences found are either at low or high speeds. The experiment does not cover the medium speed range, refer Figure 5.6. Therefore, the red histogram in Figure 5.9 is not relevant.

Since the Ispra experiment consists only of two valuable segments for *sustained stable* car-following, they cannot be evaluated under the previously mentioned aspects.

Summarising comparison for sustained stable car-following

When comparing the Southwest with the North Holland ACC experiment for *sustained stable* car-following, a similar median time-headway is come upon when considering the minimal setting for the time-headway in the Southwest experiment. The median time-headways of the Ispra-Cherasco and the North-Holland CACC experiment are in the same range as well. When splitting the time-headway distribution up for three different velocity intervals, it is outstanding that higher velocity leads to a backshift of time-headway in all regarded datasets. This backshift implies that at high velocities, the vehicles follow with a smaller time-headway, even if this does not mean that the space-headway is decreased. It is worth recalling the CTG spacing policy, Chapter 3, which controls the spatial distance based on time-gap and speed. The time-gap backshift in the North-Holland ACC experiment is around 0.12 seconds. In the North-Holland CACC experiment, it is slightly higher with 0.2 seconds. In the Southwest experiment with minimal default time-gap, the backshift is around 0.27 seconds, and with maximal default time-gap, it is 0.31 seconds. For the Ispra-Cherasco experiment,

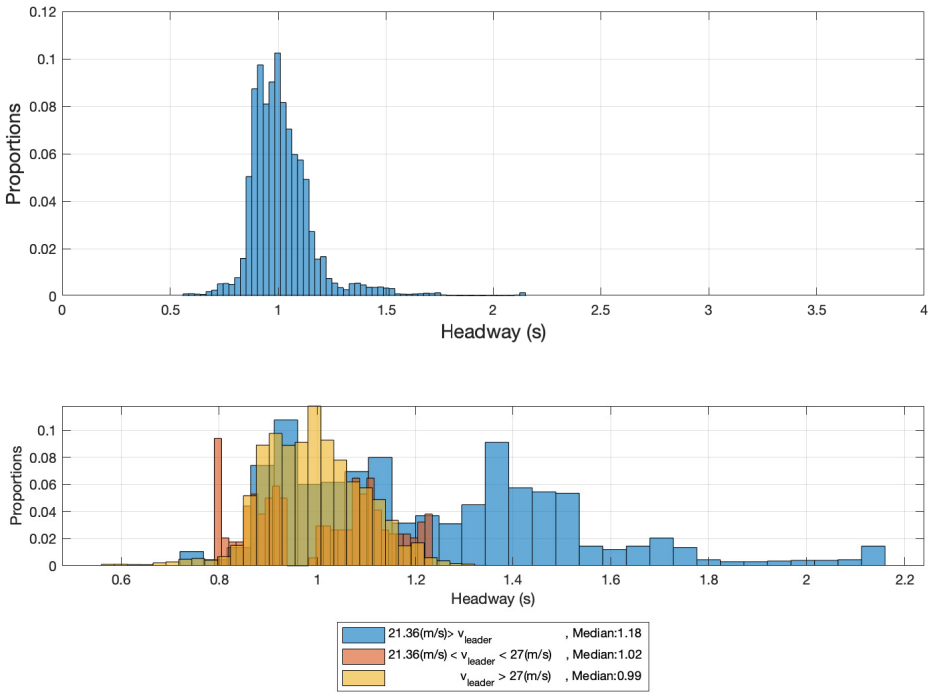

Figure 5.9: Time-headway Ispra-Cherasco experiment

it is 0.19 seconds. When considering the Southwest experiment with maximal default time-gap, the fact that the following vehicle shifts the time-headway from an assumed value of 2,6 seconds to 2,3 seconds leads to a distance error of around 4.5 meter when the speed is assumed at $15^{m}/_{s}$. As a result, the distance of the following vehicle to the vehicle in front differs by approximately 13%.

Containing frequencies in the space-headway signal:
The prior given definition of the in the space-headway signal contained frequencies to the found data sequences that are *sustained stable* is applied. Figure 5.10 presents the results for all considered FOTs. The frequency of appearance and not the proportions are used to scale the height axis, represented by the colour bar on the side, for data presentation purposes. The figure gives the first-order frequencies resulting from the FFT evaluation of the space-headway signal. For higher-order frequencies, analogue images can be generated. However, due to the prominence of first-order frequencies, this is not done in this research. Higher-order frequencies all occur with low spectral densities because of signal noise, see Figure **??**, which shows a frequency spectrum of the North-Holland ACC experiment. The idealised automated car-following behaviour shows consistently low frequencies since this avoids strong accelerations [99]. Low occurring frequencies symbolise a stable car-following behaviour where the longitudinal distance between the vehicles changes only slightly with time. High frequencies symbolise strong control interventions or signal noise.

The difference between ACC and CACC data sources is striking in the North-Holland experiment. In both data-sets, the spectrum shows an accumulation point at low frequencies.

However, in the CACC experiment, only a few outliers occur, while in the ACC data-set, the frequencies tend to scatter to higher values. This frequency distribution shows the unique quality with which the CACC system regulates the longitudinal distance. The frequencies appearing in the CACC data-set are the lowest of all experiments, and they approximately describe vehicle following where the longitudinal distance does not change due to the high frequencies.

In the Southwest experiment, mainly frequencies below 1 Hz occur. The occurrence of frequencies seems to be random, and no trend can be identified. However, the frequencies that appear cover the entire frequency range from low to high frequencies for all speeds.

Due to the data acquisition on highways in the Ispra-Cherasco experiment, which is unique in this thesis, very low frequencies occur. This can be attributed to the extended data segments found for sustained stable car-following. As the frequency is the reciprocal of the period, long segments of static car-following can cause the appearance of low frequencies as the period length can be more extensive. In other words, lower frequencies in the space-headway signal are more likely to appear when the segment of sustained stable car-following is extended. For this reason, a comparison of the experiments described above with the Ispra-Cherasco experiment is not made.

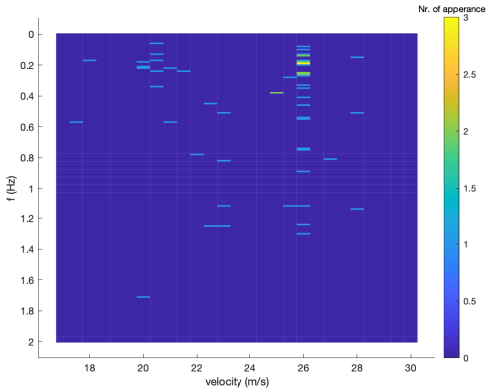

(a) North-Holland experiment ACC

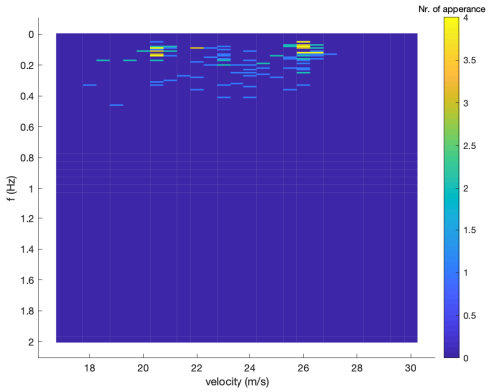

(b) North-Holland experiment CACC

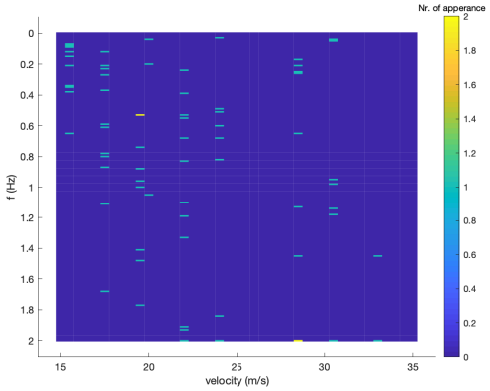

(c) Southwest experiment with maximum time-gap

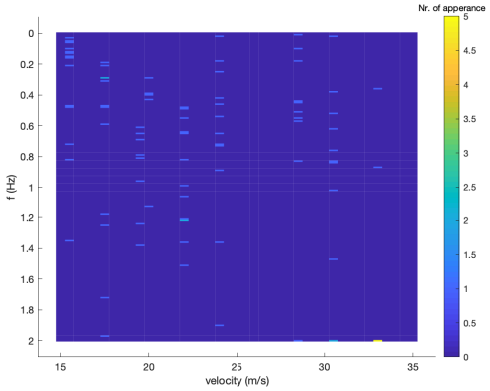

(d) Southwest experiment with minimum time-gap

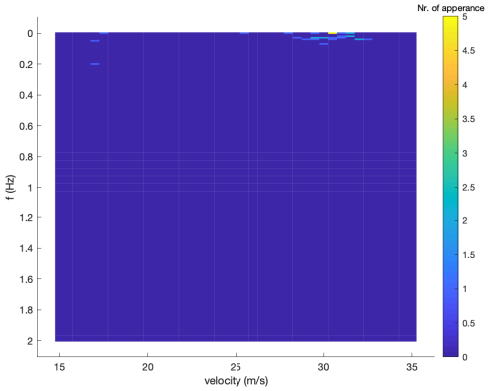

(e) Ispra-Cherasco experiment

Figure 5.10: Space-headway frequency analysis

5.1.3. Accelerated vehicle car-following

The results for *accelerated* car-following situations are presented in Figure 5.11 in a space-headway velocity graph for all regarded FOTs. Noticeable is the expected increase of the space-headway for rising velocities. The CTG spacing policy, therefore, also applies in acceleration manoeuvres. When comparing Figure 5.11 to the graph for a *stable* car-following in the previous Section, Figure 5.1, commonalities can be found. Further, for acceleration

manoeuvres, the data points in the North-Holland ACC experiment are mainly above those of the CACC experiment. This distribution implies that even during acceleration, the CACC system can maintain smaller distances to the target vehicle. The two different default settings of the time-gap in the Southwest experiment become blurred when considering acceleration manoeuvres. The reason for this is that only a few acceleration situations can be found in the data-set. In the Ispra data-set, mainly accelerations in the lower velocity range are present. There are two outliers for which the space-headway does not match and is much higher than expected. In one case, an increase in speed leads to a reduction of the distance. The behaviour in this situation is not normal, and the situation is cut out for further investigations. Due to the non-overlapping speed ranges, only the results from the North Holland and Ispra-Cherasco experiments are comparable, while the results from the Ispra and Southwest USA experiments are only comparable between driving situations.

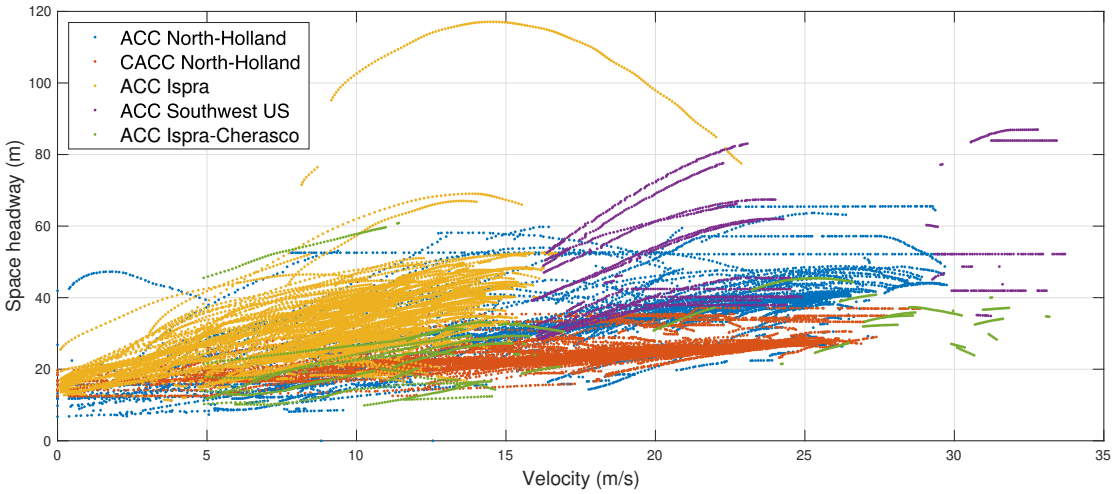

Figure 5.11: Overall space-headway for accelerated car-following

We are now considering the time-headway distribution for the *accelerated* car-following situations in the North-Holland experiment in Figure 5.12. The bandwidth of time-headway for ACC is found to be higher during acceleration situations than for *stable* car-following. The CACC mode yields less deviation than the ACC mode, but the bandwidth of time-headway is increased compared to the results for a *stable* car-following. The curve shapes for the acceleration data remain similar as for the *stable* car-following data. For ACC, the histogram shows a fast-rising flank for a lower time-headway and a flattening flank after a single peak for higher values. The CACC data shows almost an immediate increase of the distribution for lower time-headways and a flattening shape for higher values.

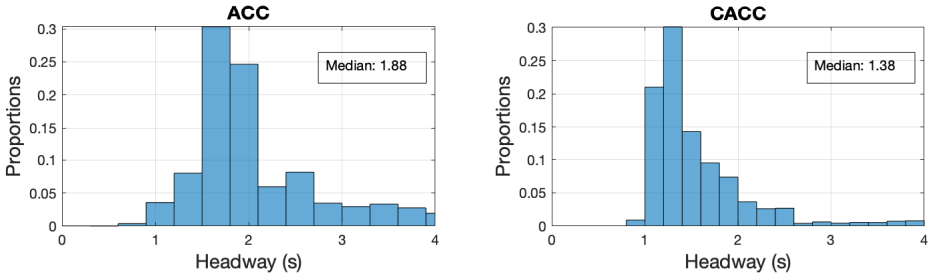

Figure 5.12: Time-headway North-Holland experiment for acceleration

In the Southwest experiment with minimum default time-gap, the values do not scatter as much as in the test runs with maximum default time-gap, Figure 5.13. This is similar to the prior discussed results for *stable* and *sustained stable* car-following. In both experiments, the distribution does not meet the expectations to be logarithmically normally distributed. Especially in the experiment with minimum time-gap, more data points were located on the left side of the occurring peak, which is unique in all experiments regarded. The median values for the time-headway in the Southwest experiment with minimal time-gap setting are comparable with the results of the North-Holland ACC experiment, accentuating the similarity of the Southwest and North-Holland ACC experiment that has already been noted. The unexpected time-headway distribution in the Southwest experiment can be attributed to the number of manoeuvres evaluated. A review of Figure 5.11 reveals the small number of data points in the FOT.

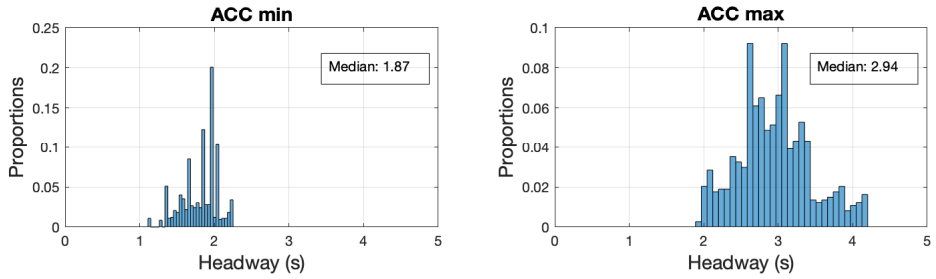

Figure 5.13: Time-headway Southwest experiment for acceleration

In the Ispra-Cherasco experiment, a broad distribution of time-headway is found. Figure 5.14 gives the results in a histogram. Fast-rising flanks of the distribution for low time-headway values and a slow falling flank for larger values are noticed. However, no peak for the median time-headway is present. With its value of 1.69 seconds, the median corresponds approximately to that of the experiments considered above. The wide distribution of the values is because of data collection on motorways as already mentioned.

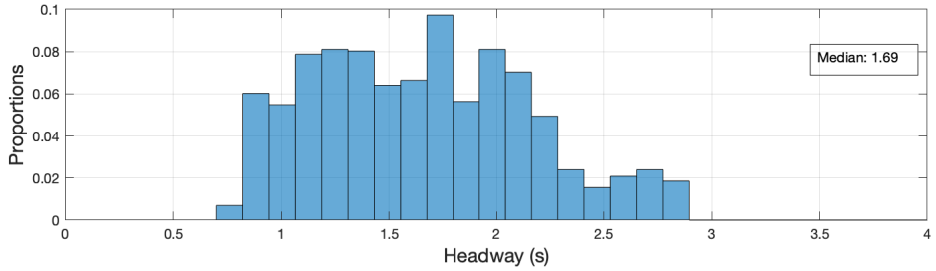

Figure 5.14: Time-headway Ispra-Cherasco experiment for acceleration

The time-headway distribution for *accelerated* car-following in the Ispra experiment is given in Figure 5.15. The expected distribution is present in the FOT. The median is the highest in all considered experiments and comes closest to that of the Southwest experiment with maximum default time-gap. The median time-headway is also in comparison to the results of *stable* car-following increased. Some outliers to high time-headways appear. These can be due to a manual driving during the data record. The record does not specify the state of the ACC system activation. Therefore, the record also contains segments in which the vehicle is manually driven. These segments are mostly filtered out, but in some cases, this is not possi-

ble. Since the majority of the segments found were recorded with the ACC system activated, the distribution is not too much influenced by the occurrence of outliers, only some extreme values occur. In the present case, the presence of outliers only leads to a widening distribution, as it can be seen from the high values of the time-headway.

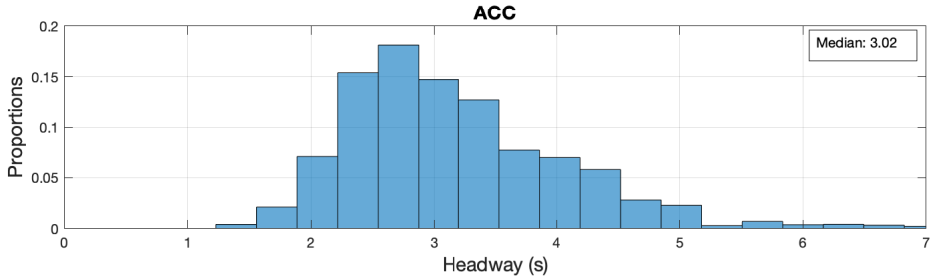

Figure 5.15: Time-headway Ispra experiment for acceleration

Summarizing comparison for accelerated car-following
The following can be determined for all data records. When *accelerating*, greater time-headways are generally observed than with *stable* or *sustained stable* car-following. The CTG spacing policy is sufficient for keeping the required safety distance also during acceleration manoeuvres. This increase can be because of the slow acceleration behaviour or of a manufacturer-dependent increase of the parameter τ_h. The intended increase of the parameter can be attributed to safety and comfort purposes. All distributions correspond to the assumed logarithmic normal distribution. An exception is the Southwest experiment due to the small number of data points to be evaluated. In this experiment, the vehicle is rarely accelerated with the minimum acceleration of $0.5^{m}/_{s^2}$ used for the evaluation.

5.1.4. Acceleration car-following manoeuvre

The following section focuses on the evaluation of the vehicle dynamics when following the defined acceleration manoeuvres from section 4.1.4. Firstly, the phenomena caused by the acceleration manoeuvre, described by the previously introduced dynamic parameters, are presented in tables. Secondly, the results of the transfer function estimation are presented. Finally, all data-sets are compared.

Describing phenomena during acceleration:
For the North-Holland ACC experiment, the results of describing the appearing phenomena are given in Table 5.1. The table lists all found acceleration manoeuvres and displays the type of system response of the velocity and the time-headway for the following vehicle. In all experiments, a distinction is made between first- and second-order system responses. In addition, the table contains information about the final speed of the underlying manoeuvre $\varnothing v$ as well as the dynamic parameters from section 4.1.4. In all detected acceleration manoeuvres, a second-order behaviour for the velocity of the following vehicle is observed. Moreover, this is the reason why a value for the speed overshoot is found in all listed manoeuvres. The response of the time-headway was in the majority of the found manoeuvres a second-order system response since vehicle velocity, and time-headway are linked values, chapter 3. This second-order response means, that when the leading vehicle has finished accelerating, the follower reduces its time-headway from an inertial error to a constant value

as time progresses. This settling time is given in the tables as T_{SH}. In case of a second-order system response for the time-headway, an undershoot of the time-headway under its mean values appears. The period between the velocity overshoot and the headway undershoot is given in the table as Δt_{vh}. In cases of a first-order system response for either velocity or time-headway, no undershoot appears. Thus, no period between the peak values can be given since there is no time-headway minimum outside the epsilon boundary for time-headway defined in Subsection 4.1.4. The manoeuvres, where a first-order system response is present, show the smallest velocity overshoots and time-headway inertial errors. In these manoeuvres, the settling time for the time-headway is the smallest. For manoeuvres where a second-order response for the time-headway is present, higher final speed leads to higher overshoots in velocity. This overshooting is visible when comparing manoeuvre 1 to manoeuvre 2. When considering manoeuvre nr three, the high velocity overshoot leads to an increased period between the velocity overshoot and the time-headway undershoot. This is due to the fact that the overshoot in velocity leads to a decrease of the time-headway between the vehicles since the ACC controller does not use the vehicle breaks to reduce the velocity of the following vehicle instantaneously. Therefore, the expanded time the vehicle needs to slow down to the leading vehicle velocity results in an increasing time between the velocity overshoot and the headway undershoot.

Table 5.1: Dynamic parameters North-Holland ACC experiment

Nr.	Rspn. Velocity	Rspn. Headway	$\varnothing$ v in $\frac{m}{s}$	$\hat{v}$ in $\frac{m}{s}$	$\hat{h}$ in s	T_{SH} in s	Δt_{vh} in s
1	2^{nd}	2^{nd}	27.866	2.164	0.176	11.6	4.7
2	2^{nd}	2^{nd}	20.594	1.566	0.435	10.9	3.7
3	2^{nd}	2^{nd}	26.139	4.321	1.739	10.9	6.7
4	2^{nd}	1^{st}	25.795	0.995	0.214	5.1	-
5	2^{nd}	1^{st}	25.854	1.016	0.227	6.9	-
6	2^{nd}	2^{nd}	23.244	1.336	0.304	12.1	4.8

For all found manoeuvres under CACC control in the North-Holland experiment, a first-order system behaviour for the following vehicle velocity is present, 5.2. During each manoeuvre, only slight overshoots of velocity are detected. The appearing overshoot $\hat{v}$ listed below is sufficiently small and does not correspond to the end of the acceleration manoeuvre of the vehicle in front. For the sake of clarity, this parameter is listed, although no overshoot occurs in a first-order system response. The initial time-headway error $\hat{h}$ is already between the limit of $0.05s$, as defined in Chapter 4.1.4, for most acceleration manoeuvres. In these cases, no settling time T_{SH} can be specified. For manoeuvres where the initial time-headway error is outside the defined limit, the settling time is remarkably low compared to all other experiments. Since neither a remarkable velocity overshoot nor a time-headway undershoot appears, it is not possible to give Δt_{vh} in the following table. The system response for the time-headway is also of first-order in all found segments. The absence of velocity overshoots is the reason why the time-headway does not show an undershoot and thus is a first-order response as well. In other words, the inertial time-headway $\hat{h}$ increases until it levels off at a fixed value. There is no difference between the manoeuvres in the final velocity reached $\varnothing v$. The longitudinal control of the following vehicle is capable of adjusting its velocity over the whole range of speeds tested in such a way that there are no overshoots, both of the speed and of the time-headway. The CACC system behaviour is more stable due to the absence of velocity overshoots, and time-headway undershoots. When considering the CACC system, the following vehicle is capable of anticipating the target vehicles movements more precisely.

The quick adjustment of velocity leads to positive results as described above and shown in the following table.

Table 5.2: Dynamic parameters North-Holland CACC experiment

Nr.	Rspn. Velocity	Rspn. Headway	$\varnothing$ v in $\frac{m}{s}$	$\hat{v}$ in $\frac{m}{s}$	$\hat{h}$ in s	T_{SH} in s	Δt_{vh} in s
1	1st	1st	26,051	0.089	0.019	0.000	-
2	1st	1st	26,148	0.512	0.069	1.0	-
3	1st	1st	20,497	0.143	0.047	0.000	-
4	1st	1st	25,923	0.097	0.014	0.000	-
5	1st	1st	21,210	1,790	0.076	4.5	-
6	1st	1st	25,810	0.060	0.043	0.000	-
7	1st	1st	26,035	0.195	0.032	0.000	-
8	1st	1st	25,965	0.125	0.016	0.000	-
9	1st	1st	26,223	0.107	0.064	1.9	-
10	1st	1st	25,858	0.242	0.027	0.000	-

The results for the Southwest experiment are presented in Table 5.3. In this FOT, a more repeatable speed profile of the leading vehicle was maintained. Therefore, all found manoeuvres accelerate up to a velocity of approximately $24^{m}/_{s}$. Throughout all manoeuvres, a second-order system response for the following vehicle velocity is detected. The system response for the headway varies between first and second-order and does not follow any recognisable rule. During test drives, carried out with minimum default time-gap, the highest speed overshoots occur. In addition, the average velocity overshoot for the experiment with minimum default time-gap is higher than for the maximum adjustable time-gap. For all other parameters, the averaged results show no significant differences. Moreover, the initial headway errors $\hat{h}$ for second-order time-headway responses are higher than for first-order responses. The time spans between the velocity overshoot and the headway undershoot are extended in comparison to the North-Holland ACC experiment.

Table 5.3: Dynamic parameters Southwest experiment

Nr.	Rspn. Velocity	Rspn. Headway	$\varnothing$ v in $\frac{m}{s}$	$\hat{v}$ in $\frac{m}{s}$	$\hat{h}$ in s	T_{SH} in s	Δt_{vh} in s
Southwest experiment ACC max							
1	2nd	1st	24,127	0.403	0.404	19.8	-
2	2nd	1st	24,098	1,903	1,152	19.8	-
4	2nd	2nd	24,133	1,935	1,629	19.8	12.0
6	2nd	1st	24,147	1,173	0.559	28.7	-
8	2nd	2nd	24,143	1,124	0.504	26.4	8.7
10	2nd	2nd	24,128	1,262	0.544	27.4	11.1
Southwest experiment ACC min							
3	2nd	1st	24,076	2,147	0.279	19.8	-
5	2nd	2nd	24,131	2,013	1,013	26.6	11.5
7	2nd	1st	24,157	1,704	0.581	31.2	-
9	2nd	2nd	24,141	1,559	0.549	18.8	10.8
11	2nd	2nd	24,169	1,965	0.769	23.8	9.9

Due to the way data was collected in the Ispra and Ispra-Cherasco FOTs, on public roads and motorways, no acceleration manoeuvres suitable for evaluation can be found in these experiments. Both experiments do not have the primary purpose of classifying the used ACC system. Therefore, neither standardised acceleration manoeuvres nor other acceleration manoeuvres suitable for evaluation are included. The use of these data-sets is thus limited to the evaluation of *stable*, *sustained stable*, and *accelerated* car-following.

Estimation of transfer functions for the acceleration manoeuvre:
In the following the estimated transfer functions for the found acceleration manoeuvres are presented. Second order transfer functions are given as $G_i(s) = \frac{a}{bs^2+cs+d}e^{-fs}$, where a is the numerator, $[b\,c\,d]$ the denominator and f the Input-Output (IO)-delay. First-order transfer function are given as $G_i(s) = \frac{a}{bs+c}e^{-fs}$, where $[b\,c]$ is the numerator. In addition, the achieved speed in the acceleration manoeuvre, the natural frequency ω_n for second-order system responses and the accuracy of the fit result is given.

The estimated transfer functions for acceleration manoeuvres in the North-Holland ACC experiment are displayed in Table 5.4. A visual representation of the step responses of these transfer functions is shown in Figure 5.16. The fitting accuracy for all estimated transfer functions is over 90%, respectively, which is sufficiently accurate. Transfer Function (TF) 1 and 3 are noteworthy, while all other graphs show approximately the same course. During the acceleration manoeuvres, 1 and 3, the vehicle accelerates to the highest velocities. For TF 1, the numerator has a small value, while the damping term c remains at a high value, so TF 1 shows a smaller overshoot and a less distinct increase in speed. In addition, the natural frequency ω_n is lower, which causes a higher period length in the step response. A similar phenomenon can be found for TF 3. The small numerator also leads to a slower speed increase. Due to the lower appearing damping term c, the function shows a widespread oscillation around the static gain of $1^m/_s$. The low natural frequency extends the period length as well, which results in a long oscillation time of TF number 3. All other TF show almost the same results for different speeds reached at high percentages of fit.

Table 5.4: Estimated transfer functions North-Holland ACC experiment

Nr.	∅ v in $\frac{m}{s}$	Numerator	Denominator	ω_n in $\frac{rad}{s}$	IO-Delay	Fit-result
1	27.866	0.1255	[1.0000 0.2442 0.1257]	0.3545	0	94.4988
2	20.594	0.2031	[1.0000 0.2977 0.2027]	0.4502	0.1	92.0154
3	26.139	0.0564	[1.0000 0.0996 0.0549]	0.2343	0.4	94.2999
4	25.795	0.2249	[1.0000 0.3138 0.2227]	0.4719	0	94.4461
5	25.854	0.2494	[1.0000 0.2871 0.2480]	0.4979	0.1	95.1872
6	23.244	0.2110	[1.0000 0.2401 0.2078]	0.4558	0	94.5966

The results for the North-Holland CACC experiment are presented in Table 5.5. As previously mentioned, the velocity response during acceleration manoeuvres was first-order in all found segments. Therefore, the found and listed transfer functions are describing a first-order system response. The step responses of the found transfer functions are presented in Figure 5.17. All responses do not show an overshoot in velocity and are approaching the static velocity value of $1^m/_s$ from below. Remarkably, two different groups of transfer functions were detected. Those who suddenly fulfil the step response and those who approach the limit value more slowly. When considering the slow approaching TFs number 3, 4, 9 and

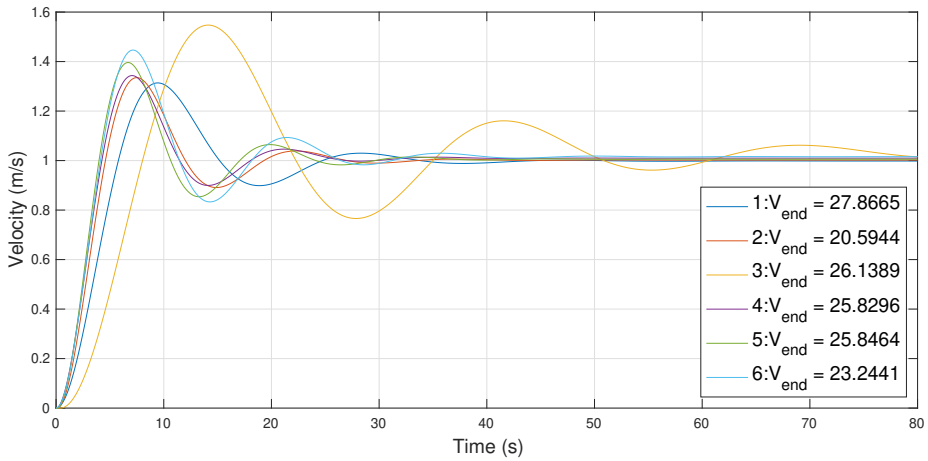

Figure 5.16: Step-response transfer functions North-Holland ACC experiment

10, it is noticeable that the numerator values for these functions are small. In addition, these functions have a high quality of regression fitting. The fit-results for these functions are the highest in the experiment. A dependence of the final speed reached in the acceleration manoeuvre, and the time constant τ cannot be determined. All other transfer functions follow the input jump almost instantly. In Figure 5.5 these fast-following TF are indistinguishable. High values of the time constant τ, like they are present here, are typical for high values of the numerator. Due to the lower quality of adaptation of the regression, the conclusion can be drawn that the vehicle control regulates the preceding and following vehicle in these manoeuvres almost identically. Thus, no transmission behaviour between the two vehicles is determined, since input and output occur almost equally. This again indicates the special quality of control of the CACC system.

Table 5.5: Estimated transfer functions North-Holland CACC experiment

Nr	∅ v in $\frac{m}{s}$	Numerator	Denominator	IODelay	FitPercent
1	26.051	179.6410	[1.0000 180.4222]	0	85.5678
2	26.148	49.4064	[1.0000 49.4574]	0	88.9266
3	20.497	1.8760	[1.0000 1.8700]	0	91.2369
4	25.923	0.7824	[1.0000 0.7793]	0	91.6258
5	21.210	50.5293	[1.0000 50.3512]	0	93.6447
6	25.810	56.8685	[1.0000 56.5710]	0	87.9795
7	26.035	36.1351	[1.0000 36.2101]	0	89.4818
8	25.965	60.8307	[1.0000 60.3344]	0	92.3427
9	26.223	2.5018	[1.0000 2.5006]	0	95.7250
10	25.858	0.9644	[1.0000 0.9606]	0	94.2614

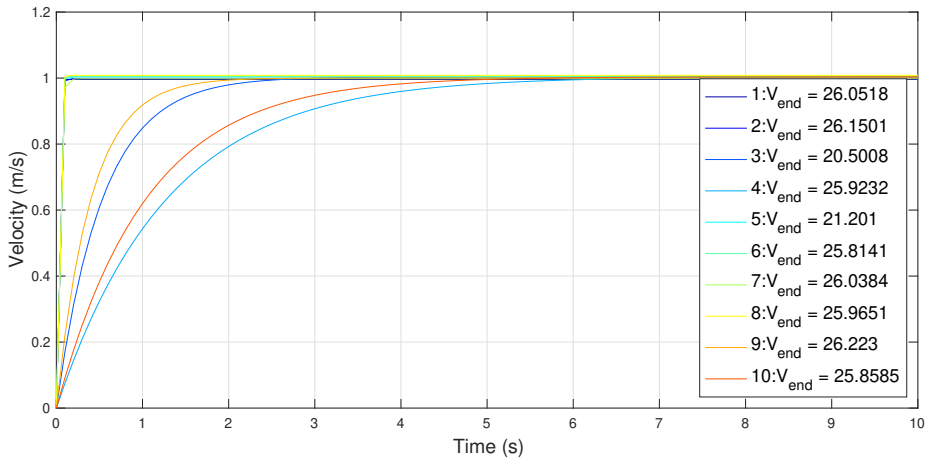

Figure 5.17: Step-response transfer functions North-Holland CACC experiment

All found acceleration manoeuvres in the Southwest experiment show a high value of the estimation fit, see Table 5.6. Due to the data acquisition with a fixed speed profile in all test runs, only acceleration manoeuvres are found where the final reached speed is around $24^{m}/_{s}$. The similar velocity profile during the FOT also leads to similar found transfer functions. The natural frequencies ω_n are lower than in the North-Holland ACC data-set. Besides, the damping parameter c is decreased in comparison. This decrease is visible by the longer settling time of velocity after the step input in Figure 5.18. No differences in the occurring time delays are found. Due to final velocities being always the same, and similarity of the acceleration manoeuvre, the signal graphs in Figure 5.18 do not show significant differences. The only striking thing is the longer settling-time aforementioned, due to the decreased damping and low natural frequencies in comparison to the North-Holland ACC FOT.

Table 5.6: Estimated transfer functions Southwest ACC experiment

Nr.	∅ v in $\frac{m}{s}$	Numerator	Denominator	ω_n	IODelay	FitPercent
1	24.0994	0.0296	[1.0000 0.1354 0.0293]	0.1711	0	93.4693
2	24.1325	0.0330	[1.0000 0.1686 0.0325]	0.1802	0	93.0898
3	24.1303	0.0435	[1.0000 0.1328 0.0431]	0.2076	0	91.6365
4	24.1461	0.0906	[1.0000 0.2106 0.0905]	0.3008	0	94.1855
5	24.1599	0.0823	[1.0000 0.1559 0.0819]	0.2861	0	94.3943
6	24.1404	0.0651	[1.0000 0.1929 0.0648]	0.2545	0.1000	93.1619
7	24.1381	0.0830	[1.0000 0.1561 0.0826]	0.2874	0	92.6980
8	24.1307	0.0611	[1.0000 0.1755 0.0609]	0.2467	0.2000	93.6613
9	24.1786	0.0448	[1.0000 0.1158 0.0449]	0.2118	0.1000	89.1133

A representation of the frequency response of the transfer functions in a Bode magnitude plot is shown in Figure 5.19. In the following, the frequency responses of the individual experiments are discussed, and a comparison between the experiments is made. For the North-Holland ACC experiment the transfer function number 3 mentioned above, from Table 5.4, is striking. This TF shows the highest magnitude at the lowest frequency. All other TFs from the North-Holland ACC experiment show a similar course. For the North-Holland CACC experiment, a frequency response typical for a first-order system can be observed. The

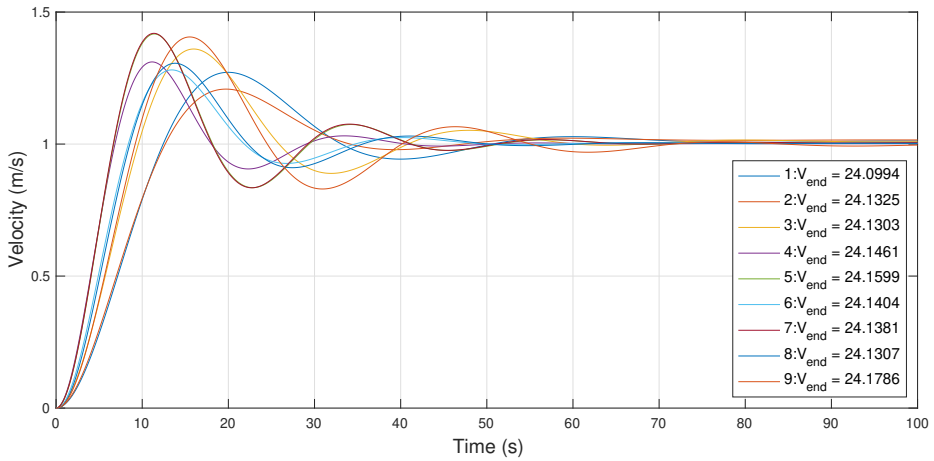

Figure 5.18: Step-response transfer functions Gunther ACC experiment

appearance of two separate groups is striking. One group consists of TF (3,4,9,10) with decreasing magnitude for lower frequencies. The other group consists of TF(1,2,5,6,7,8). Here the magnitudes only decrease at higher frequencies. Remarkably is that exactly the transfer functions with the lower cut-off frequencies show the highest fitting results from the Table 5.4. Even in the frequency response, no influence of the achieved speed in the acceleration manoeuvre on the transfer functions can be determined. In the Southwest ACC experiment, all frequency responses show a similar course, and no outliers occur. This similarity is again due to the comparable acceleration manoeuvres in the FOT. When comparing the Southwest with the North-Holland results, a lower cut-off frequency is present in the Southwest experiment. The mean cut-off frequency in the North-Holland experiment is $0.42^{rad}/_{s}$, while in the Southwest experiment it is $0.21^{rad}/_{s}$. Therefore, the vehicles in the Southwest experiment react more sensitively to lower frequencies in the speed signal of the leading vehicle. Due to air resistance, engine dynamics, human reaction time and inertia, frequencies below 1 Hz in the speed signal are more likely than higher frequencies.

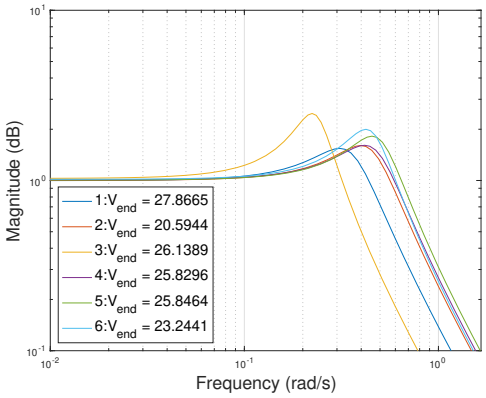

(a) North-Holland ACC experiment

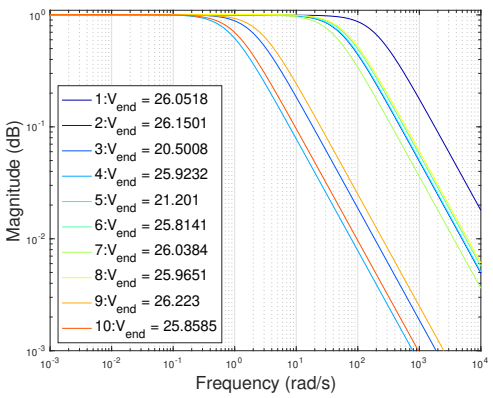

(b) North-Holland CACC experiment

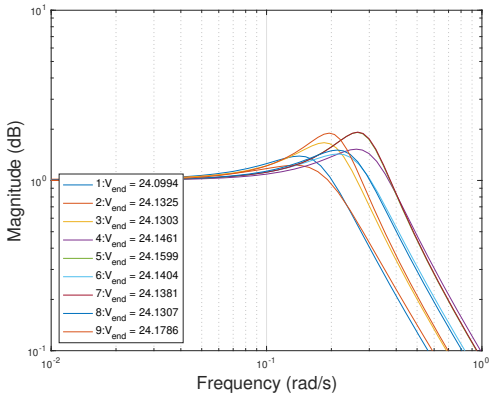

(c) Southwest ACC experiment

Figure 5.19: Frequency response for the found transfer functions

5.1.5. Decelerated vehicle following

Figure 5.20 presents the space-headways depended on the velocity for all experiments when the condition for a decelerating leading vehicle from Subsection 4.1.3 is obtained. Points that can be connected to form a continuous line represent deceleration manoeuvres that start from high speeds and high space-headways and result in lower velocities and distances. The space-headways in the Ispra experiment are, once again, the highest for the whole bandwidth of considered velocities. For the North-Holland ACC and CACC experiment, the data points are overlapping, and no remarkable difference in the headways can be seen, as it was present in Figure 5.11 and 5.1 for *accelerated* and *stable* car-following. Only at the edges of the velocity bandwidth, the data points scatter out, and a distinction between the data points can be made. For the Southwest experiment, less deceleration than acceleration situations are detected inside the data. The different default time-gap in the Southwest experiment, which is visible when considering *accelerated* and *stable* car-following in Figure 5.11 and 5.1, is much more challenging to recognise for deceleration manoeuvres due to the few data points. The space-headways in the Ispra-Cherasco experiment are, at times, the lowest of all experiments. For all data-sets consulted, it is determined that a convex curve[1] occurs during braking manoeuvres, whereas it is concave during acceleration manoeuvres. Again, is the comparability of the North-Holland and the Ispra-Cherasco experiment is given due to the same speed

[1] With positive velocity as the counting direction

range. The comparability of the Ispra and the Southwest US experiments is therefore limited.

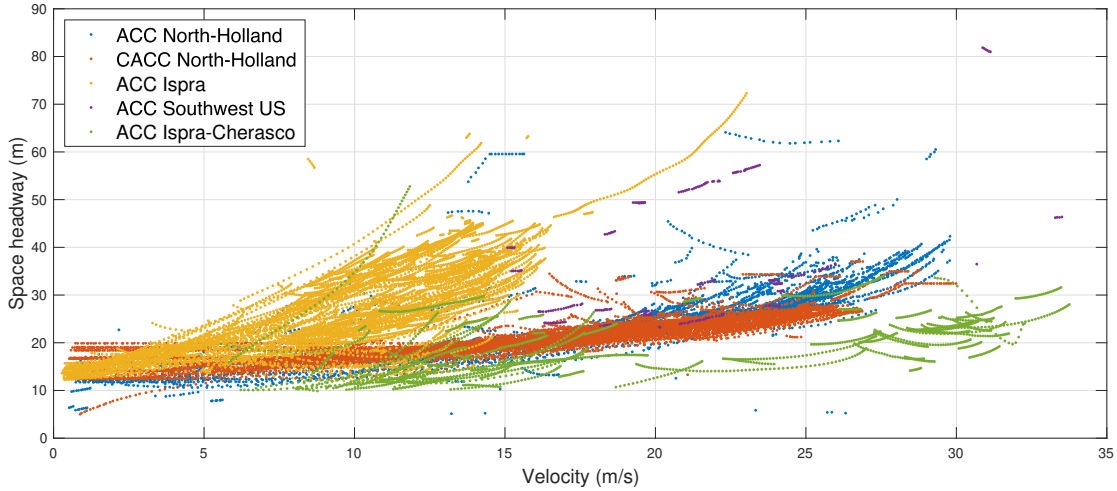

Figure 5.20: Overall space-headway for car-following with deceleration

Figure 5.21 presents the time-headways from the North-Holland experiment during decelerated car-following. The time-headways in the North-Holland experiment are for both ACC and CACC data lower than for *acceleration* manoeuvres and *stable* car-following. Furthermore, the medians of both of the records for *decelerated* car-following are equal, while ACC activation results in a thinner cluster point at 1.2 seconds. With CACC activation, the time-headway distribution scatters more towards larger values, while the extreme values for the time-headway distribution are the same in both experiments and occur with equal frequency.

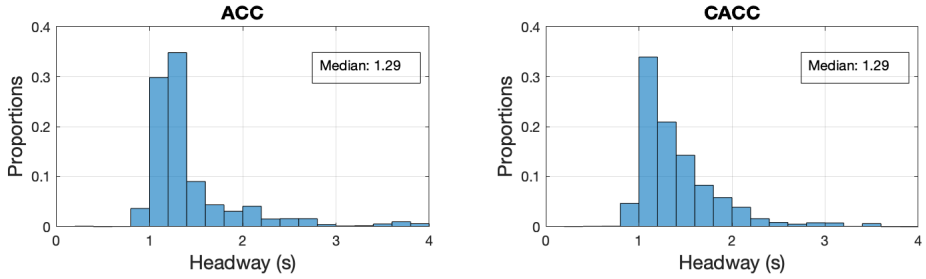

Figure 5.21: Time-headway North-Holland experiment for deceleration

The results for the Southwest FOT are shown in Figure 5.22. Due to the small number of suitable deceleration situations found in the data-set, the distribution is degenerated and does not correspond to the expectations. However, even with the limited database, a trend is noticeable. During *decelerated* car-following of the vehicles, the median time-headway for the test runs carried out with minimal time-gap setting are lower than those with the maximal time-gap setting. When comparing this to the results aforementioned for the stable or the accelerated following, it is striking that the median values of 1.38 and 2.46 seconds are precisely the same as they are present in the results for steady following, Figure 5.3. This equality leads to the conclusion that in the Southwest experiment the vehicles adapt speed reductions far more practically than speed increases and that the ACC control follows the speed profile from the target vehicle more precisely.

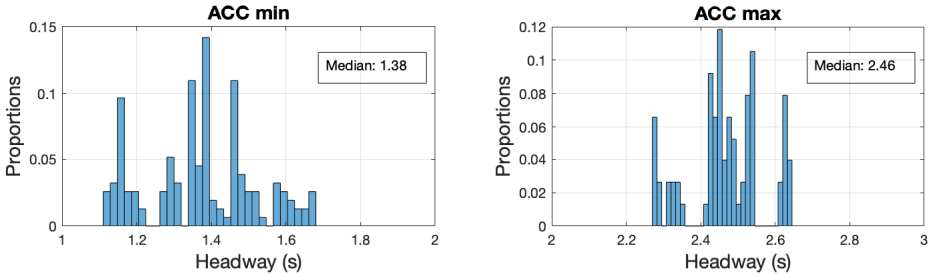

Figure 5.22: Time-headway Southwest experiment for deceleration

The time-headway distribution for *decelerated* car-following in the Ispra-Cherasco experiment is presented in Figure 5.23. The distribution shows the expected logarithmic-normal course with a lower median as for the accelerated succession (1.96s). The medians for *decelerated* and *stable* car-following (1.04s) are equal, see Figure 5.5. Once again, the ability of the ACC system to adjust deceleration situations more precisely than acceleration manoeuvres of the leading vehicle was demonstrated.

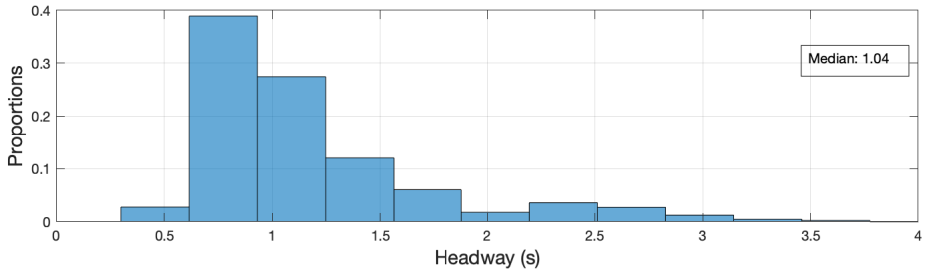

Figure 5.23: Time-headway Ispra-Cherasco experiment for deceleration

Figure 5.24 presents the time-headway distribution in the Ispra experiment for deceleration manoeuvres. Striking is the wide distribution with the highest time-headways in all considered experiments. The median time-headway is, in comparison to the median time-headway for a stable vehicle following (2.95s), see Figure 5.5 increased. However, when comparing the median for car-following during deceleration and car-following during acceleration, the median for deceleration manoeuvres is higher than for acceleration manoeuvres (3.02s). This behaviour has never been observed in any previous experiment and is unique in this data-set. This behaviour is not typical for the system and does not correspond to the expectation that the distance decreases because of the driving up during a braking manoeuvre. Instead, the following vehicle decelerates so sharply that it gains an additional safety margin.

5.1.6. Deceleration car-following manoeuvre

This subsection addresses the estimation of transfer functions during deceleration manoeuvres between the velocity of the leading vehicle as input and the velocity of the following vehicle as output. Thus the TFs are describing a SISO system for deceleration. For the North-Holland CACC experiment the transfer functions are given as $G_i(s) = \frac{as^2+bs+c}{ds^3+es^2+fs+g}e^{-hs}$, where $[a\,b\,c]$ are the numerator coefficients, $[d\,e\,f\,g]$ the denominator coefficients and h the IO-delay. For modelling reasons, additional poles and zeros are added to the transfer functions to generate fitting results over 85%. The acquired transfer functions are shown in Table 5.7. Since no IO-delay occurs, this parameter has been cut out of the table. The natural

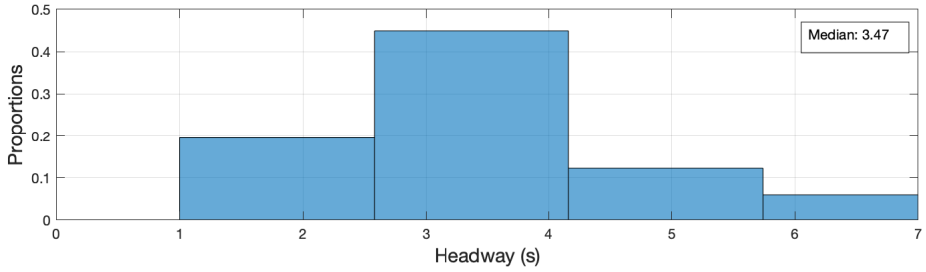

Figure 5.24: Time-headway Ispra experiment for deceleration

frequencies, specified for the second-order system responses, are also not displayed due to the higher-order transfer functions. The velocity achieved by the slowdown manoeuvre is indicated in the column for $\varnothing v$. Figure 5.25 presents the step response of the found transfer functions. Since these transfer functions describe a speed reduction, a negative input jump was selected for the sake of clarity. The result remains the same. This convention corresponds only to a change of sign. For the negative input step, it is visible that the following vehicle adapts almost immediately to the speed of the vehicle in front. The almost vertical gradients illustrate this behaviour at the beginning of the negative input jump, which occurs due to the differential component $[a\,b\,c]$ in all the transfer functions numerators. After this first immediate speed adjustment, a settling process occurs before the speed of the leading vehicle is adopted.

Table 5.7: Estimated transfer functions North-Holland CACC experiment for deceleration manoeuvres

Nr.	$\varnothing$ v ($\frac{m}{s}$)	Numerator	Denominator	Fit-result
1	23.32	[9.8864 8.0359 5.6788]	[1. 18.1300 8.7477 5.6711]	92.57
2	25.00	[799.5316 131.1842 168.7817]	[1. 826.2693 129.0605 168.6557]	87.88
3	22.57	[830.6217 314.7358 379.0282]	[1. 1178.2040 315.4775 378.3374]	95.91
4	20.36	[0.9481 0.4668 0.3862]	[1. 1.5891 0.6350 0.3852]	97.01
5	22.30	[2.5328 1.1126 1.4063]	[1. 3.9338 1.5825 1.4041]	95.92
6	22.83	[82.7267 22.0882 11.9132]	[1. 81.1587 21.8577 11.9123]	92.51
7	20.67	[2.4027 1.8356 1.5624]	[1. 5.5008 2.4312 1.5632]	85.68
8	23.13	[6.7945 6.6897 4.9593]	[1. 21.0176 5.8431 4.9548]	90.98

The estimated transfer functions from the Southwest data-set are presented in Table 5.8. In the Southwest experiment, a IO time delay does occur. To estimate the system response, an approach with three poles and two zeros of the transfer function is followed. This adjustment provided appropriate fitting results. However, the fitting results are lower than in the North-Holland CACC experiment. Remarkable is transfer function five as it has the highest IO-delay and reaches the lowest velocity during the deceleration manoeuvre. The step response of transfer function 5, shown in Figure 5.26, gives the impression that the following vehicle is speeding up at the beginning of the step input. This effect is due to the estimation error of the transfer function and not representative for the real vehicle behaviour after a decrease of the leading vehicles speed.

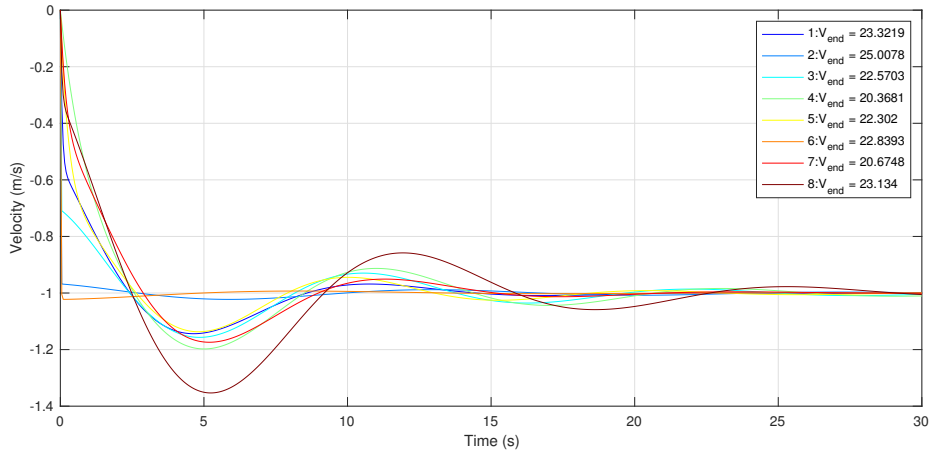

Figure 5.25: Step-response transfer functions North-Holland CACC experiment for deceleration

Table 5.8: Estimated transfer functions Southwest ACC experiment for deceleration manoeuvres

Nr.	∅ v ($\frac{m}{s}$)	Numerator	Denominator	IODelay	Fit-result
1	30.71	[0.32 0.00 0.01]	[1. 0.35 0.04 0.01]	0.1	92.91
2	28.51	[103.41 136.37 18.43]	[1. 704.25 108.19 18.12]	0	82.54
3	30.70	[12.40 474.31 49.22]	[1. 1336.62 468.74 49.04]	0	89.81
4	28.52	[0.55 0.04 0.02]	[1. 0.63 0.09 0.02]	0.1	83.08
5	17.55	[-0.05 -0.04 0.20]	[1. 1.84 0.44 0.20]	0.2	89.00

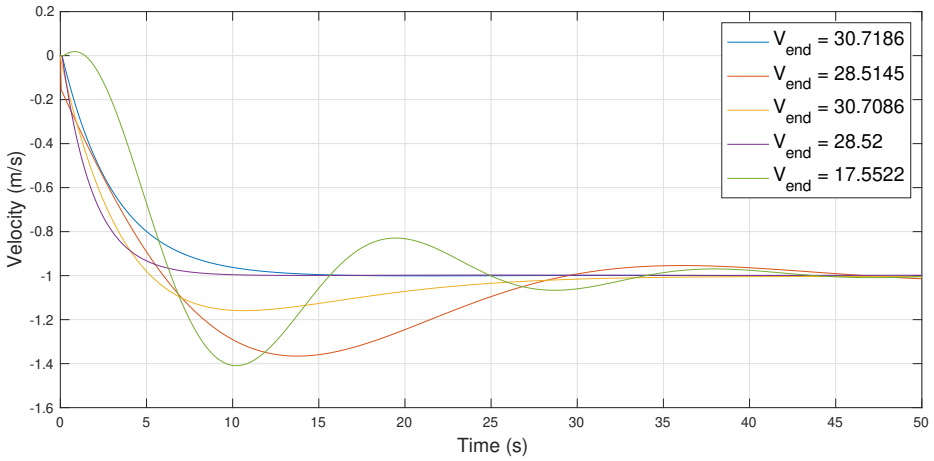

Figure 5.26: Step-response transfer functions Southwest ACC experiment for deceleration

A representation of the frequency response of the transfer functions describing the vehicle deceleration in a Bode magnitude plot is shown in Figure 5.27. Two types of TFs appear in the diagrams, those who show a maximum magnitude for a specific frequency and those whose magnitude decreases monotonically from the critical frequency. For the North-Holland CACC experiment, Figure 5.27a, the frequencies responses of transfer function 2,3 and 6 are striking. For these estimated transfer functions, the car-following behaviour is of such high quality that no magnitude maximum is occurring. The cut-off frequencies for these transfer functions are, compared to acceleration manoeuvres out of the same experiment, increased. All other TFs show an increased magnitude at lower frequencies before the magnitude starts decreasing. In the results of the Southwest experiment, Figure 5.27b, there are two groups of TFs, which are not spatially separated here, however. The increase in magnitude and the beginning of magnitude shrinkage coincide at the same frequencies. In the Southwest experiment, the almost immediate decrease in speed right after the step input is less distinct than in the North-Holland CACC experiment. For some transfer functions, the speed falls below the static value, and the settling times are extended compared to the North-Holland experiment.

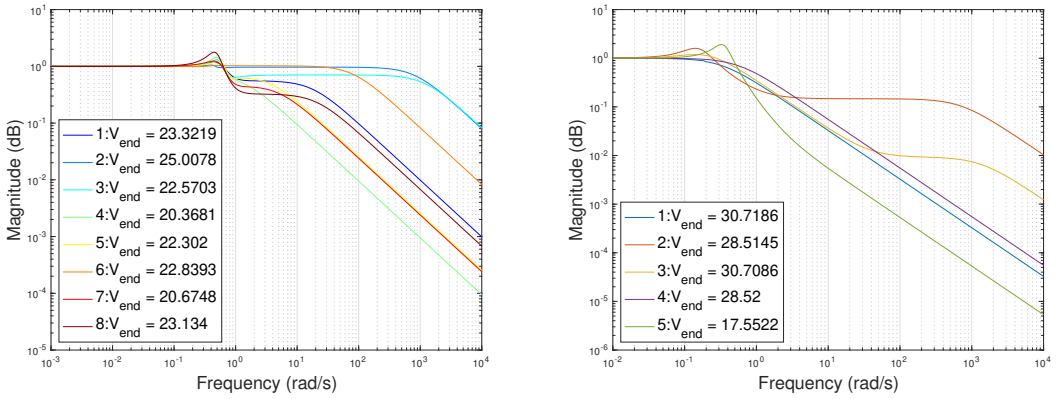

(a) North-Holland CACC experiment

(b) Southwest ACC experiment

Figure 5.27: Frequency response for the found transfer functions for deceleration manoeuvres

5.1.7. Summary for longitudinal vehicle dynamics

It was shown that in different FOT different system behaviours do appear when comparing similar driving situations. For the unaccelerated *stable* car-following, the median time-headways are in between 1.15 to 2.96 seconds for all regarded experiments. Moreover, the distributions correspond to a logarithmic normal distribution in all test.

- Time-headways in between 1.15 to 2.96 seconds
- Time-headways are logarithmic normal distributed

For the *sustained stable* car-following, the expected logarithmic normal distribution of the time-headway does not appear at first glance in all experiments. In two out of three FOTs, the time-headway distribution shows two peaks. By splitting the time-headways by the speed driven during the data record, the two-peak distributions are broken down into several individual-peak distributions of a logarithmic normal distributed shape. Furthermore, a shift of the median time-headway to lower values can be found for rising velocities in all data-sets. This shift represents a change of the parameter τ_h introduced in Section 3.1.4.

- Multiple peaks in overall time-headway evaluation
- Several logarithmic normal distributions of time-headway for different velocities
- Time-headway and velocity are correlated

Accelerated car-following with the use of ACC systems results in extended time-headways during the acceleration phase and the presence of the logarithmic normal distribution for time-headway in all experiments. If the perspective is changed from a general acceleration phase to a more fixed acceleration manoeuvre, differences in the system responses of the vehicles in each experiment become visible. By simply looking at the time-headways, only statements about the distributions and the median values of these time-headways can be made. Describing the phenomena appearing during the acceleration manoeuvre helps to understand how the following vehicle is approaching its leader's velocity and the desired headway. In particular, the system response of the speed of the following vehicle is of second-order for commercially available vehicles and of first-order for the CACC equipped vehicles in the North-Holland experiment. This knowledge is used for the estimation of transfer functions linking the following vehicle velocity as the system output and the leading vehicle velocity as the system input. Evaluating step and frequencies responses of the found transfer functions show the differences of the regarded systems. ACC systems show critical frequencies where the magnitude maximises, while the CACC system does not.

- Extended time-headways for accelerating leading vehicle
- Logarithmic normal distributed time-headways
- Second order system response for the velocity of the following vehicle to a speed change of its leader for ACC systems and first-order for CACC systems

For *decelerated* car-following the median time-headways in all experiments are lower than for *accelerated* and *steady* car-following. All experiments show the expected single peaked logarithmic normal distributions. The clear advantages of the CACC system over the ACC system, which was previously established, are no longer observed. The increased dynamics during braking operations allow both systems to react with equal quality. In addition, time-headways in the Ispra, Ispra-Cherasco, and Gunther experiments are closer to the median, and outliers occur less frequently than for *accelerated* or *stable* car-following. This shows

once again that sudden deceleration, which describes the more critical acceleration state, is faster achieved by the system of ACC controller and vehicle. These increased dynamics of the ACC and CACC system are reflected in the estimation of transfer functions, which describe the velocity of the vehicle as a SISO system for a fixed deceleration manoeuvre. In order to achieve high-quality matching results, the additional introduction of pole numbers and zeros in the transfer functions is necessary. This adjustment results in high dynamics for step responses of the velocity signals. The critical frequencies for the transfer functions of deceleration manoeuvres are in the same range as the frequencies for acceleration manoeuvres. When comparing this to the frequencies found in the space-headway signal around the average space-headway for a *sustained stable* car-following, the appearing frequencies in the space-headway signal are in the same range as the critical frequencies at which a magnitude increase occurs for both acceleration and deceleration transfer functions. Frequencies in the space-headway signal are in some cases around $0.1 Hz = 0.62^{rad}/_{s}$. Critical frequencies of the estimated transfer functions for both acceleration and deceleration manoeuvres are in the range of $0.5^{rad}/_{s}$. Therefore, following in a platoon with multiple ACC equipped vehicles is per se unstable. This was stated by [115] and [61] before.

- Lowest median time-headways during deceleration
- Logarithmic normal distributed time-headways
- Increased dynamics during braking phases of the leading vehicle
- Critical frequencies of the SISO TFs for deceleration manoeuvres meet the oscillation of space-headway for *sustained stable* car-following

5.2. Lateral vehicle dynamics

The steps carried out to calculate the lateral acceleration in the regarded Tesla experiment are given in Figure 5.28. All four figures belong to one single experiment carried out in one day. In total, there are 13 independent test rides present in the data-set. Firstly, for each of these tests, the lateral acceleration is calculated, and the lateral distance is linked to the acceleration. Finally, the linked results are summed up and compared.

Figure 5.28a presents the driven test route during the experiment starting at the *Raasdorp interchange* and ending at *Knooppunt de hoek*. It is visible that urban and suburban roads are present in the test route as well as motorways and inner-city highways. The present velocities during the test drive are given in Figure 5.28b. The occurrence of motorways and normal streets mentioned previously is also visible here. On motorways, the velocities are higher (red) than on inner-city highways (orange) and inner-city streets (green/blue). The estimated curve radii are presented in Figure 5.28c. The higher curve radii at motorway sections and the lower radii on the inner-city streets are evident. Straight sections show scattering curve radii of ±5000 (dark red/dark blue) as the algorithm is sensitive to small changes in latitude and longitude on straight roads. However, since the curve radius is the denominator of the lateral acceleration and accelerations below a certain threshold are considered representative of straight driving, as introduced in Chapter 4, the resulting scatter of curve radii is not significant. Figure 5.28d finally represents the lateral accelerations during the test drive. The lateral acceleration is mainly around $0^{rad}/_{s}$, and therefore the vehicle state is driving a straight road segment. When the vehicle is approaching a curve, the colouration of the driven path is changing. First small lateral accelerations appear right after the curve entry, then higher accelerations are present right next to the curve vertex and vice versa. This linear increase is due to the infrastructural curve shaping that is known as a clothoid shape [111], which causes

the curve radius as well as the lateral acceleration[2] to increase linearly.

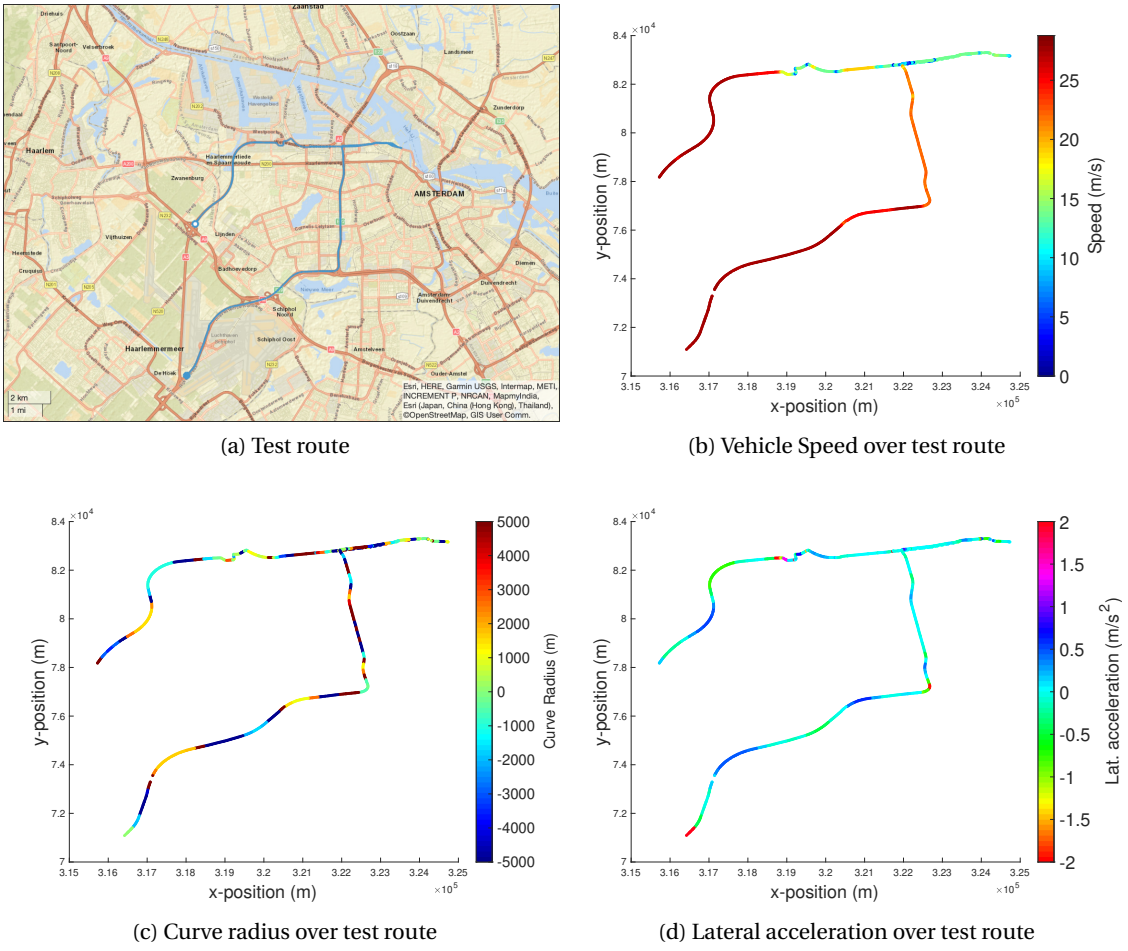

(a) Test route

(b) Vehicle Speed over test route

(c) Curve radius over test route

(d) Lateral acceleration over test route

Figure 5.28: Steps for lateral acceleration estimation

When considering the appearing and analysable[3] lateral accelerations out of all test drives, Figure 5.29 gives the present distribution. Sub-figure 5.29a presents the normalized lateral acceleration distribution for all test rides. The predominance of straight driving segments mentioned above leads to the distribution shown in this sub-figure. Mainly lateral accelerations around $0^{rad}/_{s}$ do appear corresponding to driving straight. Besides that, there is an almost symmetrically occurrence of higher lateral accelerations for either left or right turns around this mean value. The maximal lateral accelerations estimated are around $\pm 2\frac{m}{s^2}$. This value marks the functional limit of the LCA system as well. In Figure 5.29b the lateral acceleration distribution is given for values greater than $\pm 0.05^{m}/_{s^2}$ in total numbers of appearing points. Considering the total number of appearing data points for left and right curves it is outstanding that in sum, more valuable data points are found for left curves than for right curves, although the test route is an open right curve, compare Figure 5.28a. This asymmetry is due to several factors. On the one hand, sharper left-hand bends occur when driving on motorway sections, Figure 5.28c, and on the other hand, only data points are considered at which the LIDAR sensors function properly. These factors lead to an uneven distribution of

[2] Provided that the speed remains the same

[3] Only data points are considered where both, the lateral acceleration estimation and the LIDAR signal are valid.

the lateral accelerations for left and right turns. Although the lateral acceleration distribution for left and right curves are not equal and more data points for left-hand bends occur, the division into the prior introduced curve types *light* and *strong* is still done. This is maintained because for both left and right bends over 250 data points are found presenting the basic population.

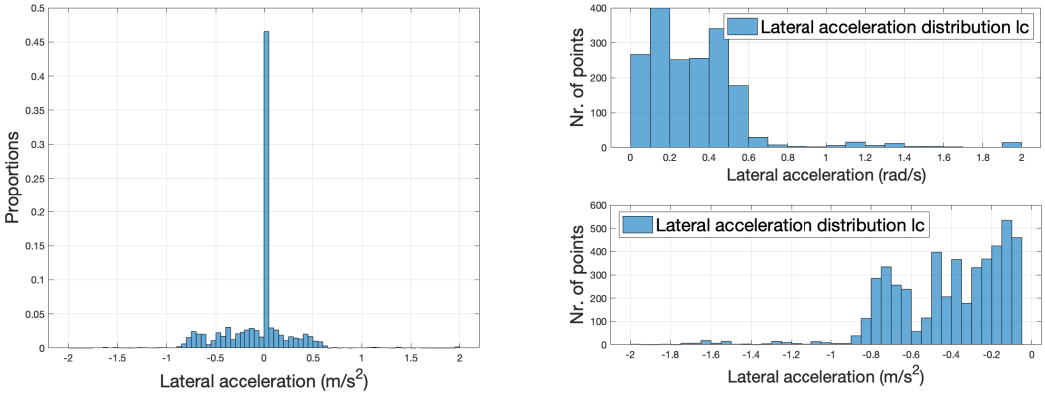

(a) Total lateral acceleration distribution in all test drives

(b) Lateral acceleration for left and right curves

Figure 5.29: Distribution of lateral acceleration in all test drives

5.2.1. Lateral vehicle dynamics when driving straight ahead

The LIDAR-distance measurement results of the sensors mounted on each side of the vehicle, as described in Chapter 4, are shown in Figure 5.30. The blue histogram shows the results of the left LIDAR sensor, the orange histogram the results of the right one. Remarkable is the high peak values of the two normalised distributions, as well as the low dispersion around these median values. The fact that the distributions of the right and left sensors do not have the same or almost the same median value indicates that the vehicle is not moving precisely in the middle of the road on straight sections. Instead, it maintains a smaller distance to the road markings on the left than to the right. Since the experimental set up is symmetrical, driving in the middle of the lane should correspond to equal distances to the left and right lane markings.

5.2.2. Lateral vehicle dynamics when driving in curves

When the vehicle is driving through curves, its position in the lane changes, as described in section 3.2, the LCA controller uses a feed-forward control strategy to minimise the lateral position error e_1 and to meet the yaw rate ψ_{des} required by the road infrastructure. Steady-state cornering, achieving both error terms to be zero simultaneously, is not possible in general for LCA systems throughout the entirety of appearing yaw-rates. Therefore, lateral deviations around the lane centre occur as a result. This lateral deviation around the lane centre in curves is shown in Figure 5.31.

Firstly, the distributions of the distance in relation to the lane centre are given for each type of detected curve, with lateral acceleration greater than $0.05^{m}/_{s^2}$ in the top graphs of sub-figures 5.31a and 5.31b. Sub-figure 5.31a represents the results for left-hand bends recorded by the left-hand LIDAR sensor. Sub-image 5.31b shows the lateral distances for right-hand curves captured by the right-hand LIDAR sensor. The two lower sub-figures represent the

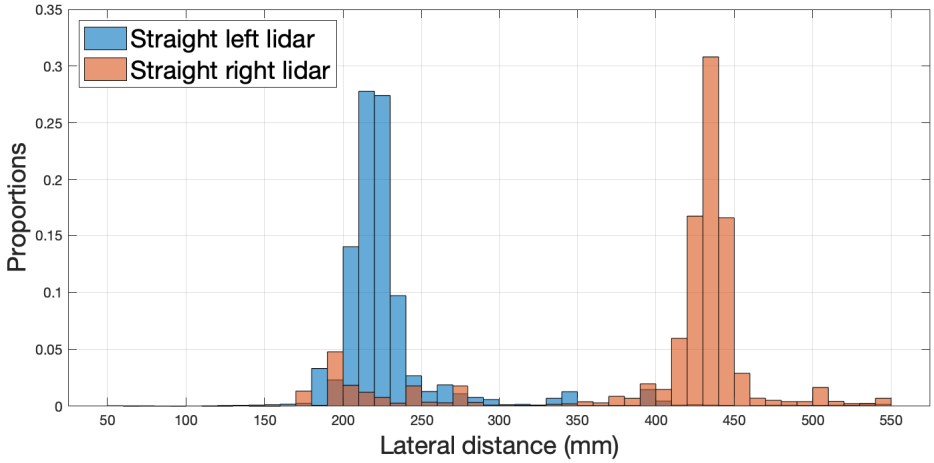

Figure 5.30: LIDAR signal from left and right sensor for straight ahead driving

Empirical Distribution Function (EDF)s of the above-shown distributions for left and right curves. It is noticeable that two peaks occur in both distance distributions. This characteristic means that during cornering, the vehicle moves back and forth between the sides of the lane or curves are driven at different distances from the road markings. In addition, when comparing the EDFs of the distance distributions in the lower graphs, the trend becomes visible that the vehicle tends to drive on the left side of the road even in right-hand bends. The EDF for left-hand bends in sub-figure 5.31a reaches a value above 0.6 for lateral deviations up to $400mm$, while the EDF for right-hand bends in sub-figure 5.31b remains below 0.5 for the same range.

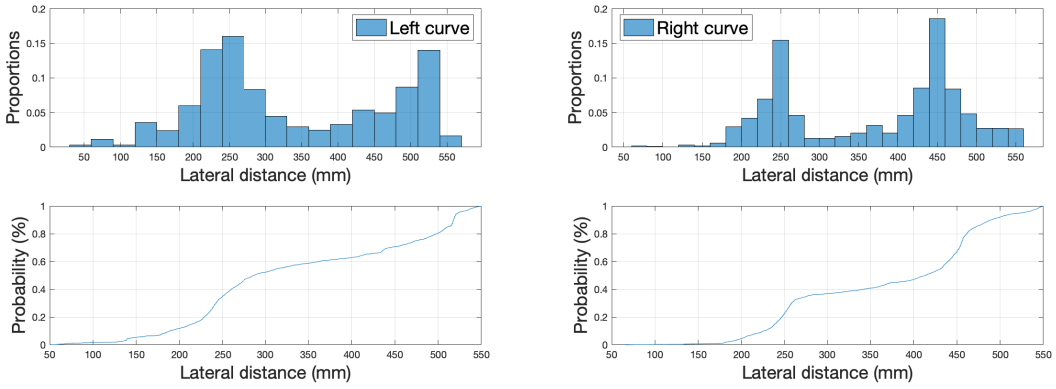

(a) Left curves

(b) Right curves

Figure 5.31: Lateral distance distribution in all curves

Splitting up the distributions prior mentioned of each curve into the introduced curve types *light* and *sharp* leads to the distributions and EDFs given in sub-figure 5.32a and 5.32b. The top graphs show the distribution of lateral distance to the lane centre for the two classes of curves. The two lover graphs represent the EDF of the top histograms. In both classes of curves, *light* and *sharp*, two peaks appear in the distance distribution, regardless of whether the curves are right or left. The above-mentioned oscillating lateral vehicle movement in its lane, therefore, occurs during all cornering, regardless of the lateral acceleration. The occur-

rence of two main distances is particularly prominent in *light* left curves. In *sharp* left turns, the vehicle drives more on the left side of the road, as it can be seen in the comparison of the EDFs for left turns. The probability that the vehicle remains at a distance under $300mm$ is above 60% in sharp turns while it is under 50% in *light* left turns. During right turns, the differences are less prominent. The vehicle is still driving more on the left lane side, shown by the fact that the probability that the vehicle is maintaining a distance to the right lane marking of less than $400mm$ is under 50%.

5.2.3. Summary for lateral vehicle dynamics

For the evaluation of automated lateral vehicle dynamics, the distance to the lane markings is evaluated. Since the road width between highways, urban motorways and urban roads changes and it is not always possible to estimate the actual road width, the distances to the road markings on the left and right side of the vehicle are considered instead of the D2CL. Different road infrastructure appears in the data-set, but this thesis is limited to straight sections and curves of different curvature divided into *sharp* and *light*.

On straight road sections, there is a tendency for the vehicle to drive on the left side of the lane. There is a logarithmic normal distribution with two asymmetrical flanks of the curve. The vehicle avoided small distances to the left and right roadside more than large ones.

This trend is also present when driving through both left and right-hand bends. It is even more evident in *sharp* curves than in *light* ones. All distributions representing the distance to both the left and right lane markings show two peak values. These peaks represent a lateral back and forth movement of the vehicle on its lane during cornering. This occurrence of two peaks was also observed during the evaluation of straight-ahead driving. Due to the changed proportions of the histogram, the second peak is not visible there.

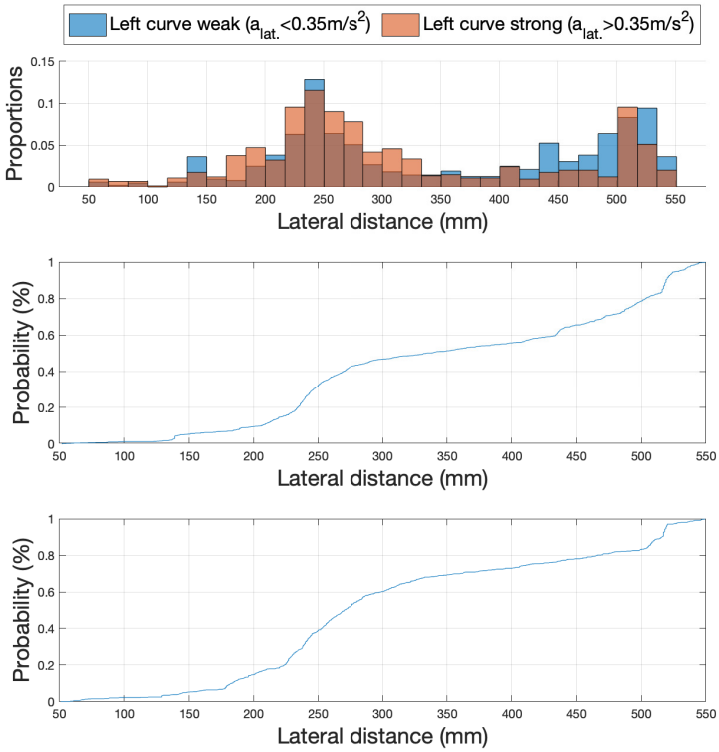

(a) Left curves

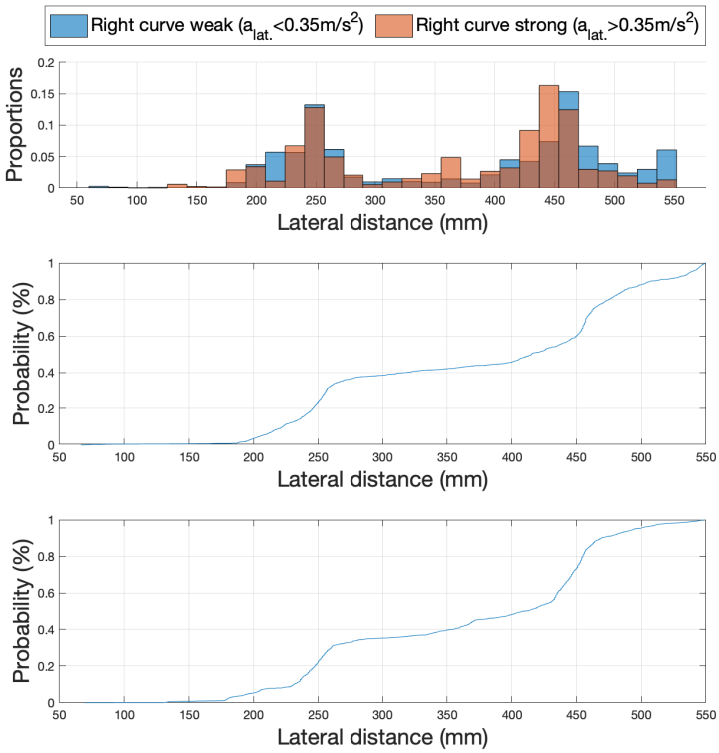

(b) Right curves

Figure 5.32: Lateral distance distribution for curves different curvature

6

Conclusion

6.1. Summary

This research developed a methodology to assess the vehicle dynamics in automated traffic. Mainly, state of the art ADAS systems are regarded. This research differed between lateral and longitudinal vehicle dynamics, and this distinction was maintained throughout. The considered systems are ACC, CACC and LCA. The results are mainly intended for the use by transportation and vehicle scientists researching in the field of automated traffic and the development of ADAS. Therefore, the results are generic for further use. The research methodology followed three steps for lateral and longitudinal vehicle dynamics respectively to archive this generality.

Firstly, the automated vehicle movement and the control strategies of the controllers involved are thoroughly described. From this accurate description of the system consisting of vehicle and controller, the variables that influence the automated vehicle movement are derived. A data-driven approach is followed using multiple FOTs.

Secondly, the methodology to investigate the prior identified parameters is developed. Since driving has multiple degrees of freedom, driving states and manoeuvres are defined to divide driving situations and to find the control system variables to describe the automated driving in these situations. For longitudinal vehicle dynamics acceleration, deceleration and steady driving are regarded. For lateral vehicle dynamics a distinction based on the infrastructure, in our case the curves, the vehicle is driving, is made.

Thirdly, the described methodology is used to evaluate multiple data sources from different research institutions. The used FOTs are described shortly, the potentials of their use, and their characteristics are presented. The data structure of the individual FOTs was adapted, and all data-sets for longitudinal and lateral vehicle dynamics are evaluated under the same condition, respectively. This evaluation derives values for the influencing variables for automated vehicle movement.

This chapter concludes the thesis by answering the research questions proposed in chapter 1, discussing the main scientific contributions of this work, listing the limitations of the thesis, and finally giving recommendations for possible further research on this field.

6.2. Answers to the research questions

In Chapter 1, research and sub-research questions were proposed concerning the necessary steps in the evaluation of vehicle dynamics for automated traffic. Here the five sub-questions are answered first, followed by the main research question.

- *What previous research is available and what methods were used to investigate vehicle dynamics?*

The impacts of ADAS have been subject to various research in the last years. Aspirations were to create models to produce realistic predictions of the effects of ADA systems on traffic. For longitudinal vehicle dynamics, with ACC and CACC systems used, research is focusing on platoon stability as well as the occurrence of congestion when variate influencing parameters like marked penetration or default headway settings. Most research is simulation-based and uses estimated parameters for system response times, default headways and other dynamic parameters. Lesser research investigates in real driving experiments. The used methods to describe longitudinal vehicle dynamics are the comparison of time or space-headways in different driving situations as well as the estimation of transfer functions to rebuild the system response on a velocity input.

For lateral vehicle dynamics, field tests have been carried out to evaluate the psychological aspects of automated lane guidance, the Operational Design Domain (ODD) the vehicle is capable of driving in or the effects of different lane marking conditions on the LCA system. All studies had in common that the surrounding environment, and in cases of psychological effects are evaluated the driver, is observed. Distances to the lane markings, captured by LIDAR or video distance estimation, therefore, is a standard method to describe the lateral driving. Simulation studies have been focusing on the impacts of certain driving manoeuvres and vehicle quantities on the accuracy the vehicle is following the lane.

- *How do the considered ADA systems work and what are their degrees of freedom?*

The considered ADA systems are ACC and its more sophisticated variant CACC for longitudinal movement and LCA systems for lateral vehicle movement.
Longitudinal vehicle control follows the approach to maintain a constant time-gap to the leading vehicle by using the vehicle's brakes and engine. This constant time-gap leads to a linear adaptation of the space-gap between the vehicles over different velocities. The default time-gap is a degree of freedom in ACC and CACC systems. Besides that, the variables τ and λ introduced in Chapter 3 describe the dynamics of the system of controller and vehicle maintaining an acceleration manoeuvre of the vehicle in front.

The purpose of lateral vehicle control systems is following the path given by the road infrastructure. The LCA mainly accesses the steering system and adjusts the steering angle. Therefore, it can affect the position of the vehicle in its lane and its turn rate around the height axis. The control strategy of LCA systems is minimizing the yaw-rate and centreline distance error terms to zero. Setting both error terms to zero is generally not possible for LCA systems. Instead, there is a trade-off between track deviation and the achievement of the required yaw-rate. There are various degrees of freedom like the feedback matrix K that is used for the controller, the properties of the FFC, the under-steer gradient K_v, and the driving dynamic quantities of the vehicle itself. Since the LCA system has multiple degrees of freedom and the experiment under consideration was carried out on real roads rather than on a test site with a defined test plan, a more objective description of the phenomena caused by the LCA system

is pursued. Therefore, the parameter under consideration is y_{off}, which is measured as an external observer and related to the lateral acceleration occurring during the test drive.

- *How to describe the lateral and longitudinal vehicle dynamics objective and generic?*

By investigating in the basic principles of ADA systems, the degrees of freedom and the system inputs are known. The longitudinal dynamics of the vehicle are described by defining different driving situations. For longitudinal automated driving suitable situations are *stable*, *sustained stable*, *accelerated* and *decelerated* car-following. All these situations cover different parts of the driving task fulfilled by the ADA system. To describe the distance between the two vehicles, the space- or the time-headway is used, whereby the time-headway is more suitable because the previously presented CTG distance policy considers the parameter τ_h as input. The time-headway is linked to the space-headway with the basic equation for velocity $v = {}^{s}/_{t}$. The parameter τ_h is calculated for all defined driving situations to evaluate what the typical distances between the vehicles in the situations are. To gain insight into dynamic manoeuvres like speeding up or decelerating, the evaluation of the time-headway on its own is insufficient. Therefore, it is searched for fixed acceleration and deceleration manoeuvres. The speed must decrease or increase by a certain amount and then remain constant for several seconds. All characteristics of the velocity of the following vehicle are discussed. Besides that, transfer functions are estimated, which have the velocity of the leading vehicle as an input signal and the followings vehicles velocity as output. This estimation allows us to make precise statements about the system's behaviour when vehicles accelerate and brake.
In lateral vehicle dynamics, further, the degrees of freedom of the ADA system are present. Due to various uncertainties and unknown control system characteristics, merely an objective description of the lateral track guidance is given. A variable for the lateral offset y_{off} to the lane centre, in the control strategy of LCA systems, is identified. This lateral offset is also determined in various driving situations while the vehicle is driving in different infrastructure. *Light* and *strong* curves are differentiated depended on the lateral acceleration in turns. The lateral lane centre offset is evaluated considering the driven curve sharpness. This approach allows us to make conclusions concerning the probabilities of the vehicle being in its lane at a defined distance from the lane centre for different kinds of turns.

- *What is the impact of different driving manoeuvres on the movement of the vehicle?*

This research question is covering longitudinal vehicle dynamics. During *stable* and *sustained stable* driving the following vehicle keeps a constant time-gap to its leader. Time-headway and velocity correlate. High velocities cause the time-headways to be smaller than for low velocities. For an accelerating leading vehicle with acceleration grader than, $0.5\,{}^{m}/_{s^2}$, the time-headways are extended as the follower tries to maintain the speed profile of the leader. Due to engine dynamics, vehicle inertia masses, and controller time lag, the velocity of the leading vehicle cannot be maintained instantaneously, and the time-headway increases. For deceleration phases where the acceleration is below a threshold of $-0.5\,{}^{m}/_{s^2}$, time-headways stay in the same range as for *stable* and *sustained stable* car-following. It is shown that deceleration of the leading vehicle can be adapted faster by the follower that acceleration. In addition to this classification of phenomena occurring during acceleration situations, the data sets are searched for fixed acceleration manoeuvres that follow a defined velocity profile. Thus, transfer functions between the speed of the leading vehicle as input and the speed of the following vehicle as output can be estimated. The evaluation of the transfer functions found also shows the increased dynamics of the following vehicle when the vehicle in front brakes. The step responses of the transfer functions for deceleration manoeuvres show higher dynamics compared to those estimated for acceleration manoeuvres.

- *How does the vehicle drive interacting with different infrastructure?*

For the LCA data-set considered, the vehicle tends to drive more on the left side of the lane in all driving situations. For *straight* driving, this effect was firstly shown by comparing the LIDAR distances to the lane markings captured on both sides of the vehicle. When evaluating curve driving, this effect remains even in right-hand bends. Striking is that in *sharp* left and right turns the vehicle tends to drive on the left side of the lane rather than in *light* curves. In all situations, whether they are classified as *straight* driving, *light*, or *sharp* curves, a lateral oscillating movement of the vehicle in its lane is present. This effect especially applies in curves.

- *What are the differences between the investigated data-sets for longitudinal and lateral driving?*

Five data-sets were used to evaluate the longitudinal vehicle dynamics. Four FOTs used ACC systems and one is using a CACC system. The differences between ACC and CACC systems are striking. CACC consistently showed better performance in terms of time-headway and stability over ACC systems. It was capable of operating at smaller time-headways in all driving situations and responded more precisely to changes in the speed of the leading vehicle. The time-headway shift for *sustained stable* car-following is found in all data sources. Besides that, there are differences in the data acquisition between the FOTs. All experiments used different state of the art ACC systems. The systems differ in the default time-gap setting and in the dynamic behaviour for acceleration and deceleration manoeuvres. The estimated transfer functions for acceleration manoeuvres showed a minimized settling time for a unit jump in the North-Holland experiment compared to the Southwest experiment. For deceleration manoeuvres, the differences are less prominent due to the increased system dynamics. The time-headways for *decelerating* do not differ as much from the time-headways for *stable* or *sustained stable* car-following as the time-headways for *accelerated* car-following do.

For the lateral vehicle dynamics, only one data source is evaluated in this thesis. Therefore, a comparison is not possible. Nevertheless, the evaluation carried out should help to gain insight into the lateral vehicle dynamics of ADA systems and to encourage further research.

In conclusion, the answer to the main research question

- *How do AVs drive interacting with different infrastructure and other vehicles on the road?*

The interaction of AVs with other road participants, in general other vehicles, are the following. The time-headways the proceeding AV maintains to the leading vehicle are in between a range of 1.13-2.96 seconds for *stable* car-following. For an accelerating leader, the time headways are increased to values of around 1.38-3.0 seconds. Deceleration of the leading vehicle causes the time-headways to shrink down to 1.04-2.43[1] seconds. During braking manoeuvres, the time-headway is closer to the values of stable car-following and therefore are deceleration phases of the leading vehicle adopted by the ACC or CACC systems with higher dynamic. The paths in a space-headway diagram going from one velocity to another are not equal for acceleration and deceleration. There is a fundamental difference in the curvature of the trajectories. Acceleration manoeuvres show concave progressions while braking

[1] Neglecting the Ispra experiment

manoeuvres are convex. The time-headway the following vehicle maintains to its predecessor is not constant over the range of velocity. Vehicle-following with higher velocities shows decreased time-headways. Thus, velocity and time-headway are correlated. The dynamic response to inputs of the leading vehicle also reveals the differences in acceleration and deceleration manoeuvres. Vehicle deceleration can be achieved faster than acceleration by the ADA system.
For the interaction of the vehicle with surrounding infrastructure, in this research curves, the following was found. The vehicle shows a biased driving on the left side of the lane, rather than being meanly centred. This bias applies to left and right curves and is noticed throughout the curve sharpness, whereby it is even more visible in curves that are, by definition, *sharp*. Additionally, a lateral oscillation of the vehicle in its lane is present.

6.3. Main contributions

Time-headways at high speeds are shorter than at low speeds
For all FOTs, it turned out that the time-headway is smaller at high driven speeds than at low speeds. The difference in time-headway is about 0.2 seconds at velocities in a range from above $21^{m}/_{s}s$ to $25^{m}/_{s}s$. This leads to the conclusion that at high velocities, the vehicle maintains a lower space-headway than it would be expected by simply observing the space-headway at low speeds. The general indication of the time-headway leaves this fact out of account. For *stable* as well as for *accelerated* and *decelerated* car-following, logarithmic normal distributions of the time-headway occur, masking the effect of time-headway variation over velocity. Only during *sustained stable* car-following, the time-headway distribution is that degenerated that it is recognized that there are several speed-dependent distributions which are added together.

The dynamics during breaking are way higher than for accelerating
It turned out that the time-headway distributions for *decelerated* and *stable* car-following are similar and have approximately equal median values in all FOTs. In contrast, the time-headway distributions for *accelerated* car-following are always shifted to larger values and the medians are increased as well. Therefore, at this point, it is concluded that decelerating can be performed with higher dynamics by the ACC system than accelerating. By estimating transfer functions for acceleration and deceleration manoeuvres, this conclusion is also supported. The transfer functions for deceleration manoeuvres show an increased dynamic for step inputs due to additional poles and zeros. The vehicles considered in the FOTs are almost capable of abruptly adjusting the speed of the driver. For CACC systems, the time-headways are slightly different. For *accelerated* car-following, the differences in time-headway compared to *stable* car-following are less large compared to ACC systems and the distributions are more stable under all driving conditions, i.e. they show conurbations.

Statistical oscillation of the space-headway around its mean value does meet the critical frequencies of the system transfer functions in some cases
The investigation of the frequency responses of the estimated transfer functions for acceleration and deceleration manoeuvres provides the critical frequencies at which an increase in magnitude is present. The investigation on the frequencies contained in the space-headway signal during *sustained stable* flowing using FFT, provides the frequencies with which the space-headway is oscillating around its mean value. The frequencies found for the space-headway oscillation around the average space-headway are for some, though not all, *sustained stable* car-following segments in the range of the critical frequencies of the estimated transfer functions of the ACC or CACC system. This can cause instability and the collapse of

vehicle platoons as already described by various scientists.

When accelerating and braking under the use of the ACC system hysteresis is present
We have seen that when the platoon of ACC vehicles is accelerating, the paths in a velocity space-headway plot are of a concave shape, whereas they are of a convex shape for deceleration manoeuvres. In other terms, the path in the diagram is not the same acceleration from one velocity to another and back. The hysteresis is less pronounced when driving with a CACC system.

The vehicle tends to drive on straight sections of road on the left-hand side of the road - this also applies to curves
The data shows that the probability that the vehicle is more likely to drive on the left side of the road is higher than for driving at the right roadside. This asymmetry was observed when comparing the distance signals from the lane markings on both sides of the vehicle. Firstly, this effect appeared when driving straight ahead and afterwards occurred in curves. When examining the distances to the road markings in curves, it was found that the effect is even more visible in curves that are, by definition, *sharp*.

There is a lateral oscillating movement of the vehicle in its lane
When the LCA system of the vehicles is activated, lateral oscillating movement of the vehicle in the lane is present. This movement happens on straight sections of the road as well as in curves. The oscillation was first detected on straight sections of the road, where it is represented by two peaks in the lateral distance distribution to the lane markings for the left and right distance. Then the movement was detected in curves as well. It is noticeable that in curves, the proportion of data points where the vehicle moves around this second peak is increased. This increase means that the vehicle drives at the second distance to the lane markings for a longer time, or the frequency with which the lateral movement occurs is raised. This observation applies particularity to *light* left curves and is less pronounced in curves that we claim as *sharp*.

6.4. Characteristic longitudinal driving manoeuvre

The following example presents the general results for the longitudinal car-following behaviour of five vehicles equipped with the same ACC system. The velocity ramp of the leading vehicle of a platoon, *Vehicle 1* is predetermined, and the same ACC system controls all following vehicles, Figure 7.1. The figure also presents the time-headway between the first three vehicles. *Vehicle 1* drives with a speed of $10^{m}/_{s}$, then it increases its speed twice by $10^{m}/_{s}$ in a period of $15s$ respectively. After a phase without acceleration, the leading vehicle brakes twice. It reduces its speed by $10^{m}/_{s}$ in a period of $10s$ respectively until it reaches the final speed.

Firstly, the driving behaviour of the following vehicles is modelled with the CTG Spacing Policy specified in (3.4) and coupled with a first-order vehicle model specified in (3.9). The results of this simulation are presented in Figure 7.1a. The used calibration parameters are $\tau_h = 2s$, $\lambda = 0.4^{1}/_{s}$ and $\tau = 1s$. The acceleration is limited to the thresholds provided by ISO 15622. Visible are the occurring speed overshoots, which are higher for deceleration phases than for acceleration phases. It is also noticeable that the time-headway error[2] is speed depended as it is less high for speed changes in the lower speed range than for higher speeds. This observation applies to brake and acceleration manoeuvres and is indicated by the higher peaks in the time-headway signal.

Secondly, a VTG spacing policy is implemented regarding the noticed time-headway shift at high velocities mentioned in Chapter 5. The default time-headway values are changed as $\tau_h = -0.04\,v + 2.73$, derived from the North-Holland ACC experiment. All other calibration parameters remain the same. It is striking that the overshoots in velocity are less severe during deceleration manoeuvres than during acceleration manoeuvres. Besides, the time-headway overshoot[3] is higher in deceleration manoeuvres than in acceleration manoeuvres. Dependence of the time-headway overshoot on the driven speed is present as well. In the lower speed range, the overshoots are more prominent.

Finally, the estimated transfer functions from the North-Holland ACC experiment for acceleration manoeuvres and the Southwest experiment for deceleration manoeuvres are implemented, referring to Chapter 5. Figure 7.1c presents the results. At a time of 130 seconds, the use of the acceleration transfer function ends, and the deceleration transfer function is activated and used until the end of the simulation. The simulation uses saturation of acceleration regarding ISO 15622 as well. Remarkable is the amplifying velocity of the vehicles downstream. Especially velocity increases in the lower speed range lead to high overshoots. For deceleration phases, the amplifying overshoots lead to instability of the vehicle platoon. The time-headways also show this instability. By adding up the amplifying values, the time-headway errors increase. This increase of the time-headway shows that the estimated transfer functions can help to understand the acceleration and deceleration behaviour of the vehicles but are not sufficient to model the whole car-following behaviour. A precise model has to take the time-headways for *steady* driving phases additional into account.

Since in this thesis only global phenomena were described, which are present during the activation of a LCA system, and not the control strategy the LCA system follows, no simulative comparison of the results can be provided. Nevertheless, the discovered global lane deviation towards the left lane side is already a very pictorial result

[2] Deviation from the default setting ($1s$)
[3] Overshoot because here the default value is changed

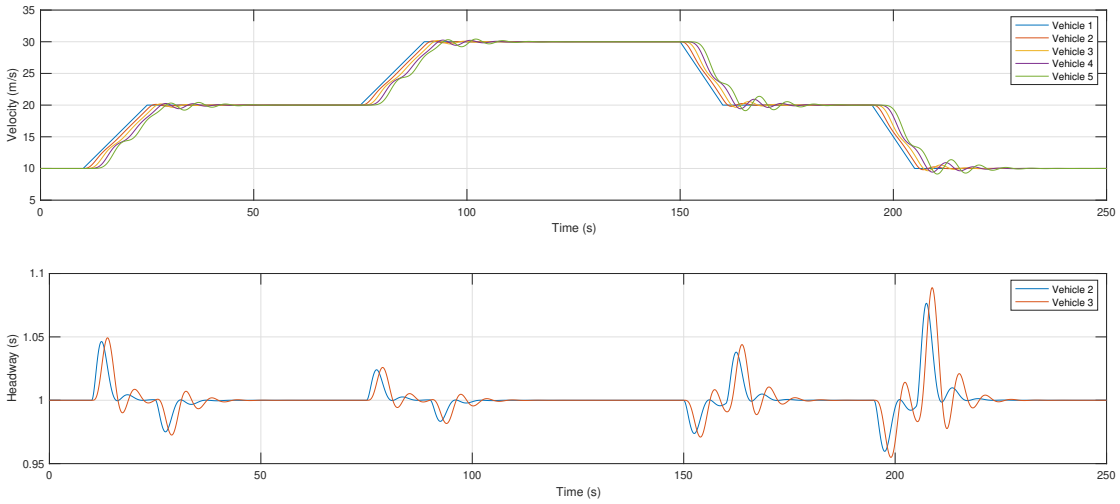

(a) CTG spacing policy

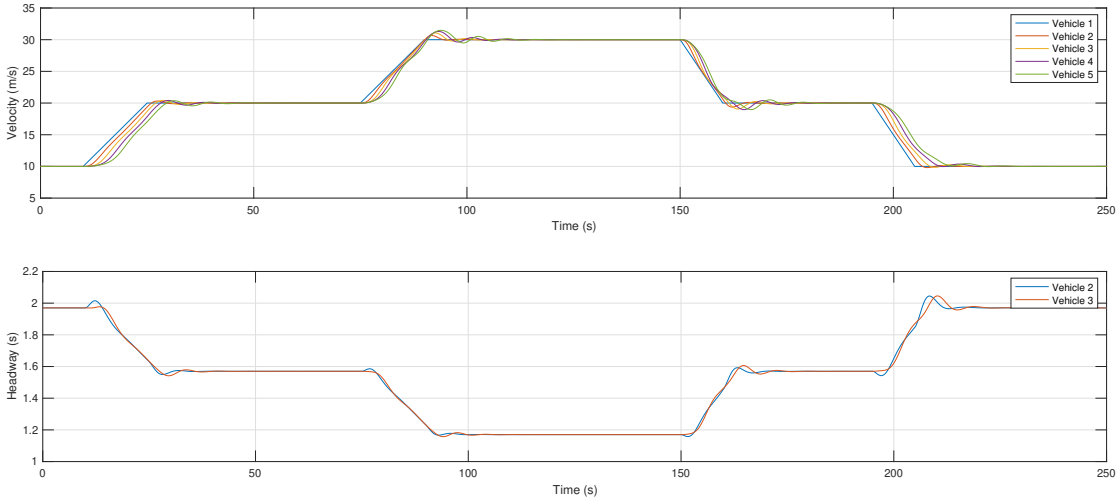

(b) VTG spacing policy

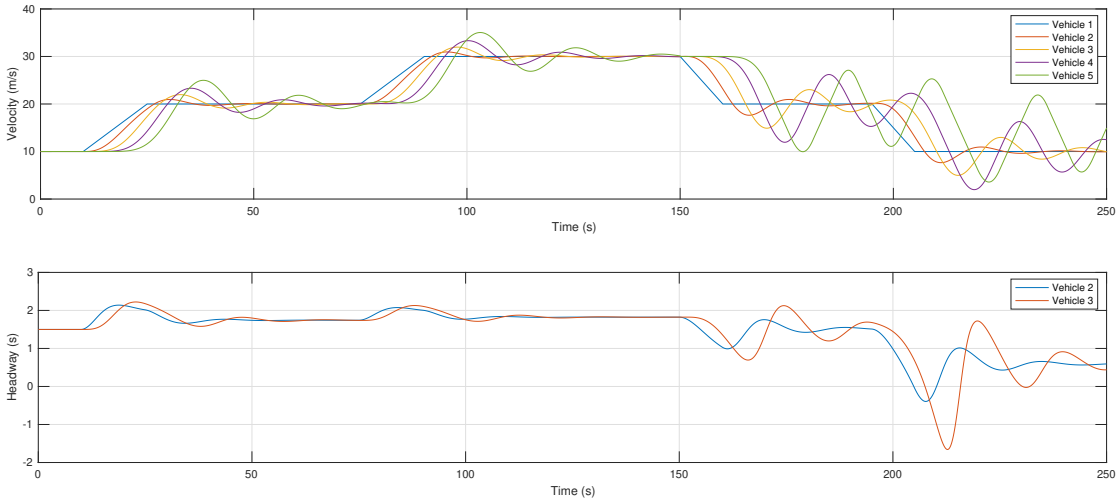

(c) Estimated transfer functions

Figure 6.1: Comparison of the CTG with the VTG spacing policy and the estimated transfer functions

6.5. Research limitations

As with any scientific work, there are limitations to this research. They are discussed hereinafter.

- For all specified driving conditions, whether they are described as *stable*, *sustained stable* or *accelerated*, the influence of the human driver must be avoided. In data-sets in which the system state of the ACC or CACC is classified, it is easy to detect human intervention. In data sources that do not contain this information, the present research uses different approaches to exclude situations of human intervention for evaluation. This concerns mainly the Ispra experiment.
- Due to the unique data acquisition of each experiment, their comparability is limited. Some data sources are not suitable for one analysis but for another. Regardless of every effort made to show comparable situations within the data-sets, we had to make assumptions, for example, for the vehicle environment and environmental influences. A genuinely accurate comparison of different ACC systems for automated driving can only be guaranteed by using the same unified test for all vehicles.
- Since no uniform test is performed to evaluate acceleration and deceleration manoeuvres, the descriptions of the phenomena caused by these manoeuvres, e.g., speed overshoot of the following vehicle or the settling time for the speed, differ widely for the data sources considered. Differences in the speed ramps and temporary drops or increases of the vehicle's acceleration that are not excluded by the manoeuvre definition lead to different speed outputs. This effect is because there are infinite ways to connect two points in a velocity-time diagram. For this reason, the estimation of transfer functions is better suited to classify the system responses to acceleration and deceleration inputs instead of the description of phenomena.
- For the estimation of the transfer functions, approaches are chosen, which show high results of the fitting accuracy of more than 85% each. It is not the aim of this research to classify the ACC systems used in their entirety and to cover all the subtleties of the control strategy. Hence, the ACC system is a SISO black box. It should be mentioned that the use of other approaches for the estimation of transfer functions can provide even higher fitting results.
- This research is limited in the field of infrastructural interaction of the vehicle as only one suitable data-set is evaluated. The considered data showed a clear trend, but it is of further interest whether other vehicles of other brands behave in the same way. Furthermore, this research only focuses on phenomena caused by automated driving with LCA systems, instead of investigating the control strategy to obtain more generic and reusable results, as it is the case with ACC and CACC systems.

6.6. Recommendations and next steps

The research field of automated driving will prospectively increase in the next years. Research that connects to the results of this work could include the following subjects. Possible next scientific steps are divided for longitudinal and lateral automated vehicle movement.

Longitudinal vehicle dynamics:

- Investigate the connection of the estimated transfer functions and the ACC and CACC control system. Try to fit the dynamic CTG ACC control parameters λ and τ to the estimated transfer functions and investigate how the differences in acceleration and deceleration behaviour can be implemented in the controller.
- A possible next step can be to study the threshold and response times of the systems. For this purpose, uniform test manoeuvres are essential to determine the exact times for leader and follower actions. A detailed knowledge of these reaction times is of high interest for traffic planning and safety assessments.
- A cross-correlation study, taking into account vehicle dynamics quantities such as engine power and vehicle mass, can be conducted to make predictions about the behaviour of the ACC system when implemented in different vehicles. Thus, the longitudinal behaviour of a vehicle can be predicted even better.

Longitudinal vehicle dynamics:

- A goal for further research is to find more suitable data-sets to prove or debunk the general hypothesis that LCA systems drive the automated vehicle on the left side of the road rather than exactly in the middle.
- In addition, future research can investigate the performance of different LCA systems in the same test environment and find out what differences exist when performing the same driving manoeuvres. Possible identification tests could be trajectory return or an open loop circular driving test following ISO 4138:2012.
- Further investigations of the LCA control strategy and influencing parameters, in particular by feed-forward road curvature estimation and linking the results with driving performance tests, are also a possible field for further research.
- If further details concerning the LCA control strategy are revealed, the oscillating vehicle movement in its lane, as shown in this thesis, can be further investigated. Especially the occurring frequencies are of interest as well as whether there are differences in the occurrence of the oscillation in curved and straight road sections.

Acronyms and Abbreviations

ACC Adaptive Cruise Control

ADAS Advanced Driver Assistance Systems

ADA Advanced Driver Assistance

AVs Automated Vehicles

AV Automated Vehicle

CACC Cooperative Adaptive Cruise Control

CSG Constant Space Gap

CTG Constant Time Gap

D2CL Distance to Centre Line

EDF Empirical Distribution Function

FFC Feed Forward Controller

FFT Fast Fourier Transformation

FD Fundamental Diagram

FOT Field Operational Test

FOTs Field Operational Tests

GPS Global Positioning System

HMI Human Machine Interface

IDM Intelligent Driver Model

IO Input-Output

LCA Lane Centering Assistant

LKS Lane Keeping System

LKA Lane Keeping Assistant

LIDAR light detection and ranging

MLIT Ministry of Land, Infrastructure, Transport and Tourism

OEM Original Equipment Manufacturers

ODD Operational Design Domain

SFC State Feedback Controller

SISO Single Input Single Output

SRQ sub-research questions

TF Transfer Function

VM Vehicle Model

VTG Variable Time Gap

V2V Vehicle to Vehicle

V2I Vehicle to Infrastructure

A

Appendix I

Data sets for longitudinal vehicle dynamics

Province Noord-Holland Prius experiment

Location:	Noord Holland, The Netherlands
Institution:	TNO
Date:	15 February 2019
Contact person:	Simeon C. Calvert
Documentation:	[54]
Derived articles:	[11]
Used System:	ACC and CACC
Test environment:	Public road
Short description:	This field operated test is focusing on inter vehicle movement, V2V communication as well as on V2I communication. The used vehicles where seven Toyota Prius equipped with the Toyota ACC system and an by TNO developed CACC system.

European Commission Joint Research Center Ispra ACC experiment

Location:	Ispra, Italy
Institution:	European Commission Joint Research Center
Date:	2018
Contact person:	Michail Makridis
Documentation:	To be searched
Derived articles:	[66] [65]
Used System:	ACC
Test environment:	Test track
Short description:	This field operated test is focusing on inter vehicle movement. The used vehicles where one Fiat and one BMW booth equipped wit a on board ACC system. The BMW is following the human driven Fiat.

Vanderbilt ACC string stability experiment

Location:	Southwest, USA
Institution:	Vanderbilt University
Date:	2019
Contact person:	George Gunter
Documentation:	[36]
Derived articles:	[36]
Used System:	ACC
Test environment:	Public road
Short description:	This experiment assess the string stability of several newer date model year adaptive cruise control ACC equipped vehicles. The research analyzes seven distinct vehicle models using data collected from more than 1900 kilometer of driving in a car-following constellation with ACC engaged by the following vehicle.

Data sets for lateral vehicle dynamics

Shubhams Data set i have to find the proper name

Location:	Amsterdam, The Netherlands
Institution:	Royal HaskoningDHV, TU Delft
Date:	2019
Contact person:	Shubham Bhusari
Documentation:	[7]
Derived articles:	[24]
Used System:	LKA
Test environment:	Public road
Short description:	This experiment assess the position of a vehicle in a test drive both on motorways and in cities. The used vehicle is a Tesla model s whose autopilot is permanently activated. When the vehicle asks the driver to take over, the driver only intervenes briefly.

Bibliography

[1] Kayvan Aghabayk, Majid Sarvi, and William Young. Understanding the dynamics of heavy vehicle interactions in car-following. *Journal of Transportation Engineering*, 138 (12):1468–1475, 2012.

[2] T. P. Alkim, G. Bootsma, and S. P. Hoogendoorn. Field operational test "the assisted driver". In *2007 IEEE Intelligent Vehicles Symposium*, pages 1198–1203, 2007.

[3] Florent Altché and Arnaud de La Fortelle. An lstm network for highway trajectory prediction. In *2017 IEEE 20th International Conference on Intelligent Transportation Systems (ITSC)*, pages 353–359. IEEE, 2017.

[4] Dennis N Assanis, Zoran S Filipi, Scott B Fiveland, and Michalis Syrimis. A predictive ignition delay correlation under steady-state and transient operation of a direct injection diesel engine. *J. Eng. Gas Turbines Power*, 125(2):450–457, 2003.

[5] Zevi Bareket, Paul S Fancher, Huei Peng, Kangwon Lee, and Charbel A Assaf. Methodology for assessing adaptive cruise control behavior. *IEEE Transactions on Intelligent Transportation Systems*, 4(3):123–131, 2003.

[6] Andre Benine-Neto, Stefano Scalzi, Said Mammar, and Mariana Netto. Dynamic controller for lane keeping and obstacle avoidance assistance system. In *13th International IEEE Conference on Intelligent Transportation Systems*, pages 1363–1368. IEEE, 2010.

[7] Shubham Bhusari. A methodology for the assessment of operational design domain for lane keeping system equipped vehicles: The case of tesla model s. Master's thesis, TU Delft, 2018.

[8] Shubham Bhusari. A methodology for the assessment of operational design domain of lane keeping assistance system equipped vehicles: The case of tesla model s. Master's thesis, TU Delft, 2018.

[9] Arnab Bose and Petros A Ioannou. Analysis of traffic flow with mixed manual and semiautomated vehicles. *IEEE Transactions on Intelligent Transportation Systems*, 4(4):173–188, 2003.

[10] Simeon C. Calvert and B van Arem. A generic multi-level framework for microscopic traffic simulation with automated vehicles in mixed traffic. *Transportation Research Part C: Emerging Technologies*, 110:291–311, 2020.

[11] Simeon C. Calvert and Bart van Arem. Cooperative adaptive cruise control and intelligent traffic signal interaction: A field operational test with platooning on a suburban arterial in real traffic. Unpublished, 2019.

[12] Simeon C. Calvert, TH A van den Broek, and Martijn van Noort. Cooperative driving in mixed traffic networks—optimizing for performance. In *2012 IEEE Intelligent Vehicles Symposium*, pages 861–866. IEEE, 2012.

[13] Christopher R Carlson, J Christian Gerdes, and J David Powell. Practical position and yaw rate estimation with gps and differential wheelspeeds. In *Proceedings of AVEC 6th International Symposium*, 2002.

[14] Bo-Chiuan Chen, Bi-Cheng Luan, and Kangwon Lee. Design of lane keeping system using adaptive model predictive control. In *2014 IEEE International Conference on Automation Science and Engineering (CASE)*, pages 922–926. IEEE, 2014.

[15] Yan Chen and Junmin Wang. Adaptive vehicle speed control with input injections for longitudinal motion independent road frictional condition estimation. *IEEE Transactions on Vehicular Technology*, 60(3):839–848, 2011.

[16] Swaroop Darbha and K.R. Rajagopal. Intelligent cruise control systems and traffic flow stability. *Transportation Research Part C: Emerging Technologies*, 7(6):329 – 352, 1999. ISSN 0968-090X. doi: https://doi.org/10.1016/S0968-090X(99)00024-8. URL `http://www.sciencedirect.com/science/article/pii/S0968090X99000248`.

[17] Swaroop Darbha and KR Rajagopal. Intelligent cruise control systems and traffic flow stability. *Transportation Research Part C: Emerging Technologies*, 7(6):329–352, 1999.

[18] LC Davis. Effect of adaptive cruise control systems on traffic flow. *Physical Review E*, 69 (6):066110, 2004.

[19] Kakan C Dey, Li Yan, Xujie Wang, Yue Wang, Haiying Shen, Mashrur Chowdhury, Lei Yu, Chenxi Qiu, and Vivekgautham Soundararaj. A review of communication, driver characteristics, and controls aspects of cooperative adaptive cruise control (cacc). *IEEE Transactions on Intelligent Transportation Systems*, 17(2):491–509, 2015.

[20] Edmund Donges. Aspekte der aktiven sicherheit bei der führung von personenkraftwagen. *Automob-Ind*, 27(2), 1982.

[21] Edmund Donges. A conceptual framework for active safety in road traffic. *Vehicle System Dynamics*, 32(2-3):113–128, 1999.

[22] Daniel J Fagnant and Kara Kockelman. Preparing a nation for autonomous vehicles: opportunities, barriers and policy recommendations. *Transportation Research Part A: Policy and Practice*, 77:167–181, 2015.

[23] P Fancher, Z Bareket, and R Ervin. Human-centered design of an acc-with-braking and forward-crash-warning system. *Vehicle System Dynamics*, 36(2-3):203–223, 2001.

[24] Haneen Farah, Shubham Bhusari, Paul van Gent, Freddy Antony Mullakkal Babu, Peter Morsink, Riender Happee, and Bart van Arem. An empirical analysis to assess the operational design domain of lane keeping system equipped vehicles combining objective and subjective risk measures. *IEEE Transactions on Intelligent Transportation Systems*, 2020.

[25] Björn Filzek and Bert Breuer. Distance behavior on motorways with regard to active safety˜ a comparison between adaptive-cruise-control (acc) and driver. Technical report, SAE Technical Paper, 2001.

[26] Carlos Flores, Vicente Milanés, and Fawzi Nashashibi. A time gap-based spacing policy for full-range car-following. In *2017 IEEE 20th International Conference on Intelligent Transportation Systems (ITSC)*, pages 1–6. IEEE, 2017.

[27] Bernhard Friedrich. The effect of autonomous vehicles on traffic. In *Autonomous Driving*, pages 317–334. Springer, 2016.

[28] Hans-Thomas Fritzsche. A model for traffic simulation. *Traffic Engineering+ Control*, 35(5):317–21, 1994.

[29] Andreas Geiger, Martin Lauer, Frank Moosmann, Benjamin Ranft, Holger Rapp, Christoph Stiller, and Julius Ziegler. Team annieway's entry to the 2011 grand cooperative driving challenge. *IEEE Transactions on Intelligent Transportation Systems*, 13 (3):1008–1017, 2012.

[30] Sebastian Geyer, Stephan Hakuli, Hermann Winner, Benjamin Franz, and Michaela Kauer. Development of a cooperative system behavior for a highly automated vehicle guidance concept based on the conduct-by-wire principle. In *2011 IEEE Intelligent Vehicles Symposium (IV)*, pages 411–416. IEEE, 2011.

[31] Christian Günter Gold. *Modeling of take-over performance in highly automated vehicle guidance*. PhD thesis, Technische Universität München, 2016.

[32] Siyuan Gong, Anye Zhou, and Srinivas Peeta. Cooperative adaptive cruise control for a platoon of connected and autonomous vehicles considering dynamic information flow topology. *Transportation Research Record*, 2673(10):185–198, 2019.

[33] Michael A Goodrich and Erwin R Boer. Model-based human-centered task automation: a case study in acc system design. *IEEE Transactions on Systems, Man, and Cybernetics-Part A: Systems and Humans*, 33(3):325–336, 2003.

[34] CM Gorter. Adaptive cruise control in practice: A field study and questionnaire into its influence on driver, traffic flows and safety. Master's thesis, TU Delft, 2015.

[35] Jürgen Guldner, Han-Shue Tan, and Satyajit Patwardhan. Analysis of automatic steering control for highway vehicles with look-down lateral reference systems. *Vehicle System Dynamics*, 26(4):243–269, 1996.

[36] George Gunter, Derek Gloudemans, Raphael E Stern, Sean McQuade, Rahul Bhadani, Matt Bunting, Maria Laura Delle Monache, Roman Lysecky, Benjamin Seibold, Jonathan Sprinkle, et al. Are commercially implemented adaptive cruise control systems string stable? *arXiv preprint arXiv:1905.02108*, 2019.

[37] Levent Guvenc, Ismail Meriç Can Uygan, Kerim Kahraman, Raif Karaahmetoglu, Ilker Altay, Mutlu Senturk, Mümin Tolga Emirler, Ahu Ece Hartavi Karci, Bilin Aksun Guvenc, Erdinç Altug, et al. Cooperative adaptive cruise control implementation of team mekar at the grand cooperative driving challenge. *IEEE Transactions on Intelligent Transportation Systems*, 13(3):1062–1074, 2012.

[38] Jibo He, Jason S McCarley, and Arthur F Kramer. Lane keeping under cognitive load: performance changes and mechanisms. *Human factors*, 56(2):414–426, 2014.

[39] Marika Hoedemaeker and Karel A Brookhuis. Behavioural adaptation to driving with an adaptive cruise control (acc). *Transportation Research Part F: Traffic Psychology and Behaviour*, 1(2):95–106, 1998.

[40] Raymond Hoogendoorn, Bart van Arerm, and Serge Hoogendoom. Automated driving, traffic flow efficiency, and human factors: Literature review. *Transportation Research Record*, 2422(1):113–120, 2014.

[41] Xiaoyu Huang and Junmin Wang. Lightweight vehicle control-oriented modeling and payload parameter sensitivity analysis. *IEEE Transactions on Vehicular Technology*, 60 (5):1999–2011, 2011.

[42] P. A. Ioannou and C. C. Chien. Autonomous intelligent cruise control. *IEEE Transactions on Vehicular Technology*, 42(4):657–672, Nov 1993. ISSN 1939-9359. doi: 10.1109/25.260745.

[43] Petros A Ioannou and Margareta Stefanovic. Evaluation of acc vehicles in mixed traffic: Lane change effects and sensitivity analysis. *IEEE Transactions on Intelligent Transportation Systems*, 6(1):79–89, 2005.

[44] Rolf Isermann. *Fahrdynamik-Regelung: Modellbildung, Fahrerassistenzsysteme, Mechatronik*. Springer-Verlag, 2006.

[45] K. Jerath and S. N. Brennan. Analytical prediction of self-organized traffic jams as a function of increasing acc penetration. *IEEE Transactions on Intelligent Transportation Systems*, 13(4):1782–1791, Dec 2012. doi: 10.1109/TITS.2012.2217742.

[46] Kshitij Jerath and Sean N Brennan. Analytical prediction of self-organized traffic jams as a function of increasing acc penetration. *IEEE Transactions on Intelligent Transportation Systems*, 13(4):1782–1791, 2012.

[47] Fangjun Jiang and Zhiqiang Gao. An application of nonlinear pid control to a class of truck abs problems. In *Proceedings of the 40th IEEE Conference on Decision and Control (Cat. No. 01CH37228)*, volume 1, pages 516–521. IEEE, 2001.

[48] Shivaram Kamat. Lane keeping of vehicle using model predictive control. In *2019 IEEE 5th International Conference for Convergence in Technology (I2CT)*, pages 1–6. IEEE, 2019.

[49] Parampreet Kaur and Rajeev Sobti. Current challenges in modelling advanced driver assistance systems: Future trends and advancements. In *2017 2nd IEEE International Conference on Intelligent Transportation Engineering (ICITE)*, pages 236–240. IEEE, 2017.

[50] Arne Kesting, Martin Treiber, Martin Schönhof, Florian Kranke, and Dirk Helbing. Jam-avoiding adaptive cruise control (acc) and its impact on traffic dynamics. In *Traffic and Granular Flow'05*, pages 633–643. Springer, 2007.

[51] Arne Kesting, Martin Treiber, Martin Schönhof, and Dirk Helbing. Adaptive cruise control design for active congestion avoidance. *Transportation Research Part C: Emerging Technologies*, 16(6):668–683, 2008.

[52] Bo-Ah Kim, Seung-Hi Lee, Young Ok Lee, and Chung Choo Chung. Comparative study of approximate, proximate, and fast model predictive control with applications to autonomous vehicles. In *2012 12th International Conference on Control, Automation and Systems*, pages 479–484. IEEE, 2012.

[53] ByeoungDo Kim, Chang Mook Kang, Jaekyum Kim, Seung Hi Lee, Chung Choo Chung, and Jun Won Choi. Probabilistic vehicle trajectory prediction over occupancy grid map via recurrent neural network. In *2017 IEEE 20th International Conference on Intelligent Transportation Systems (ITSC)*, pages 399–404. IEEE, 2017.

[54] Gerdien Klunder, Michel Legius, Hettie Boonman, Ron Wouters, Simeon Calvert, Paco Hamers, Stefan Talen, Isabel Wilmink, Maurice Kwakkernaat, and Joke Welten. Cacc proef noord-holland. Technical report, TNO, 2019.

[55] Kristofer D Kusano and Hampton C Gabler. Safety benefits of forward collision warning, brake assist, and autonomous braking systems in rear-end collisions. *IEEE Transactions on Intelligent Transportation Systems*, 13(4):1546–1555, 2012.

[56] Mohammad Lavasani, Xia Jin, and Yiman Du. Market penetration model for autonomous vehicles on the basis of earlier technology adoption experience. *Transportation Research Record*, 2597(1):67–74, 2016.

[57] Kibeom Lee, Shengbo Eben Li, and Dongsuk Kum. Synthesis of robust lane keeping systems: impact of controller and design parameters on system performance. *IEEE Transactions on Intelligent Transportation Systems*, 20(8):3129–3141, 2018.

[58] Shengbo Li, Keqiang Li, Rajesh Rajamani, and Jianqiang Wang. Model predictive multiobjective vehicular adaptive cruise control. *IEEE Transactions on Control Systems Technology*, 19(3):556–566, 2010.

[59] Shengbo Eben Li, Qiangqiang Guo, Long Xin, Bo Cheng, and Keqiang Li. Fuel-saving servo-loop control for an adaptive cruise control system of road vehicles with step-gear transmission. *IEEE transactions on vehicular technology*, 66(3):2033–2043, 2016.

[60] Shengbo Eben Li, Yang Zheng, Keqiang Li, Le-Yi Wang, and Hongwei Zhang. Platoon control of connected vehicles from a networked control perspective: Literature review, component modeling, and controller synthesis. *IEEE Transactions on Vehicular Technology*, 2017.

[61] Chi-Ying Liang and Huei Peng. String stability analysis of adaptive cruise controlled vehicles. *JSME International Journal Series C Mechanical Systems, Machine Elements and Manufacturing*, 43(3):671–677, 2000.

[62] Amara Loulizi, Youssef Bichiou, and Hesham Rakha. Steady-state car-following time gaps: An empirical study using naturalistic driving data. *Journal of Advanced Transportation*, 2019:1–9, 05 2019. doi: 10.1155/2019/7659496.

[63] Tyron Louw and Natasha Merat. Are you in the loop? using gaze dispersion to understand driver visual attention during vehicle automation. *Transportation Research Part C: Emerging Technologies*, 76:35–50, 2017.

[64] Haneet Singh Mahajan, Thomas Bradley, and Sudeep Pasricha. Application of systems theoretic process analysis to a lane keeping assist system. *Reliability Engineering & System Safety*, 167:177–183, 2017.

[65] Michail Makridis, Konstantinos Mattas, Daniele Borio, and Biagio Ciuffo. Estimating empirically the response time of commercially available acc controllers under urban and freeway conditions. In *2019 6th International Conference on Models and Technologies for Intelligent Transportation Systems (MT-ITS)*, pages 1–7. IEEE, 2019.

[66] Michail Makridis, Konstantinos Mattas, and Biagio Ciuffo. Response time and time headway of an adaptive cruise control. an empirical characterization and potential impacts on road capacity. *IEEE Transactions on Intelligent Transportation Systems*, 2019.

[67] Huajian Mao, Wuman Luo, Haoyu Tan, Lionel M Ni, and Nong Xiao. Exploration of ground truth from raw gps data. In *Proceedings of the ACM SIGKDD International Workshop on Urban Computing*, pages 118–125, 2012.

[68] Vicente Milanés and Steven E Shladover. Modeling cooperative and autonomous adaptive cruise control dynamic responses using experimental data. *Transportation Research Part C: Emerging Technologies*, 48:285–300, 2014.

[69] Vicente Milanés, Steven E Shladover, John Spring, Christopher Nowakowski, Hiroshi Kawazoe, and Masahide Nakamura. Cooperative adaptive cruise control in real traffic situations. *IEEE Transactions on Intelligent Transportation Systems*, 15(1):296–305, 2013.

[70] Xavier Mosquet, Michelle Andersen, and Aakash Arora. A roadmap to safer driving through advanced driver assistance systems. *Auto Tech Review*, 5(7):20–25, 2016.

[71] Freddy Antony Mullakkal-Babu, Meng Wang, Haneen Farah, Bart van Arem, and Riender Happee. Comparative assessment of safety indicators for vehicle trajectories on highways. *Transportation Research Record*, 2659(1):127–136, 2017.

[72] Thomas J Nagle et al. Global positioning system (gps) civil monitoring performance specification. Technical report, United States. Dept. of Transportation, 2009.

[73] Attila M Nagy and Vilmos Simon. Survey on traffic prediction in smart cities. *Pervasive and Mobile Computing*, 50:148–163, 2018.

[74] Gerrit JL Naus, Rene PA Vugts, Jeroen Ploeg, Marinus JG van De Molengraft, and Maarten Steinbuch. String-stable cacc design and experimental validation: A frequency-domain approach. *IEEE Transactions on vehicular technology*, 59(9):4268–4279, 2010.

[75] Hans-Jürgen Negele. *Anwendungsgerechte Konzipierung von Fahrsimulatoren für die Fahrzeugentwicklung*. PhD thesis, Technische Universität München, 2007.

[76] Julia Nilsson, Mattias Brännström, Erik Coelingh, and Jonas Fredriksson. Lane change maneuvers for automated vehicles. *IEEE Transactions on Intelligent Transportation Systems*, 18(5):1087–1096, 2016.

[77] JF O'Hanlon. Driving performance under the influence of drugs: rationale for, and application of, a new test. *British journal of clinical pharmacology*, 18(S1):121S–129S, 1984.

[78] Sinan Öncü, Jeroen Ploeg, Nathan Van de Wouw, and Henk Nijmeijer. Cooperative adaptive cruise control: Network-aware analysis of string stability. *IEEE Transactions on Intelligent Transportation Systems*, 15(4):1527–1537, 2014.

[79] Hendrik Oschlies. *Komfortorientierte Regelung für die automatisierte Fahrzeugquerführung*. Springer, 2019.

[80] Jeroen Ploeg, Bart TM Scheepers, Ellen Van Nunen, Nathan Van de Wouw, and Henk Nijmeijer. Design and experimental evaluation of cooperative adaptive cruise control. In *2011 14th International IEEE Conference on Intelligent Transportation Systems (ITSC)*, pages 260–265. IEEE, 2011.

[81] Jeroen Ploeg, Elham Semsar-Kazerooni, Guido Lijster, Nathan van de Wouw, and Henk Nijmeijer. Graceful degradation of cacc performance subject to unreliable wireless communication. In *16th International IEEE Conference on Intelligent Transportation Systems (ITSC 2013)*, pages 1210–1216. IEEE, 2013.

[82] Jeroen Ploeg, Dipan P Shukla, Nathan van de Wouw, and Henk Nijmeijer. Controller synthesis for string stability of vehicle platoons. *IEEE Transactions on Intelligent Transportation Systems*, 15(2):854–865, 2013.

[83] Jeroen Ploeg, Nathan Van De Wouw, and Henk Nijmeijer. Lp string stability of cascaded systems: Application to vehicle platooning. *IEEE Transactions on Control Systems Technology*, 22(2):786–793, 2013.

[84] Vincenzo Punzo and Fulvio Simonelli. Analysis and comparison of microscopic traffic flow models with real traffic microscopic data. *Transportation Research Record*, 1934 (1):53–63, 2005.

[85] Rajesh Rajamani. *Vehicle dynamics and control*. Springer, New York, 2012. ISBN 978-1-4614-1432-2.

[86] Vasili Ramanishka, Yi-Ting Chen, Teruhisa Misu, and Kate Saenko. Toward driving scene understanding: A dataset for learning driver behavior and causal reasoning. In *Proceedings of the IEEE Conference on Computer Vision and Pattern Recognition*, pages 7699–7707, 2018.

[87] Jens Rasmussen. Skills, rules, and knowledge; signals, signs, and symbols, and other distinctions in human performance models. *IEEE transactions on systems, man, and cybernetics*, (3):257–266, 1983.

[88] Gilles Reymond, Andras Kemeny, Jacques Droulez, and Alain Berthoz. Role of lateral acceleration in curve driving: Driver model and experiments on a real vehicle and a driving simulator. *Human factors*, 43(3):483–495, 2001.

[89] Bryan Riley, George Kuo, Brian Schwartz, Jon Zumberge, and Kevin Shipp. Development of a controlled braking strategy for vehicle adaptive cruise control. Technical report, SAE Technical Paper, 2000.

[90] Federico Roselli, Matteo Corno, Sergio M Savaresi, M Giorelli, D Azzolini, A Irilli, and Giulio Panzani. $H\mathbb{F}_1$ control with look-ahead for lane keeping in autonomous vehicles. In *2017 IEEE Conference on Control Technology and Applications (CCTA)*, pages 2220–2225. IEEE, 2017.

[91] Wouter J Schakel, Bart Van Arem, and Bart D Netten. Effects of cooperative adaptive cruise control on traffic flow stability. In *13th International IEEE Conference on Intelligent Transportation Systems*, pages 759–764. IEEE, 2010.

[92] Bernhard Schick, Florian Fuhr, Manuel Höfer, and Peter E Pfeffer. Eigenschaftsbasierte entwicklung von fahrerassistenzsystemen. *ATZ-Automobiltechnische Zeitschrift*, 121 (4):70–75, 2019.

[93] Li Shengbo, Bin Yang, Li Keqiang, Hiroshi Ukawa, Dongsheng Bai, and Masatoshi Handa. A control strategy of acc system considering fuel consumption. In *Proc 2006 Adv Vehi Eng Control Conf*, pages 851–855, 2006.

[94] Steven E Shladover, Dongyan Su, and Xiao-Yun Lu. Impacts of cooperative adaptive cruise control on freeway traffic flow. *Transportation Research Record*, 2324(1):63–70, 2012.

[95] Julian Staiger, Luka Popovic, and Christian Bienias. Impact on the quality of automated lateral driving when implementing an 2dof steering model and vary driving dynamic quantities. In *2020 International Conference on Intelligent Vehicles (ICoIV)*. Hong Kong Society of Robotics and Automation, in print.

[96] D. Swaroop. *String stability of interconnected systems: An application to platooning in automated highway systems*. PhD thesis, UC Berkeley: California Partners for Advanced Transportation Technology., 1997. Retrieved from https://escholarship.org/uc/item/86z6h1b1.

[97] Darbha Swaroop and KR Rajagopal. A review of constant time headway policy for automatic vehicle following. In *ITSC 2001. 2001 IEEE Intelligent Transportation Systems. Proceedings (Cat. No. 01TH8585)*, pages 65–69. IEEE, 2001.

[98] Hedrick J K SWAROOP D. String stability of interconnected. In *American Control Conference, Proceedings of the 1995. Washington: IEEE*, volume 3, pages 1806–1810, 1995.

[99] Meirav Taieb-Maimon and David Shinar. Minimum and comfortable driving headways: Reality versus perception. *Human factors*, 43(1):159–172, 2001.

[100] Alireza Talebpour and Hani S Mahmassani. Influence of connected and autonomous vehicles on traffic flow stability and throughput. *Transportation Research Part C: Emerging Technologies*, 71:143–163, 2016.

[101] Tamás Tettamanti, István Varga, and Zsolt Szalay. Impacts of autonomous cars from a traffic engineering perspective. *Periodica Polytechnica Transportation Engineering*, 44 (4):244–250, 2016.

[102] Felix Tigges, F Krauns, A Hafner, R Henze, and F Kücükay. Controller concept for automated lateral control. In *8th International Munich Chassis Symposium 2017*, pages 465–481. Springer, 2017.

[103] Olivér Törő, Tamas Becsi, and Szilárd Aradi. Design of lane keeping algorithm of autonomous vehicle. *Periodica Polytechnica Transportation Engineering*, 44(1):60–68, 2016.

[104] Martin Treiber and Arne Kesting. Traffic flow dynamics: data, models and simulation. *Physics Today*, 67(3):54, 2014.

[105] Stefan Trommer, Lars Kröger, and Tobias Kuhnimhof. Potential fleet size of private autonomous vehicles in germany and the us. In *Road Vehicle Automation 4*, pages 247–256. Springer International Publishing, 06 2018. ISBN 978-3-319-60933-1. doi: 10.1007/978-3-319-60934-8_20.

[106] Kakin K Tsoi, Mark Mulder, and David A Abbink. Balancing safety and support: Changing lanes with a haptic lane-keeping support system. In *2010 IEEE international conference on systems, man and cybernetics*, pages 1236–1243. IEEE, 2010.

[107] Eser Ustunel and Engin Masazade. Vision-based road slope estimation methods using road lines or local features from instant images. *IET Intelligent Transport Systems*, 13 (10):1590–1602, 2019.

[108] Bart Van Arem, Cornelie JG Van Driel, and Ruben Visser. The impact of cooperative adaptive cruise control on traffic-flow characteristics. *IEEE Transactions on intelligent transportation systems*, 7(4):429–436, 2006.

[109] Ellen van Nunen, Maurice RJAE Kwakkernaat, Jeroen Ploeg, and Bart D Netten. Cooperative competition for future mobility. *IEEE Transactions on Intelligent Transportation Systems*, 13(3):1018–1025, 2012.

[110] Francesco Viti, Serge P Hoogendoorn, Tom P Alkim, and Gerben Bootsma. Driving behavior interaction with acc: results from a field operational test in the netherlands. In *2008 IEEE Intelligent Vehicles Symposium*, pages 745–750. IEEE, 2008.

[111] Jurate Vitkiene and Virgaudas Puodziukas. Design of road based on the applicable design methods used in western european countries. In *Environmental Engineering. Proceedings of the International Conference on Environmental Engineering. ICEE*, volume 9, page 1. Vilnius Gediminas Technical University, Department of Construction Economics . . . , 2014.

[112] Junmin Wang and Rajesh Rajamani. Adaptive cruise control system design and its impact on highway traffic flow. In *Proceedings of the 2002 American Control Conference (IEEE Cat. No. CH37301)*, volume 5, pages 3690–3695. IEEE, 2002.

[113] Meng Wang, Serge Paul Hoogendoorn, Winnie Daamen, Bart van Arem, Barys Shyrokau, and Riender Happee. Delay-compensating strategy to enhance string stability of adaptive cruise controlled vehicles. *Transportmetrica B: Transport Dynamics*, 6(3): 211–229, 2018.

[114] Ziran Wang, Guoyuan Wu, and Matthew J Barth. A review on cooperative adaptive cruise control (cacc) systems: Architectures, controls, and applications. In *2018 21st International Conference on Intelligent Transportation Systems (ITSC)*, pages 2884–2891. IEEE, 2018.

[115] Lingyun Xiao and Feng Gao. Practical string stability of platoon of adaptive cruise control vehicles. *IEEE Transactions on intelligent transportation systems*, 12(4):1184–1194, 2011.

[116] Lingyun Xiao, Swaroop Darbha, and Feng Gao. Stability of string of adaptive cruise control vehicles with parasitic delays and lags. In *2008 11th International IEEE Conference on Intelligent Transportation Systems*, pages 1101–1106. IEEE, 2008.

[117] Long Xin, Pin Wang, Ching-Yao Chan, Jianyu Chen, Shengbo Eben Li, and Bo Cheng. Intention-aware long horizon trajectory prediction of surrounding vehicles using dual lstm networks. In *2018 21st International Conference on Intelligent Transportation Systems (ITSC)*, pages 1441–1446. IEEE, 2018.

[118] Yao-Ming Yuan, Rui Jiang, Mao-Bin Hu, Qing-Song Wu, and Ruili Wang. Traffic flow characteristics in a mixed traffic system consisting of acc vehicles and manual vehicles: A hybrid modelling approach. *Physica A: Statistical Mechanics and its Applications*, 388 (12):2483–2491, 2009.

[119] Yang Zheng, Shengbo Eben Li, Jianqiang Wang, Keqiang Li, et al. Influence of information flow topology on closed-loop stability of vehicle platoon with rigid formation. In *17th International IEEE Conference on Intelligent Transportation Systems (ITSC)*, pages 2094–2100. IEEE, 2014.